TRANSIENT HEAT TRANSFER MEASUREMENTS ON A FLAT PLATE IN TURBULENT FLOW USING AN ELECTRICAL ANALOG

THESIS

Richard K. Rockwell
Captain, USAF

DEPARTMENT OF THE AIR FORCE
AIR UNIVERSITY
AIR FORCE INSTITUTE OF TECHNOLOGY

Wright-Patterson Air Force Base, Ohio

AFIT/GAE/ENY/89D-31

TRANSIENT HEAT TRANSFER MEASUREMENTS ON A FLAT PLATE IN TURBULENT FLOW USING AN ELECTRICAL ANALOG

THESIS

Presented to the Faculty of the School of Engineering
of the Air Force Institute of Technology
Air University
in Partial Fulfillment of the
Requirements for the Degree of
Master of Science in Aeronautical Engineering

Richard K. Rockwell, B.S.
Captain, USAF

December 1989

Approved for public release; distribution unlimited

PREFACE

The primary purpose of this study was to develop, test and build an electrical circuit to be used for heat transfer measurement in a transient test facility. The method currently used to calculate heat transfer involves performing a numerical differentiation of recorded surface temperature. This procedure is cumbersome and has not yielded satisfactory results when used with the shock tube at AFIT. The numerical procedure is inherently noisy since, as with many numerical schemes where a derivative is approximated using a finite difference, errors are magnified as the numerical procedure marches forward. With the analog, heat transfer measurements are recorded directly, allowing for time savings and drastically simplifying the data reduction.

Writing this thesis and performing the experimentation, although much work, has been quite enjoyable. There have been struggles, as is to be expected when any work of this magnitude is performed under a time constraint. Many times the data would not come out as expected. However, upon further examination, certain parameters would appear which would tie everything together. This is what makes experimentation so satisfying. One can take unexpected results and, with a little theory and insight, explain the results then perform another experiment and verify and understand the phenomena.

I have had a great deal of help from others in perform-

ing the experimentation and in writing this thesis. I am deeply indebted to my thesis committee, Lt Col Paul King, Dr. William Elrod, and Capt Daniel Fant, for their hours of patience and consultation. I also wish to thank Jay Anderson, Orville Wright, Tim Major and Jack Tiffany for their help in building the necessary test equipment. Finally, I wish to thank my wife, Lil, for her love and understanding on those occasions when I was tied to my desk with work.

Richard K. Rockwell

Table of Contents

List of Figures

Figure

List of Tables

List of Symbols

Symbol	Description	Units
A	Undetermined Coefficient in Appendix B	
a	Speed of Sound,	m/s
	x^0 Coefficient in Turbulence Calculation Constant in Appendix B	
b	x^1 Coefficient in Turbulence Calculation, Constant in Appendix B	
B	Undetermined Coefficient in Appendix B	
c	Capacitance per Unit Volume,	$\frac{\mu Farad}{m^3}$
	x^2 Coefficient in Turbulence Calculation	
C_f'	Local Skin Friction Coefficient	
C_p	Constant Pressure Specific Heat	$\frac{J}{kgK}$
G	Amplifier Gain	
h	Convective Heat Transfer Coefficient	$\frac{Watt}{m^2\ K}$
i	Current	Amp
k	Thermal Conductivity	$\frac{Watt}{mK}$
ℓ	Thin Film Thickness	μm
m	Slope of a Calibration Curve	
M	Mach Number	
Nu	Nusselt Number	
P	Power	Watt
Pr	Prandtl Number	
q	Heat Flux	$\frac{Watt}{m^2}$
Q	Laplace Transform of Heat Flux	

r	Recovery Factor, Resistance per unit length	$\frac{Ohm}{m}$
R	Resistance, Gas Constant	Ohm $\frac{J}{g\ ^{\circ}C}$
Re	Reynolds Number	
s	Laplace Variable	
St	Stanton Number	
t	Time	s
T	Temperature	K
U	Velocity	$\frac{m}{s}$
V	Electrical Potential	V
x	Position, Hot wire Overheat Parameter	m
α	Empirical Parameter used to calculate the Recovery Factor,	
	Thermal Diffusivity,	$\frac{m^2}{s}$
	Thin Film Temperature Coefficient, Hot-Wire Temperature Coefficient,	$\frac{1}{^{\circ}C}$
β	Empirical Parameter	
γ	Ratio of Specific Heats	
ε	Curve Fit Error	
λ	Empirical Parameter	
μ	Dynamic Viscosity	Pa s
ν	Kinematic Viscosity	$\frac{m^2}{s}$
π	Arithmetic constant (3.1415297)	
ρ	Density	$\frac{kg}{m^3}$
τ	Time integration Variable, Thermocouple Time Constant, Laplace Transform of Temperature (Appendix A)	ms

ω	Frequency	$\frac{1}{s}$

Subscripts

air	Pertaining to air
aw	Adiabatic wall
decade	Hot-wire decade box
elbow	Hot-wire probe joint
g	Gauge (Heat Flux Gauge), Gas
int	Internal
j	Thermocouple Junction
mean	Arithmetic Average
min	Minimum
probe	Hot-wire Probe
ref	Reference
rms	Root Mean Square
s	Surface, Shock
sum	Summation
support	Hot-wire Support Rod
t	Stagnation
0	Initial, At T = 0 °C, At T = Flow Stagnation Temperature
1	Driven Condition, First Resistor in Analog, Thin Film (Appendix A)
2	Behind Normal Shock, Substrate (Appendix A)
4	Driver Section
20	20 °C
w	Wall

x	Local
θ	Momentum (Momentum Reynolds Number)
∞	Free Stream

ABSTRACT

In this study an electrical analog, for heat flux measurement from surface mounted thin film temperature gauges, was built and tested. Typically, the determination of heat transfer from thin film gauges requires the numerical evaluation of an integral. The electrical analog enables the heat transfer to be recorded directly without incorporating numerical error.

Once built and tested, the analog is used to measure transient flat plate heat flux with free-stream turbulence. The time varying flow is produced using a low pressure shock tube, with free stream turbulence generated by flow injection upstream of the flat plate. The "steady flow" portion of the test data is compared to the theoretical flat plate solution for constant free stream and constant plate temperatures.

A constant temperature hot-wire technique is used to determine free stream turbulence. The hot-wire procedure requires performing several experiments with the same flow conditions, but different hot-wire operating temperatures. A quadratic least squares curve fit is performed using the data from the hot-wire experiments to determine the turbulence level.

TRANSIENT HEAT TRANSFER MEASUREMENTS ON A FLAT PLATE IN TURBULENT FLOW USING AN ELECTRICAL ANALOG

INTRODUCTION

Thin film heat flux gauges have been used with considerable success in measuring heat transfer in shock tubes and other short duration test facilities by Oldfield, 1978 and 1984, Schultz, 1973, Schmitz, 1963 and others. A thin film heat flux gauge (also known as a thin film surface thermometer) consists of a thin metallic film, usually gold, platinum or rhodium, deposited on an insulating material (substrate). Commonly used insulating materials are quartz, pyrex and soda glass [Meyer, 1963: 1]. The metal films are typically 0.1 μm thick [Schultz, 1973: 19]. Since the thin films are small and have negligible heat capacity they offer little resistance to heat flow. Hence, the thin film is assumed to be at the same temperature as the substrate surface. If the test duration is sufficiently small (on the order of 10^{-3} seconds), then the heat flow into the insulating material may be taken as one-dimension heat flow into a semi-infinite slab. For this situation, the relation between heat flux and surface temperature is given by [Skinner, 1960: 4]

$$q(t) = \sqrt{\frac{k\rho C_p}{\pi}} \left\{ \frac{T(0^+) - T(0^-)}{\sqrt{t}} + \int_0^t \frac{\left.\frac{dT}{dt}\right|_{(t-\tau)}}{\sqrt{\tau}} \, d\tau \right\} \qquad (1.1)$$

For all but simplified solutions, this integral must evaluated numerically. Several theses at AFIT have used this numerical procedure to obtain heat flux from recorded surface temperature data (Gochenaur, 1984, Fillingham, 1985, Smith, 1986 and Novak, 1987). The results obtained in these studies do not agree with the constant free stream velocity, constant free stream temperature, iso-thermal flat plate solution. Perhaps part of the explanation for the disagreement is the error inherent in the numerical procedure, since the discrete time derivative of temperature must be evaluated in order to evaluate (1.1).

A method for measuring heat transfer directly would be much preferred. Such a method exists and is referred to as the electrical analog for heat transfer. The thin film voltage signal can be used as the input to an electrical circuit for which there exists an analogy between temperature and heat flux to voltage and current. The voltage output of this circuit is related to heat flux and can be recorded at the time of the experiment. The goal of this thesis was to build an electrical analog for heat transfer measurements, then use the analog to measure transient heat flux in a shock tube. The major benefit of using the heat transfer analog is that no numerical differentiation is required. Heat flux is recorded directly, which also saves time in data reduction since multiplying the analog signal by a cal-

ibration constant is much less cumbersome than performing numerical integration/differentiation.

Background of the Electrical Analog

The earliest research on the electrical analog for heat transfer measurements were performed by Lawson and McGuire in 1953. They used the analog to measure heat flow through an insulated wall separating two rooms. In one room a fire was ignited while the other room remained at ambient conditions. Later, Meyer [1960] proposed using the analog in conjunction with thin film heat flux gauges to measure heat flow in shock tubes and other transient test facilities. The analog used by both Lawson and Meyer consisted of a series of constant value resistor-capacitor elements. These R-C elements were introduced in three configurations, the "T" configuration, the "L" configuration and the "PI" configuration. An example of each configuration is given in figure 1.1. The number of elements needed depends on the application, as the test duration increases, more R-C elements that are required. Typically, 30 to 40 elements are required when using the Meyer circuit to measure heat flux in a shock tube.

Skinner [1960] examined the electrical analog about the same time as Meyer. Both the Meyer and Skinner circuits consisted of constant value R-C elements. The "infinite medium" was approximated by using more elements. Later,

Skinner and Meyer [1963] considered using values of R-C elements in an arithmetic progression, increasing the resistance and capacitance values in a predetermined way, to better approximate the infinite medium.

Oldfield [1984] has designed the most practical electrical analog for heat transfer measurement to date. The Oldfield analog uses R-C components which increase in a logarithmic progression, allowing for an analog design of only 9 sections (as opposed to 20 or 30 for the Meyer analog), with a working frequency range of 0.02 Hz to 100 kHz [Oldfield, 1984: 253]. The Oldfield analog was used as the model for the analog developed in this study.

Objectives

The primary objective of this research was to develop and test an electrical circuit for direct measurement of heat transfer in a transient test facility (the shock tube). Once the analog (circuit) is built and tested, it was used to measure heat transfer to a flat plate in turbulent flow. A turbulence injector just upstream of the flat plate was used to generate free stream turbulence. An algorithm was developed which uses a constant temperature hot-wire data to determine the turbulence level. In summary, the objectives were:

1. Build and test an electrical analog for heat transfer measurement.

2. Develop the tools required (computer software) to perform the constant temperature hot-wire procedure to determine turbulence levels.

3. Measure the shock tube turbulence levels with and without turbulence injection.

4. Perform shock tube experiments with and without turbulence injection, then compare heat transfer rates with those for no free stream turbulence and with free stream turbulence present.

THEORY

Shock Tube Principles

A shock tube is a device in which a plane shock wave is formed by the rupturing of a diaphragm which separates a higher pressure gas from a lower pressure gas. The high pressure section is called the driver section, the low pressure section is called the driven section. The shock wave strength is a function of the driver to driven pressure ratio (P_4/P_1). Higher pressure ratios produce higher strength shock waves. The equations for shock tube performance are given in Appendix A. A simple shock tube is depicted in Figure 2.1.

When the diaphragm is burst compression waves move in the direction of low pressure and quickly coalesce to form a normal shock wave. At the same moment, expansion waves move in the opposite direction, into the high pressure gas. The flow properties behind the normal shock, which constitute the test conditions of interest for this study, can be computed using the equations of Appendix A.

Boundary Layer Theory

Passage of a shock wave though still air imparts a forward velocity to the air behind the shock (forward being the direction of shock travel). If a flat plate is placed in the shock tube, a boundary layer is formed on the plate behind the normal shock. Flow is started along the plate as

the shock moves down the passage. Since the shock has finite velocity, flow along the plate at each streamwise location is started at different moments in time [Schlichting, 1979: 439-443]. For the ratio of flow speed to shock speed equal to zero $(U_2/U_s = 0)$, this boundary layer problem is the same as Stokes first problem, the suddenly accelerated flat plate [Schlichting, 1979: 90-91, 440-441].

Flat Plate Heat Transfer

Heat transfer to a flat plate is governed by the temperature difference, between the plate and flow, and the effectiveness at which the temperature difference is imposed on the plate (or fluid). This heat flow effectiveness is determined by properties of the fluid-plate interface, namely the boundary layer. Four flat plate heat transfer solutions are considered in this study, namely steady laminar, steady turbulent, unsteady laminar and unsteady turbulent. Laminar/turbulent refers to the state of the boundary layer and steady/unsteady refers to the state of the free stream. The underlying assumptions for these simplified solutions are that the plate remains at constant temperature and the heat transfer is one-dimensional.

The equation for heat flux is:

$$q = h\ (T_\infty - T_w) \qquad (2.1)$$

For high velocity flows, the adiabatic wall temperature is used in place of the free-stream temperature.

$$q = h\,(T_{aw} - T_w) \tag{2.2}$$

The adiabatic wall temperature is given by Schlichting [1979: 442]

$$T_{aw} = T_\infty \left\{ 1 + \frac{\gamma-1}{2} M_\infty^2\, r \right\} \tag{2.3}$$

The adiabatic wall temperature reduces to the stagnation temperature for r=1. The recovery factor, r, is also given by Schlichting [1979: 442] as

$$r = Pr^{\alpha} \tag{2.4}$$

Where

$$\alpha = 0.39 - \frac{0.02}{1 - U_\infty/U_s} \tag{2.5}$$

Two important parameters used to study heat transfer are the local Nusselt number (Nu_x) and the Stanton number (St). These parameters are defined as:

$$Nu_x \equiv \frac{h\,x}{k} \tag{2.6}$$

$$St \equiv \frac{h}{\rho\, U_\infty\, C_p} \tag{2.7}$$

Fluid Properties. All fluid properties are evaluated at the reference (or film) temperature unless otherwise noted. Kays and Crawford [1980: 304] give the reference temperature as:

$$T_{ref} = T_\infty + 0.5\,(T_w - T_\infty) + 0.22\,(T_{aw} - T_\infty) \tag{2.8}$$

Kinematic viscosity is defined as:

$$\nu \equiv \frac{\mu}{\rho} \tag{2.9}$$

According to Schlichting [1979: 9], dynamic viscosity can be taken to be independent of pressure (to a first approximation). Density, on the other hand, is a strong function of both temperature and pressure. Therefore, whenever kinematic viscosity is used, it is calculated using

$$\nu = \frac{\mu(T_{ref})}{\rho(T_{ref}, P_2)} , \qquad (2.10)$$

unless otherwise noted.

Steady Laminar Solution. Kays and Crawford [1980: 134-137] give the heat transfer solution for the case of constant free-stream velocity flow along a constant-temperature semi-infinite plate with a laminar boundary layer. The solution is:

$$Nu_x = 0.332\ Pr^{1/3}\ Re_x^{1/2} \qquad (2.11)$$

This equation is good for moderate Prandtl numbers, $0.5 \le Pr \le 15$.

Unsteady Laminar Solution. The heat transfer solution for unsteady free-stream velocity, laminar boundary layer, constant free-stream temperature semi-infinite plate is given by Schlichting [1979: 439-443].

Nu_x = Local Nusselt number
Re_x = Local Reynolds number
C_f' = Skin Friction coefficient
Pr = Prandtl number
U_∞ = Flow velocity behind the shock

ν_w = kinematic viscosity at the wall
x = distance from reference point (i.e., leading edge)
t = time since shock passed reference point

$\left.\begin{matrix}\beta \\ \lambda\end{matrix}\right\}$ Emperical parameters

$$Nu_x = \frac{1}{2} C_f' \, Re_x \, Pr^{\lambda} \tag{2.12}$$

Where

$$Re_x = \frac{U_\infty^2}{\nu_w} \left(t - \frac{x}{U_s} \right) \tag{2.13}$$

$$\text{Note:} \quad \nu_w = \frac{\mu(T_w)}{\rho(P_2, T_w)}$$

$$C_f' \sqrt{Re_x} = 1.128 \sqrt{1 - \beta \frac{U_\infty}{U_s}} \tag{2.14}$$

$$\beta = 0.346 \tag{2.15}$$

$$\lambda = 0.35 + \frac{0.15}{1 - U_\infty / U_s} \tag{2.16}$$

Steady Turbulent Solution. Kays and Crawford [1980: 134-137] give the heat transfer solution for the case of constant free-stream velocity flow along a constant-temperature semi-infinite plate with a turbulent boundary layer. The solution is:

$$St \, Pr^{0.4} = 0.0287 \, Re_x^{-0.2} \tag{2.17}$$

This equation is good for gases, where $0.5 \leq Pr \leq 1$ and

$5 \times 10^5 \leq Re_x \leq 5 \times 10^6$ Recall,

$$Nu_x = St\ Pr\ Re_x \tag{2.18}$$

Substitute Stanton number from equation (2.17) to get,

$$Nu_x = 0.0287\ Pr^{0.6}\ Re_x^{0.8} \tag{2.19}$$

Unsteady Turbulent Solution. The solution for unsteady free-stream velocity, turbulent boundary layer, constant free-stream temperature, constant temperature semi-infinite plate is given by using the unsteady Reynolds number from equation (2.13) in equation (2.19).

Electrical Analog for Heat Transfer

The governing equations for one-dimensional heat transfer to a semi-infinite medium are:

$$\frac{\partial q}{\partial x} = -\rho C_p \frac{\partial T}{\partial t} \tag{2.20}$$

$$q = -k \frac{\partial T}{\partial x} \tag{2.21}$$

These are reduced to the diffusion equation by substitution, to get:

$$\frac{\partial T}{\partial t} = \frac{k}{\rho C_p} \frac{\partial^2 T}{\partial x^2} \tag{2.22}$$

Equations (2.20), (2.21) and (2.22) may be solved for the heat flux at the surface of the semi-infinite medium in terms of the surface temperature T (see Appendix A) to give [Oldfield, 1978]:

$$Q = \sqrt{\rho\, C_p\, k}\ \sqrt{s}\ \tau \qquad (2.23)$$

The governing equations for one-dimensional diffusion of electrical charge through a medium with a distributed capacitance per unit volume (c) and resistance per unit length (r) is given by Oldfield [1978]:

$$\frac{\partial i}{\partial x} = -c\,\frac{\partial V}{\partial t} \qquad (2.24)$$

$$i = -\frac{1}{r}\,\frac{\partial V}{\partial x} \qquad (2.25)$$

Which can be combined to give:

$$\frac{\partial V}{\partial t} = \frac{1}{r\,c}\,\frac{\partial^2 V}{\partial x^2} \qquad (2.26)$$

Equations (2.24), (2.25) and (2.26) can be solved to get:

$$\bar{i} = \sqrt{c/r}\ \sqrt{s}\ \bar{V} \qquad (2.27)$$

Equations (2.22) and (2.26) have identical form so that analogous thermal and electrical systems may be constructed. The respective analogies are given in Table 2.1. Combining (2.23) and (2.27) yields:

$$\frac{\bar{I}}{\bar{V}}\sqrt{r/c} = \frac{Q}{\tau}\,\frac{1}{\sqrt{\rho C_p k}} \qquad (2.28)$$

V is related to T, the change in surface temperature (T=0 at t=0), by the thermal coefficient of resistivity of the thin film heat flux gauge [Oldfield, 1984]. We know,

$$R_g = R_{g0}\alpha T \qquad (2.29)$$

Table 2.1: Thermal-Electrical Analogies [Meyer, 1960: 4]

Thermal			Electrical		
Property	Symbol	Unit	Property	Symbol	Unit
Temperature	T	°C	Voltage	V	Volts
Time	t	sec	Time	t	sec
Heat Flux	q	$\frac{\text{Joule}}{\text{sec m}^2}$	Current	i	Amp
Heat Capacity	ρC_p	$\frac{\text{Joule}}{\text{m}^3\ ^\circ\text{C}}$	Capacitance	c	$\frac{\text{Farad}}{\text{m}^3}$
Conductivity	k	$\frac{\text{Joule}}{\text{sec m}\ ^\circ\text{C}}$	Conductivity	$\frac{1}{r}$	$\frac{\text{m}}{\text{Ohm}}$
Length	x	m	Length	x	m

Define $$V_0 \equiv R_{g0} i$$

where i is the current in the thin film gauge. Therefore, a change in voltage (V=0 at t=0) across the thin film due to a change in surface temperature is

$$V_{in} = V_0 \alpha T$$

and

$$\bar{V}_{in} = \bar{V}_o \alpha \tau \qquad (2.30)$$

The current, i, is found by taking the analog output voltage across resistor R_1 (see Figure 2.2, or Figures 3.3 to 3.5 for more detailed circuit diagrams)

$$i = V'_{out}/R_1 \qquad (2.31)$$

If the analog output is passed through an amplifier, then

$$V_{out} = G\, V'_{out} \tag{2.32}$$

where G is the amplifier gain, and

$$i = \frac{V_{out}}{G\, R_1}$$

or

$$\bar{I} = \frac{\bar{V}_{out}}{G\, R_1} \tag{2.33}$$

Substituting (2.30) and (2.33) into (2.28) yields:

$$\frac{\bar{V}_{out}}{R_1}\,\frac{1}{V_0 \alpha \tau}\,\frac{1}{G}\,\sqrt{r/c}\,\rceil = \frac{Q}{\tau}\,\frac{1}{\sqrt{\rho C_p k}\,\rceil}$$

The Laplace variable for temperature, τ, is canceled from both sides, after which the Inverse Laplace Transform can be performed (s does not appear on either side of the equation) to give:

$$\frac{V_{out}}{R_1}\,\frac{1}{V_0 \alpha}\,\frac{1}{G}\,\sqrt{r/c}\,\rceil = q\,\frac{1}{\sqrt{\rho C_p k}\,\rceil} \tag{2.34}$$

Finally, reducing and solving for heat flux yields:

$$\boxed{q = \sqrt{\rho C_p k}\,\rceil\,\frac{1}{G}\,\sqrt{r/c}\,\rceil\,\frac{V_{out}}{R_1 V_0 \alpha}} \tag{2.35}$$

The $V_0\alpha$ term is the slope of the heat flux calibration curves given in Appendix E, the product $\rho C_p k$ is a property of the gauge substrate and $\frac{1}{GR_1}\sqrt{\frac{r}{c}\rceil}$ is determined from calibration.

Turbulence Measurement

The method used to measure free-stream turbulence is taken from Oldfield [1978]. The turbulence injector to be used injects cold air (at room temperature, ≈ 293 K) into a hot gas (T_2 = 369 K for M = 1.4) which could give rise to temperature fluctuations in the flow [Oldfield, 1978: 746]. Since hot wire measurements are extremely sensitive to temperature fluctuations, a technique for separating the temperature fluctuations from the velocity (Re) fluctuations is needed. The electrical power supplied to a hot wire can be written as [Oldfield, 1978: 747]

$$P = C(R - R_0)Re^{0.5} \tag{2.36}$$

where R is the resistance of the constant temperature hot wire, R_0 is the hot wire resistance at the flow stagnation temperature T_t and C is a constant. Differentiate (2.36) logarithmically and keeping R constant for a constant temperature hot wire gives:

$$\ln P = \ln C + \ln (R - R_0) + 0.5 \ln Re \tag{2.37}$$

$$d\left(\ln(R - R_0)\right) = \frac{d(R-R_0)}{R - R_0} = \frac{-dR_0}{R - R_0} \tag{2.38}$$

$$dP/P = \frac{-R_0}{R - R_0}\frac{dR_0}{R_0} + 0.5\, dRe/Re \tag{2.39}$$

Define the hot wire overheat parameter, x as

$$x \equiv \frac{R_0}{R - R_0} \tag{2.40}$$

Re-write (2.37) to get

$$dP/_P = -x \frac{dR_0}{R_0} + 0.5\, dRe/_{Re} \qquad (2.41)$$

Square both sides and average,

$$\overline{\left(\frac{dP}{P}\right)^2} = \overline{\left(\frac{1}{2} \frac{dRe}{Re} - x \frac{dR_0}{R_0} \right)^2} \qquad (2.42)$$

$$\frac{\overline{dP^2}}{\overline{P^2}} = \frac{1}{4} \frac{\overline{dRe^2}}{\overline{Re^2}} - x \frac{\overline{dR_0\, dRe}}{\overline{R_0}\ \overline{Re}} + x^2 \frac{\overline{dR_0^2}}{\overline{R_0^2}} \qquad (2.43)$$

Let

$$c \equiv \frac{\overline{dR_0^2}}{\overline{R_0^2}} \qquad (2.44)$$

$$b \equiv - \frac{\overline{dR_0\, dRe}}{\overline{R_0}\ \overline{Re}} \qquad (2.45)$$

$$a \equiv \frac{1}{4} \frac{\overline{dRe^2}}{\overline{Re^2}} \qquad (2.46)$$

Substitute (2.44), (2.45) and (2.46) into (2.43) to get

$$\frac{\overline{dP^2}}{\overline{P^2}} = a + bx + cx^2 \qquad (2.47)$$

The power can be related to the hot wire bridge voltage, since

$$P = V^2/_R$$

$$dP = 2VdV/_R$$

$$\frac{dP^2}{P^2} = \frac{4V^2 dV^2/R^2}{V^4/R^2}$$

So,
$$\frac{\overline{dP^2}}{\overline{P^2}} = 4\,\frac{\overline{dV^2}}{\overline{V^2}} \qquad (2.48)$$

and

$$4\,\frac{\overline{dV^2}}{\overline{V^2}} = a + bx + cx^2 \qquad (2.49)$$

Equation (2.49) is quadratic in x, the hot wire overheat parameter. The turbulence level can be obtained by fitting a least squares second order curve fit to the hot wire bridge voltage as a function of the overheat parameter. The turbulence level is related to the curve fit coefficients as follows [Oldfield, 1978: 747]:

Reynolds turbulence level (the same as velocity turbulence level at low Mach numbers)

$$\sqrt{\overline{dRe^2}/\overline{Re^2}} = 2\sqrt{a} \qquad (2.50)$$

Flow temperature variation

$$\sqrt{\overline{dT_t^2}/\overline{T_t^2}} = \sqrt{\overline{dR_0^2}/\overline{R_0^2}}\;\frac{R_0}{\alpha_{20}R_{20}T_t} = \sqrt{c}\;\frac{R_0}{\alpha_{20}R_{20}T_t} \qquad (2.51)$$

Correlation coefficient

$$\frac{\overline{dR_0\,dRe}}{\sqrt{\overline{dR_0^2}\;\overline{dRe^2}}} = -\frac{b}{2\sqrt{ac}} \qquad (2.52)$$

Fast Fourier Transform

The Fourier Transform (FT) is a method for determining the frequency components of a signal. The Fast Fourier Transform (FFT) is an algorithm which performs the FT quickly. Such an algorithm is given in Chapter 12 of the Numerical Recipes text [Press, 1986]. The algorithms described in Chapter 12, REALFT and FOUR1, were adapted from FORTRAN source code to QuickBASIC and were used extensively in this study to examine signal frequency components and for digital filtering.

Experimental Apparatus

Shock Tube

All experiments were performed in the AFIT low pressure shock tube. This shock tube has four main parts, the driver section, the driven section, the test section and the dump tank chamber. A schematic of the shock tube used is given in Figure 3.1. Mylar diaphragms were used to separate the driver and driven sections. Three diaphragm thicknesses were used, 2 mil (0.002") diaphragms for weak shocks, 5 and 7 mil diaphragms for stronger shocks. The laboratory air supply was used to pressurize the driver section, with a maximum pressure of 120" Hg gauge. Ambient pressure was used in the driven section, P_1, for each experiment. The diaphragm was ruptured using a pneumatic plunger.

Pressure Transducers. Two Endevco model 8530A-100 pressure transducers were flush mounted in the top wall of the shock tube. These transducers measure absolute pressure and produce approximately 3 mV per PSI. The forward transducer was located 46.5 inches upstream of the plate leading edge, the rear transducer was located 18.5 inches upstream of the plate leading edge (see Figure 3.2). The forward transducer was used to trigger the transient recorders and the Schlieren spark source. Neff Type 119 amplifiers were used to increase both the forward and rear pressure transducer sig-

nals. The ten volt transducer excitation voltage was produced using a Power Mate Corporation DC power supply. The pressure transducers were calibrated using the AMETEK Model HK-500 pneumatic dead weight tester, with the Neff amplifiers set for a gain of 10. The calibration results are given in Appendix E.

Instrumented Flat Plate

An instrumented flat plate installed on the test section center line was used for the heat transfer study. The plate was thirty inches long, four inches wide and three-quarters inch thick. The flat plate had a cylindrical leading edge with a row of cooling holes located two inches downstream. Each cooling hole was one milli-meter in diameter. Forty-one cooling holes formed a line parallel with the plate leading edge. The cooling air injection angle is 90° (perpendicular to the flow).

Seven thin film heat flux gauges were mounted in the plate, proportionally spaced downstream of the cooling holes. See Figure 3.2 for the flat plate instrumentation spacing. The thin film gauges made of a platinum film 0.5 mm wide, 0.1 μm thick, deposited on a pyrex 7740 substrate. For 7740 pyrex,

$$\sqrt{\rho\ C_p\ k} = 1388.84\ \frac{J}{sec^{0.5}m^2K},$$

taken from the Thermo-physical Properties of Matter refer-

ence text. The thin film gauges were calibrated for amplifier output voltage as a function of temperature. The slope of the calibration curves give the $V_0\alpha$ term used in Equation 2.35. The calibration procedure and results are given in Appendix D.

Each heat flux gauge was placed in a Wheatstone bridge configuration using the PSC 8115 Bridge Supply Module. The heat flux signals were amplified, with a gain of 1000, and filtered with a 10 kHz Low Pass Filter to improve the signal to noise ratio. The filter and amplification were provided by the PSC 8015-1 Programmable DC amplifiers.

Heat Transfer Analog

The overall circuit design is depicted in Figure 2.2. The circuit consists of constant current source, an AD524 Instrumentation amplifier and the R-C analog. The PSC 8015-1 output voltage provides the analog input. The analog output is taken across resistor R_1 (see Figure 3.3), then amplified using the AD524. The AD524 output is then fed into the transient recorder (DL1200).

Constructing the Heat Transfer Analog. The heat flux analog was modeled after that developed by Oldfield [1984: 252]. The design operating range of the Oldfield analog is 0.02 Hz to 100 kHz. The analog built here does not incorporate all of the Oldfield components. The current to voltage conver-

ter and 100 kHz low pass filter are not incorporated into the analog designed here. These differences will reduce the bandwidth, or working range, of the heat flux gauge. However, an AD524 Instrumentation Amplifier is used in place of the LF357 operational amplifier. The AD524 has a much better frequency response than the LF357 and has built-in gain settings of 1, 10, 100 and 1000. This will offset, somewhat, the omission of the current to voltage converter in terms of working frequency range.

Resistor and Capacitor Selection. Oldfield [1984: 247] gives a method where low tolerance capacitors may be used in conjunction with higher tolerance resistors to build the R-C network. Standard size (22, 47, 100 etc) low tolerance (5%) polyester film capacitors are used. These capacitors are relatively inexpensive and readily available. Once the capacitors are purchased, the value of each capacitor is measured. The resistor values are then chosen using [Oldfield, 1984: 250]

$$\gamma_i = C_i/C_{i-1} \qquad i = 1...9 \qquad (3.1)$$

$$R_1 = \frac{r}{c}\frac{C_1}{1 + \sqrt{\gamma_2}} \qquad (3.2)$$

$$R_i = \frac{r}{c}\frac{C_i}{\sqrt{\gamma_i}} \qquad i = 2...9 \qquad (3.3)$$

Given R_i is made up of two resistors. The first resistor is

chosen as the largest standard size smaller than the desired value. The value of the first resistor is measured (to within 0.5%) and a smaller resistor is chosen so that the combination is within 1% of the desired value. The value r/c is determined by the working frequency range [Oldfield, 1984: 249-250]. For the analog designed here,

$$\frac{r}{c} = 1.9 \times 10^{10}$$

The capacitor and corresponding resistor values used for the seven circuits built in this study are given in Tables 3.1 to 3.7.

All components were purchased from local vendors using Impress funds. Two types of capacitors were purchased, polyester film and electrolytic. The electrolytic capacitors were used because polyester film capacitors were not available in the required sizes. All capacitors were purchased from

MCM Electronics
2582 East River Rd
Moraine, Ohio 45439
(513) 434-0031

The resistors used were precision (0.1%) wire wound resistors and carbon film resistors (5%). The wire wound resistors were purchased at

Rixan Associates
5062 Wadsworth
Dayton, Ohio 45424

The wire wound resistors were counter-wound on two spools to reduce inductance problems. It was felt that the wire wound

resistors may have too much inductance, creating noise problems, but this has not been observed. The precision wire wound resistors were very expensive (about $3.00 each), compared to the carbon film resistors ($0.35 for a package of ten). Many of the carbon film resistors were within 2% tolerance. Looking back, it would have much cheaper, and just as easy, to have used all carbon film resistors, since two resistors were used in series to form a non-standard resistor size for each resistor-capacitor lump.

The AD524 Instrumentation Amplifiers were available in-house and did not have to be purchased. The AD524 amplifiers had pre-set gain settings of 1, 10, 100 and 1000. Other gain settings could be achieved using an external resistor across two of the AD524. Using this procedure (see Figure 3.5 and AD524 documentation), the amplifier was configured for a gain of 300 using an external 200 Ohm resistor.

Having selected the components and circuit design, the next stage was to build a printed circuit (PC) board on which to assemble the components. The PC board design was first laid out on a mylar grid in 2 to 1 proportions (the artwork was twice the size of the actual circuit). This was accomplished using colored black tape specifically designed for circuit artwork. Orville Wright, of the Electrical Engineering department, was good enough to pre-view the art-

work to check for technical errors. Once the artwork was completed, it was taken to building 5, along with a work order from Jack Tiffany of the AFIT shop, so that the PC boards could be made. Building 5 personnel reduced the artwork and deposited a copper circuit (where the black tape had been) on a ceramic (composite) board. Eight of these PC boards were produced, seven of which were used. Once the boards were obtained from building 5, component mounting holes were drilled using Orville Wright's miniature drill press. The components were then soldered to the PC board by Tim Major, an technician for the department, and the analog complete.

Since a separate analog was used for each heat flux channel (seven in all), a box was designed to contain the seven circuits, providing a common power supply and BNC input and output connections. The analog container was built out of $\frac{1}{8}$" thick plexy glass and designed so that each board could be removed separately. The analog container and connections are shown in Figure 4.1.

Table 3.1: Resistor-Capacitor Values for Circuit 31-105

Circuit Number: 31-105	
Capacitance (μf)	Resistance (Ohm)
0.02184	100 + 70 = 170
0.04659	600 + 10 = 610
0.1012	1k + 300 = 1.3k
0.2276	2k + 900 = 2.9k
0.4571	3k + 3.3k = 6.3k
1.083	10k + 3.6k = 13.6k
2.272	20k + 9k = 2.9k
4.720	60k + 3k = 63k
10.54	100k + 36k = 136k

Table 3.2: Resistor-Capacitor Values for Circuit 31-790

Circuit Number: 31-790	
Capacitance (μf)	Resistance (Ohm)
0.02186	100 + 70 = 170
0.04671	600 + 10 = 610
0.1021	1k + 300 = 1.3k
0.2265	2k + 900 = 2.9k
0.4901	6k + 100 = 6.1k
1.024	10 + 3.3k = 13.3k
2.301	30k
4.682	60 + 2k = 62k
11.12	100 + 33k = 133k

Table 3.3: Resistor-Capacitor Values for Circuit 31-820

Circuit Number: 31-820	
Capacitance (μf)	Resistance (Ohm)
0.02175	100 + 70 = 170
0.04625	510 + 90 = 600
0.1005	1.3k
0.2241	2.5k + 350 = 2.85k
0.4700	6k + 200 = 6.2k
1.092	10k + 3.6k = 13.6k
2.325	30k + 200 = 30.2k
4.865	60k + 4k = 64k
10.57	100k + 36k = 136k

Table 3.4: Resistor-Capacitor Values for Circuit 31-850

Circuit Number: 31-850	
Capacitance (μf)	Resistance (Ohm)
0.02195	100 + 70 = 170
0.04764	600
0.1044	1k + 300 = 1.3k
0.2211	2k + 900 = 2.9k
0.4851	6k + 200 = 6.2k
1.040	10k + 3.6k = 13.6k
2.299	20k + 9.1k = 29.1k
4 782	60k + 3k = 63k
10.21	100k + 33k = 133k

Table 3.5: Resistor-Capacitor Values for Circuit 31-870

Circuit Number: 31-870	
Capacitance (μf)	Resistance (Ohm)
0.02180	100 + 70 = 170
0.0463	600
0.1010	1k + 300 = 1.3k
0.2290	2k + 900 = 2.9k
0.4563	6k + 120 = 6.12k
1.019	10k + 3k = 13k
2.295	20k + 9k = 29k
4.778	60k + 3k = 63k
11.13	100k + 40k = 140k

Table 3.6: Resistor-Capacitor Values for Circuit 32-100

Circuit Number: 32-100	
Capacitance (μf)	Resistance (Ohm)
0.02187	100 + 70 = 170
0.04596	600
0.1017	1k + 300 = 1.3k
0.2312	2k + 900 = 2.9k
0.4931	6k + 400 = 6.4k
1.006	10k + 3.3k = 13.3k
2.272	20k + 9K = 29k
4.640	60k + 2k = 62K
10.56	100k + 33k = 133k

Table 3.7: Resistor-Capacitor Values for Circuit 32-200

Circuit Number: 32-200	
Capacitance (μf)	Resistance (Ohm)
0.02162	100 + 70 = 170
0.04636	511 + 90 = 601
0.1049	1.3k + 10 = 1.31k
0.2335	2.01k + 920 = 2.93k
0.4767	3k + 3.29k = 6.33k
1.080	13k + 509 =13.51k
2.333	30k + 100 = 30.1k
4.740	60k + 3.28k =63.28k
10.61	98.6k + 36.4k = 135k

Calibrating the Heat Transfer Analog. Each circuit used for heat flux measurement was calibrated. The calibration procedure is to determine

$$R_1 G \sqrt{\frac{C}{r}}$$

which is used in equation (2.35) to obtain the heat flux. Re-writing equation (2.27) yields

$$\frac{\bar{I}}{\bar{V}} = \sqrt{\frac{C}{r}}\ \sqrt{s}$$

or, in the frequency domain

$$\frac{i}{V} = \sqrt{\frac{C}{r}}\ \sqrt{\omega} \qquad (3.4)$$

where ω is the frequency (radians/sec) and $V=V_{in}$, the analog input voltage. Recall (2.33)

$$i = \frac{V_{out}}{R_1 G}$$

So,

$$\frac{V_{out}}{V_{in}} = GR_1 \sqrt{\frac{C}{r}}\ \sqrt{\omega} \qquad (3.5)$$

The goal of the calibration procedure is to find

$$GR_1 \sqrt{\frac{C}{r}}$$

The calibration is performed by connecting a frequency generator to the input of the analog. The RMS voltage input and output values are recorded for various frequencies and the ratio V_{out}/V_{in} is plotted as a function of the square root of frequency. This curve will be linear for the working range of the analog. A least squares linear curve fit is performed, where the slope is taken to be

$$m = G\ R_1 \sqrt{\frac{C}{r}} \qquad (3.6)$$

Hence, Equation (2.35) becomes

$$q = \sqrt{\rho\, C_p k}\ \frac{V_{out}}{m V_0 \alpha} \qquad (3.7)$$

Since V_{out}/V_{in} versus $\sqrt{\omega}$ is linear in the working range for the analog, points are chosen so that the curve fit yields a correlation of 0.999. Points of increasing frequency are included in the calibration until the correlation falls below 0.999. The calibration results for each circuit are given in Table 3.8 and Figures 3.6 to 3.12.

Circuit	Slope	Standard Deviation	Correlation
31-105	0.74371	1.928	0.99945
31-790	0.78699	1.957	0.99942
31-820	0.73212	1.670	0.99958
31-850	0.73852	2.000	0.99941
31-870	0.79757	1.248	0.99955
32-100	0.73695	2.018	0.99939
32-200	0.70370	2.149	0.99927

Table 3.8: Calibration of the Heat Flux Circuits

Free-Stream Turbulence Generator

Free-stream turbulence is generated with flow injection 2.5 inches upstream of the flat plate leading edge. High pressure air is injected perpendicular to the flow at twelve locations (4 on each side wall, 2 each top and bottom). A diagram of the turbulence injector is given in Figure 3.13.

Hot Wire Anemometer

A TSI model 1054A constant temperature hot wire anemometer provided the hot wire bridge output voltage. The

hot wire sensor used was the TSI 1214-10 thin film hot wire. Other hot wire sensors were explored, including the TSI 1214-TI.5 thin wire and the TSI 1214-20 thin film, but neither were as suitable as the TSI 1214-10. The 1214-TI.5 had poor vibration characteristics (when hit with a shock wave) and the 1214-20 was slower to respond (did not reach full voltage in a short enough time) than the 1214-10.

The hot-wire was placed in the shock tube using two configurations (See Figure 3.14). Configuration 1 proved to be inappropriate because the hot wire supports would vibrate after shock passage, destroying the data integrity. These vibrations were reduced by using configuration 2, so configuration 2 was used for all hot wire measurements.

Thermocouple

A K-type (Chromel-Alumel) thin foil thermocouple was used in conjunction with a battery powered ice point (OMEGA, Model MCP) to measure the flow temperature behind the normal shock. The thermocouple signal was amplified using an AD524 Instrumentation amplifier with a gain setting of 100. The thermocouple probe was at the same location as the hot-wire probe (see Figure 3.14).

Flow Visualization

Schlieren flow visualization was used to obtain photographs of the shock patterns and boundary layer behind the

normal shock. The spark source was triggered using a delayed pressure signal from the forward pressure transducer. The delay was produced using the Cordin model 453 Time Delay Generator. The images were captured on two types of film, Polaroid Type 47 (ASA 3000) and Polaroid Type 42 (ASA 200). The Type 47 film gave better contrast, however the lower speed film had a smaller grain size and produced slightly cleaner pictures. The spark lamp and mirror configuration are depicted in Figure 3.15.

DataLab Transient Recorder

The DataLab DL1200 transient recorder was used to acquire all test data. The DL1200 has 8 channels, each channel with its own analog to digital (AD) converter. The recorder was used in the 8 channel mode, allowing for 4096 samples to be collected for each channel. The sample interval, time between samples, can be varied from 2 μsec to 20 msec. Each channel has its own gain settings, which were normally set to different levels depending on which parameter was being measured on a given channel. The recorder can be triggered using one of the eight data channels (an internal trigger) or from an external trigger.

Data Collection and Reduction

All transient experimental data was recorded using the DataLab DL1200 recorder. A Zenith Z-248, which had been modified using the 386 upgrade kit, was connected to the DL1200 via an IEEE-488 parallel interface card. The data was recorded on the DL1200 then transferred to the Z-248 for analysis. The DL1200 was normally set for a 2 μsec sample interval, using the forward pressure transducer as the trigger source. A 5% pre-delay (5%, or 204, of the 4096 samples were acquired prior to the trigger) was used so that an accurate measurement of shock speed could be obtained. Two software programs were developed during the course of the study, NEWDL and POST, both written using QuickBasic 4.5. The NEWDL software package was used to interface between the Z-248 and the DL1200. Post processing and data analysis were performed using the POST software package. The instrumentation/hardware interface is depicted in Figure 4.1.

Shock Mach Number. The shock Mach number was measured on each heat transfer run. The time of shock passage at each sensor location (2 pressure and 4 heat flux gauges) was determined by close examination of the respective voltage signals. Since the distance between transducers is known, the shock speed is given by

$$U_s = \frac{\Delta x}{\Delta t}$$

where Δx is the distance between sensors and Δt is the time for the shock to travel Δx. A shock speed was calculated between the forward and rear pressure transducers and between the forward pressure sensor and each of the heat flux gauges. These five shock speeds were averaged and the shock Mach number computed using the ambient air temperature by

$$M_s = \frac{U_s}{\sqrt{\gamma R_{air} T_1}}$$

where $R_{air} = 287 \frac{J}{g^\circ C}$. The five Mach numbers did not differ by much, typically only in the third or fourth significant digit.

Heat Transfer

The heat transfer analog output voltages were recorded directly at the time of the experiment using the heat transfer analog. A different analog circuit was used for each heat flux channel recorded. Figure 4.1 depicts how the analogs were connected during testing. After testing, the analog output voltages were multiplied by the calibration constant (see equation 3.6) for the respective heat flux circuit to obtain heat flux.

Turbulence Intensity

The turbulence level, or intensity, was determined by making several tests at the same driver pressure but with

different values of the hot wire overheat parameter. For each of these runs, the mean and RMS values of the hot wire bridge voltage were calculated. The RMS voltage level divided by the mean voltage level ($4V^2_{rms}/V^2_{mean}$) was then plotted as a function of the hot wire overheat parameter, x. A least squares quadratic curve fit was performed, giving the turbulence intensity by equation (2.50). A problem was encountered when the hot wire measurements were performed using configuration 1 (See Figure 3.4). The hot wire prongs would vibrate after being hit by the initial shock wave, producing an erroneous hot wire signal. This phenomenon has been seen on other theses as well. McQueen [1984] performed a hot wire study in the AFIT high pressure shock tube. McQueen concluded that the natural frequency of the hot wire support for the TSI 1214-10 thin film probe was 22.134 kHz. The hot wire bridge output voltage for a typical run using configuration 1 is shown in Figure 4.3. An FFT was performed on this data, the results of which are shown in Figure 4.4. There is a pronounced spike in the FFT at 20 kHz, which would presumably be due to the vibration of the hot wire probe supports. A similar run was performed using hot wire configuration 2 (see Figure 3.4). The probe vibrations were reduced, but there were still significant spikes above 10 kHz (see Figures 4.4 and 4.5). Also, these frequency spikes were more pronounced when the TSI 1214-10 thin

film hot-wire probe was used (compared to the 1214-20), and more pronounced at higher shock speeds. To diminish the amplitude of the frequency components above 10 kHz, all hot wire data used for turbulence measurement was digitally filtered using an algorithm in the POST software package. This algorithm performs an FFT on the given data then displays the FFT so the user may select a band of frequency components. The magnitude of all frequency components outside this window is set equal to 0. An inverse FFT is then performed on the remaining frequency components to re-create the original signal, minus the discarded frequencies. Figures 4.7 and 4.9 show time domain data before and after the filtering process, Figures 4.8 and 4.10 show frequency data before and after filtering.

Overheat Parameter. Recall the definition of the hot-wire overheat parameter (2.40)

$$x \equiv \frac{R_0}{R - R_0}$$

Where R_0 is the hot-wire resistance at the gas stagnation temperature and R is the wire resistance set by the constant-temperature anemometer. When the probe is connected to the hot-wire anemometer, the wire resistance is set by dialing in the decade box resistance. The decade resistance, R_{decade}, is related to the hot-wire resistance by

$$R_{decade} = R_{int} + R \qquad (4.1)$$

Where R_{int} is the internal resistance of the probe configuration due to the probe internal resistance, the probe support resistance and the elbow resistance (see Figure 3.5). R_{int} = 0.38 Ohm for the hot-wire probe and supports used in these experiments (R_{elbow} = 0.09 Ohm, R_{probe} = 0.14 Ohm and $R_{support}$ = 0.15 Ohm).

Shock Mach Number

A theoretical shock Mach number, based on P_4/P_1, was used to calculate the theoretical heat transfer early in the data analysis. Upon further examination it became apparent that this procedure was not accurate enough. The shock Mach number can very as much as ten percent from the theoretical value. Table 5.1 gives the results of the shock

Table 5.1: Measured and Theoretical Shock Mach Numbers

Run Number	P_4	Diaghram Thickness (mil)	Measured M_s	Theoretical M_s
r040	50	2	1.2096	1.2370
r041	100	7	1.2926	1.3688
r043	115	7	1.3343	1.4007
r044	115	7	1.3262	1.4007
r054	100	7	1.3023	1.3697
r057	90	7	1.2730	1.3477
r059	70	7	1.1829	1.2975
r060	60	2	1.2377	1.2691
r061	90	7	1.2766	1.3477
r063	70	7	1.1999	1.2975
r064	60	2	1.2366	1.2691
r080	100	5	1.3196	1.3675
r102	70	3	1.2562	1.2958
r103	80	4	1.2762	1.3218
r104	115	5	1.3448	1.3990
r105	120	7	1.3407	1.4087
Average Error: 4.9%				
Standard Deviation: 2.0%				

speed calculations. The largest error occurred when the thick (7 mil) diaphragm was used at the low (70" Hg gauge) driver pressures. However, the average deviation from the theoretical value is five percent, with a standard deviation

of two percent. Since all fluid properties are determined by the shock speed, the shock Mach number was measured on all heat transfer runs. The shock speed was not measured on the runs taken to measure turbulence intensity. Table 5.2 gives an example of the effect of Mach number error on Stanton number.

Table 5.2: Effect of shock Mach number error on Heat Transfer Solution

P_1 = 29.00" Hg, T_1 = 20 °C				
	P_2 ("Hg)	T_2 (°C)	U_2 (m/sec)	St (gauge 1)
M_s = 1.2500	48.03	66.7	128.7	0.00232
M_s = 1.3125	53.45	78.24	157.4	0.00221

Flow Characteristics

Diaphragm Burst Characteristics. The mylar diaphragm burst characteristics are not well understood when thick diaphragms (7 mil) are used at low driver pressures (50" Hg gauge). On the runs performed using these conditions, the pressure and hot-wire sensors exhibited an isentropic rise in pressure and velocity (or temperature) prior to shock passage. These pressure and velocity gradients could affect the gas properties, shock Mach number and turbulence intensity. These conditions, low driver pressure with thick diaphragms, were not examined during this study.

Flow Characteristics: Schlieren Photography. Flow char-

acteristics were measured qualitatively with the use of Schlieren photography. The shock pattern over the flat plate is quite complicated as shown by Figure 5.1. The pictures in Figure 5.1 place the shock in different locations along the plate. Photographs were taken with and without turbulence injection (10% and 12% turbulence intensity, respectively) and with and without the film cooling holes covered. These different configurations, for the most part, did not noticeably change the shock structure over the plate. However on some runs where turbulence injection was used the shock below the plate appears to be ahead of the shock on top of the plate (see Figure 5.1(a) and 5.1(b).

Flow Properties: Temperature and Pressure. The flow properties (temperature, pressure and velocity) behind the normal shock determine the heat transfer solution. If there are errors in these fluid properties, then a certain amount of error will be present in the heat transfer. The normal shock relationships for temperature and pressure can be verified by measuring the flow temperature and pressure behind the shock wave. If the measured temperature and pressure agree favorably with the theoretical values then this will lend some confidence in the temperature difference to the flat plate and the fluid velocity (via the static pressure).

All theoretical properties (temperature, pressure and velocity) were determined using the normal shock relations for a normal shock having the measured shock speed, and the

measured ambient conditions prior to shock passage. The equations for these relationships are given in Appendix A.

The measured and theoretical (equation A.1 multiplied by the measured P_1) pressures behind the normal shock are plotted in Figure 5.2. As indicated, the theoretical and measured pressure agree quite well for the first 4 milliseconds after shock passage. This indicates the useful test time to be approximately 4 milliseconds. After 4 msec, the pressure begins to drop dramatically, signaling the passage of an expansion wave.

The temperature behind the shock could not be so easily measured. The rise time of the K-type thermocouple used is on the order of milliseconds. The thermocouple could not reach the temperature of the flow before the flow temperature changed. To circumvent this problem, the thermocouple trace was curve fit to match the response of a first order system to a step input. The equation to be solved for the curve fit is

$$\frac{V_g - V_j(t)}{V_g - V_j(0)} = e^{-t/\tau} \qquad (5.1)$$

Where,

V_g = thermocouple output voltage at the gas temperature

$V_j(t)$ = thermocouple output as a function of time

τ = thermocouple time constant

A least squares method is used to perform the curve fit.

Define

$$\varepsilon_i \equiv \left(V_g - V_j(t_i)\right) - \left(V_g - V_j(0)\right) e^{-t_i/\tau} \qquad (5.2)$$

The "best" curve that fits the given data is the one given by the V_g and τ which minimize

$$\varepsilon^2_{sum} = \sum_{i=1}^{N} \varepsilon_i^2 \ , \qquad (5.3)$$

where N is the number of data points and ε_i is computed using the i^{th} data point for a given V_g and τ. The minimum curve fit error as a function of τ is plotted in Figure 5.3. Each point on the curve represents the optimum τ for a given V_g. The minimum of the curve represents the optimum τ-V_g combination. This optimum combination is:

$$\tau = 9.9 \text{ msec}$$

$$V_g = 325 \text{ mV}$$

The gas temperature corresponding to a thermocouple voltage of 325 mV is determined by using the reference table for a K type thermocouple (pg T-42 of the OMEGA reference catalog) and recalling that the thermocouple amplifier was set for a gain of 100. The measured gas temperature is 80 °C which agrees with the theoretical temperature of 76 °C, determined using:

$$M_s = 1.30$$
$$P_1 = 29.0\text{" Hg}$$

$$T_1 = 20\ ^{\circ}\text{C}$$

and equation (A.2). The first order curve fit, measured thermocouple voltages and thermocouple voltage corresponding

to the theoretical temperature behind the shock are plotted on Figure 5.4.

Turbulence Intensity

The turbulence levels encountered in the shock tube were measured. The background turbulence level was found to be 10%. The turbulence level increased only slightly, to 12%, when the turbulence injector was used. Both turbulence measurements were performed using a driver pressure of 100" Hg gauge. Table 5.3 gives the run numbers and hot-wire

Table 5.3: Run numbers and Hot-wire resistance values for turbulence level calulations

Background Turbulence		Turbulence Injection	
Run Number	R_{decade}(Ohm)	Run Number	R_{decade}(Ohm)
r045	8.25	r085	8.25
r046	8.10	r086	8.15
r047	7.95	r087	8.05
r048	7.80	r088	7.95
r049	7.65	r089	7.85
r050	7.50	r090	7.75
r051	7.35	r091	7.65
r052	7.20	r093	7.45
r053	7.05	r094	7.35
r054	6.90	r095	7.20
r055	6.75	r096	7.05

resistance values for both the background turbulence and turbulence injection experiments. The TSI 1214-10 thin film hot-wire probe was used for both measurements. The hot-wire data was digitally filtered, using the POST computer program,

to remove the 20 KHz frequency spike from each run.

Table 5.4 gives the curve fit parameters for both the no turbulence and turbulence injection measurements. The turbulence levels are given in Table 5.5. The curve fit for the case of no turbulence injection is plotted on Figure 5.5, the curve fit for the case with turbulence injection is plotted on Figure 5.7. The accompanying plots, Figures 5.6 and

Table 5.4: Turbulence Curve Fit Coefficients

	a	b	c
Background Turbulence	0.2304×10^{-2}	$-.9991 \times 10^{-3}$	0.1334×10^{-3}
Turbulence Injection	0.3569×10^{-2}	$-.9477 \times 10^{-3}$	0.9756×10^{-4}

Table 5.5: Measured Turbulence Intensities

	Reynolds	Temperature	Correlation
Background Turbulence	9.60 %	5.54 %	0.90
Turbulence Injection	11.95 %	4.65 %	0.80

5.8, gives the mean hot-wire power output as a function of decade resistance. The linearity of Figures 5.6 and 5.8 lends confidence to the turbulence calculations, since the hot-wire power output was assumed to be a linear function of hot-wire resistance (equation 2.36). The results of the least squares analysis for Figures 5.6 and 5.8 are given in

Table 5.6.

Table 5.6: Least Squares Curve Fit for Hot-Wire Power Output as a Function of Decade Resistance

	Slope	Standard Deviation	Correlation
Background Turbulence	10.87	0.0367	0.99293
Turbulence Injection	12.87	0.0561	0.99179

Heat Transfer

Heat Flux Measurements. Typical temperature and the corresponding heat flux as a function of time are shown in Figures 5.9 to 5.12. Figures 5.9 and 5.10 were from runs with only background turbulence, Figures 5.11 and 5.12 were taken from runs where turbulence injection was used. Cross plots were made of heat flux as a function of thin film gauge temperature to confirm that the heat flux was relatively constant over the test duration. The cross plots are presented in Figures 5.13 and 5.14. These plots indicate that the heat flux is fairly constant with thin film temperature. If the cross plots did not show constant heat flux, then the heat flux for an isothermal flat plate would have to be extrapolated to the heat flux corresponding to t=0, since that would be the only time for which the plate could be considered isothermal.

To reduce the data from the heat flux time histories to something more manageable, the average heat flux was computed over the usable test time. The usable test time was typically taken as 4 to 8 milliseconds, depending on the gauge location and the heat transfer characteristics (spikes were avoided). The usable test time for run r043 was 4 to 5 msec (gauge #4, Figure 5.9) and 4 to 6 msec (gauge #4, Figure 5.11) for run r044. Once mean heat flux was determined, the Stanton number could be calculated using

$$St_{th} = \frac{q_{th}}{(\rho C_p U_\infty)_{th}} \qquad (5.5)$$

$$St = \frac{q}{(\rho C_p U_\infty)_{th}} \qquad (5.6)$$

Combining (5.5) and (5.6) yields

$$St = St_{th}\, {}^{q}/_{q_{th}} \qquad (5.7)$$

Where St_{th} and q_{th} are theoretical values (based on the fluid properties obtained using the measured shock Mach number and equations 2.2 and 2.17) and q is the measured (mean) heat flux (equation 3.6). Nusselt number and convective heat transfer coefficient were computed in a similar manner. Data summaries for each run are given in Appendix E.

When the first heat transfer measurements were performed, the measured heat flux was much higher than what theory predicted, much higher even than the theoretical values for 10% free-stream turbulence. After much delibera-

tion it was realized that the film cooling holes were just upstream of the heat transfer gauges and ingesting air during the run. The heat flux discrepancy was most noticeable on the first heat flux gauge, the one closest to the film cooling holes.

For this study, film cooling was not being investigated and hence the film cooling holes and supply lines were not pressurized during testing. This would cause a pressure gradient between the air behind the shock and that in the film cooling network. This pressure gradient would tend to bleed off the boundary layer just upstream of the first heat flux gauge. The warmer boundary layer would then generate high heat flux, with the cooler boundary layer having been sucked away.

On a following run the cooling holes were covered with black electrical tape (the electrical tape being stronger and easier to apply and remove than cellophane tape). The measured heat flux with the holes covered was greatly reduced and fell more in line with the predicted values.

The theoretical Stanton numbers, with no turbulence injection, were plotted as a function of Reynolds number on Figure 5.16. The theoretical curves corresponding to zero free-stream turbulence and 10% free-stream turbulence are plotted for comparison. A Prandtl number of 0.7 was used for theoretical calculations. The measured Stanton numbers group about the line corresponding to 10% free-stream turbulence.

This agrees with the calculated free-stream turbulence of 9.60%. The 10% turbulence line was calculated using the correlation to Simonich and Bradshaw [1978: 676].

$$\frac{St}{St_o} = 1 + 5\ T \qquad (5.6)$$

Where St_o is the zero turbulence Stanton number (equation 2.17) and Tu is the turbulence intensity (in %/100).

There is some scatter in the data, both in Reynolds number and gauge location. The Reynolds number scatter may be due to the shock Mach number variations (which determine the flow properties and possibly the turbulence level). The scatter due to gauge location (relative to the 10% turbulence line) may be due to the variance among heat flux gauge substrate properties. Close examination of Figure 5.15 reveals that there is a correlation between heat flux gauges. Each symbol set on these two figures correspond to a different run. The first symbol (corresponding to the lowest Re_x for each run) corresponds to the first heat flux gauge, the second symbol (of a given set) to the second operative heat flux gauge (gauge 4), and so on. Data from the first heat flux gauges tend to group together as does data the fourth, sixth and seventh gauges. This phenomena suggests that there is some difference between the heat flux gauges, possibly different substrate $\rho C_p k$ values, or different turbulence levels at different locations along the plate.

The temperature uncertainty (≈3%) will move the heat

flux curve up or down but will not reduce the scatter, unless there is an axial temperature gradient.

The measured Stanton numbers, with turbulence injection, are plotted on Figure 5.17. The theoretical curves corresponding to zero free-stream turbulence (Equation 2.17) and 12% free-stream turbulence (Equations 2.17 and 5.6) are plotted for comparison. A Prandtl number of 0.7 was used for the theoretical calculations. The measured Stanton numbers group about the line corresponding to 12% free-stream turbulence. This agrees with the calculated free-stream turbulence of 11.95%. The 12% turbulence line was calculated using the Simonich-Bradshaw correlation.

Blair [1983] performed a study to measure the effect of free-stream turbulence on heat transfer through a turbulent boundary layer. Blair considered $St/St_o\big|_{Re_\theta}$ (Stanton number ratio for constant Reynolds number based on momentum thickness) to be a function of turbulence intensity. Figure 5.18 shows $St/St_o\big|_{Re_\theta}$ as a function of Tu, with Blair's data, the Simonich-Bradshaw correlation (Equation 5.6) and the present data. Blair's investigation was performed with much lower turbulence levels than this study. Blair's data indicates a non-linear heat transfer-turbulence correlation at the higher turbulence levels, as opposed to the linear Simonich-Bradshaw correlation (Equation 5.6). The present data, however, does correspond well to (5.6).

From Schlichting [1979: 638] the momentum Reynolds

number is related to Re_x by

$$\theta/_x = 0.036\ Re_x^{-0.2} \qquad (5.7)$$

So,

$$Re_\theta = 0.036\ Re_x^{0.8} \qquad (5.8)$$

Hence, constant Re_x implies constant Re_θ, assuming the turbulence intensity does not affect Re_θ.

Heat Flux Analog. The heat flux analog appears to have work as designed. The linear V_{out}/V_{in} versus $\sqrt{\omega}$ calibration curves indicate the working range of the analog to be the designed bandwidth of 0.1 Hz to 100 kHz. The heat flux measurements are consistent with what has been done in the past (as far as magnitude) in this shock tube (the AFIT low pressure shock tube). Also, the heat flux measurements correlate with the turbulence levels according to the correlations of Blair [1983] and Simonich [1978], although only marginally so with Blair's results.

Conclusions and Recommendations

Conclusions

Heat Transfer and Heat Flux Analog.

1. The heat flux analog designed for this study performed as predicted. The calibration curves match the theoretical relation

$$\frac{V_{out}}{V_{in}} = (\text{constant})\ \sqrt{\omega}$$

2. The measured heat flux matches the theoretical values (Eqn. 2.17) when adjusted for the free-stream turbulence levels using the Simonich-Bradshaw correlation (Eqn. 5.6).

Turbulence Level.

1. The background free-stream turbulence in the shock tube is high, on the order of 10%.

2. The turbulence injection does increase the free-stream turbulence level, although only marginally (by 2%)

3. The reason for using the constant temperature hot-wire method, to separate velocity and temperature fluctuations, is justified since significant temperature fluctuations (5%) were measured.

4. The constant temperature hot-wire procedure for calculating turbulence level works, although care must be taken in reducing the data due to the vibrations of the hot-wire support prongs and possibly the hot-wire itself. This

claim is supported by the fact that the turbulence calculations and the heat flux measurements, obtained by independent means, compliment one another. The turbulence-heat flux correlation agrees with those of Blair [1983] and Simonich [1978].

Recommendations

1. A calibration was not performed to measure heat flux gauge substrate properties. Some of the scatter in the heat transfer data may be reduced if the substrate properties were known. Such a calibration should be performed if accurate heat flux measurements are desired.

2. A new method for determining heat transfer is now in place (the heat flux analogs). Shock tube heat transfer studies should be performed with more complex flow geometries (turbine blades or cascades) to study the effects in configurations more representative of turbo-machinery.

3. There is some interesting phenomena occurring as the shock passes the flat plate leading edge and as the shock passes the film cooling holes. A new test section should be developed so that the flow around these critical areas can be photographed. The current test section is too far aft of the flat plate leading edge. Also, a high speed camera would aid in the shock pattern determination.

4. The diaphragm burst characteristics are not well understood when thick diaphragms (7 mil) are used at low driver pressures (50" Hg gauge). On the runs performed

using these conditions, the pressure and hot-wire traces exhibited an isentropic rise in pressure and velocity (temperature) prior to shock passage. A study should be performed to characterize the flow around the diaphragm as the diaphragm is ruptured. A high speed camera would aid in this study.

REFERENCES

Ayra, S.P.S. and Plate, E.J. (1969), *Hot-wire Measurements in Non-isothermal Flow*, Instruments and Control Systems, March 1969, pg 87.

Blair, M.F., *Influence of Free-Stream Turbulence on Turbulent Boundary Layer Heat Transfer and Mean Profile Development, Part I - Experimental Data,* ASME Journal of Heat Transfer, Vol 105, No. 1, February 1983.

Blair, M.F., *Influence of Free-Stream Turbulence on Turbulent Boundary Layer Heat Transfer and Mean Profile Development, Part II - Analysis of Results,* ASME Journal of Heat Transfer, Vol 105, No. 1, February 1983.

Bradshaw, P., An Introduction to Turbulence and its Measurement, Pergammon Press, 1971.

Burden, R.L. and Faires, J.D., Numerical Analysis, 3rd Ed., PWS Publishers, 1985.

Carlson, A.B. and Gisser, D.G., Electrical Engineering Concepts and Applications, Addison-Wesley Publishing Company, 1981.

Doebelin, E.O., Measurement Systems Application and Design, McGraw-Hill Book Company, Inc., 1966.

Echert, E.P.G. and Goldstein, B.J., Measurements in Heat Transfer, 2nd Ed., McGraw-Hill Book Company, New York, 1976.

Fillingham, Patrick K., *Flat Plate and Turbine Vane Cascade Heat Transfer Investigation Using a Shock Tube*, Masters Thesis, School of Engineering, Air Force Institute of Technology (AU), Wright-Patterson AFB OH, December 1985.

Frost, W. and Moulden, T., Handbook of Turbulence, Volume 1, Plenum Press, 1977.

Fu-Kang Tsou, S.J. Chen, *Measurement of Heat Transfer rates using a Transient Technology*, ASME, January 1989.

Gaydon, A.G. and Hurle, I.R., The Shock Tube in High Temperature Chemical Physics, Reinhold Publishing Corporation, 1963.

Glass, I.I., *Shock Tubes, Part I: Theory and Performance of Simple Shock Tubes.* Utia Review No. 12, Toronto, Canada: Institute of Aerophysics, University of Toronto, 1959.

Gochenaur, John E., *Investigation of Heat Transfer to a Turbine Cascade using a Shock Tube*, Masters Thesis, School of Engineering, Air Force Institute of Technology (AU), Wright-Patterson AFB OH, December 1984.

Hinze, J.O., Turbulence: An Introduction to its Mechanism McGraw-Hill Book Company, 1959.

Kays, W.H. and Crawford, M.E., Convective Heat and Mass Transfer, McGraw-Hill Book Company, 1980.

Lawson, D.I. and McGruire, J.H., *The Solution of Transient Heat-flow Problems by Analogous Electrical Networks,* Institute of Mechanical Engineers (Great Britian), Vol 167, No. 3, pg. 275-287, 1953.

McQueen, Stephen M., *Velocity and Transient Measurements in a Shock Tube using a Hot-Wire Anemometer*, Masters Thesis, School of Engineering, Air Force Institute of Technology (AU), Wright-Patterson AFB OH, December 1984.

Meyer, R.F., *A Heat Flux Meter for use with Thin Film Surface Thermometers*, NRC Canada, Aero. Rep. LR-279, 1960.

Meyer, R.F., *Further Comments on Analogue Networks to Obtain Heat Flux from Surface Temperature Measurements*, NRC Canada, Aero. Rep. LR-375, 1963.

Mirels, H. *Boundary Layer Behine Shock or Thin Expansion Wave Moving into a Stationary Fluid*, NACA TN 37 12, 1956.

Morkovin, Mark V., *Fluctuations and Hot-wire Anemometry in Compressible Flows,"* AGARDograph 24, November 1956.

Novak, Joseph T., *Investigation of Heat Transfer to a Flat Plate in a Shock Tube,* Masters Thesis, School of Engineering, Air Force Institute of Technology (AU), Wright-Patterson AFB OH, December 1987.

Oldfield, M.L.G., Jones, T.V. and Schultz, D.L., *On Line Computer for Transient Turbine Cascade Instrumentation*, IEEE Transactions on Aerospace and Electronic Systems, Vol AES-14, Number 5, September, 1978.

Oldfield, M.L.G., Burd, H.J. and Doe, N.G., *Design of Wide Bandwidth Analogue Circuits for Heat Transfer Instrumentation in Transient Wind Tunnels*, 16th Symposium of the International Centre for Heat and Mass Transfer (Heat and Mass Transfer in Rotating Machinery) Dubrovnik, D.E. Metzger, Ed., Hemisphere Publishing Corp., New York, 1984.

Press, W.H., Flannery, B.P. Tuekolsky, S.A. and Vetterling, W.T., Numerical Recipies, The Art of Scientific Computing, Cambridge University Press, 1986.

Schlichting, Hermann, Boundary Layer Theory (Seventh Edition), McGraw-Hill Book Company, Inc., New York, NY, 1979.

Schmitz, L.S., *Nonlinear Analog Network to Convert Surface Temperature to Heat Flux*, Cornell Aeronautical Labortory, Inc., CAL Report No. 130, 1963.

Schultz, D.L. and Jones, T.V., *Heat-Transfer Measurements in Short-Duration Hypersonic Facilities*, AGARDograph No. 165, February 1973.

Skinner, George T., *Analogue Network to Convert Surface Temperature to Heat Flux*, Report No. CAL-100, Cornell Aeronautical Laboratory, Inc., Buffalo, New York, February, 1960.

Simonich, J.C. and Bradshaw, P., *Effect of Free Stream Turbulence on Heat Transfer through a Turbulent Boundary Layer*, ASME Journal of Heat Transfer, Vol 100, No. 4, November 1978.

Smith, Bret J., *Investigation of Heat Transfer to a Sharp Edged Flat Plate Using a Shock Tube*, Masters Thesis, School of Engineering, Air Force Institute of Technology (AU), Wright-Patterson AFB OH, December 1986.

Wise, B. and Schultz, D.L., *Turbulence measurements in supersonic flow with the hot-wire anemometer*, Aero. Res. Council, C.P. 366, 1955.

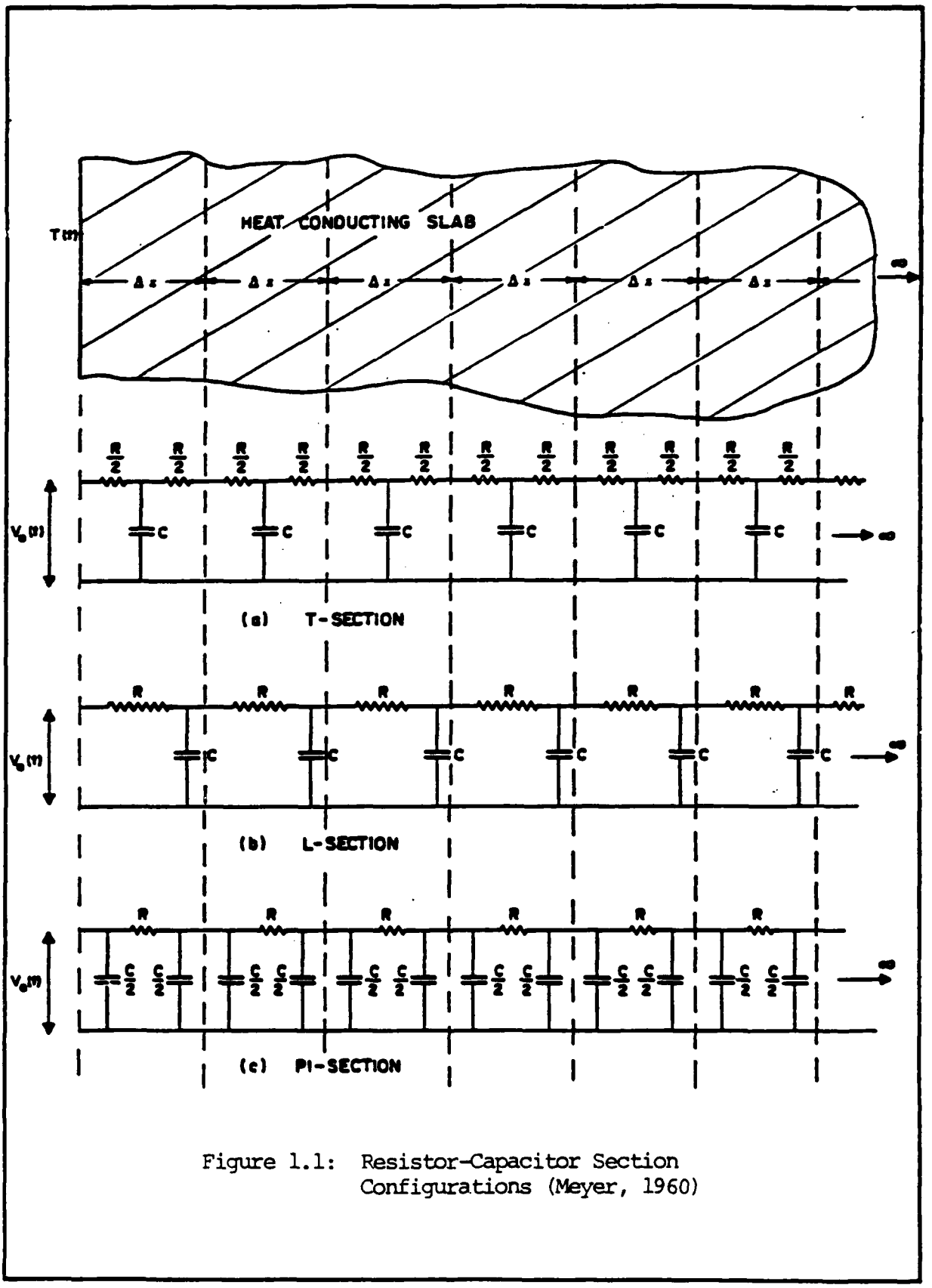

Figure 1.1: Resistor-Capacitor Section Configurations (Meyer, 1960)

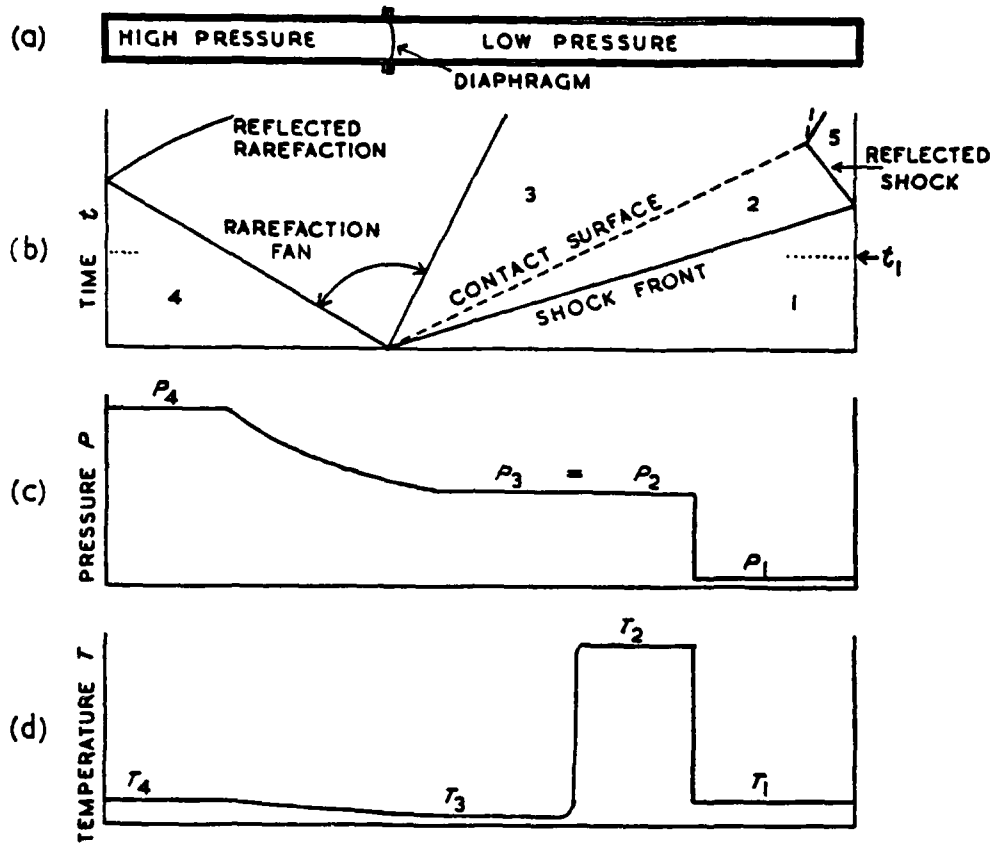

Figure 2.1: (a) Conventional Shock Tube (b) An x-t diagram showing progress of the shock wave (c) The pressure distribution along the tube at time t_1 (d) The temperature distribution at time t_1 (Gaydon: 1)

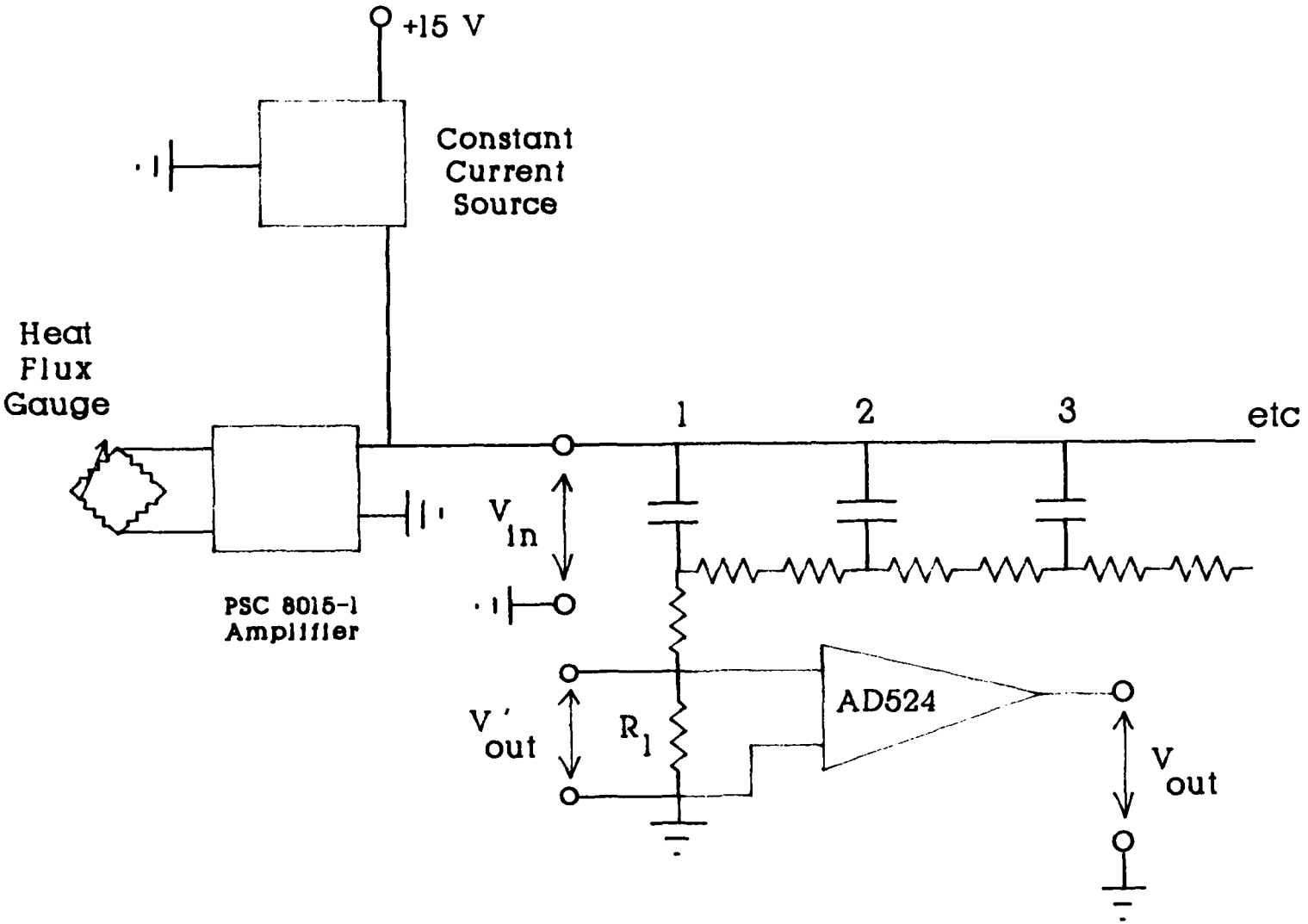

Figure 2.2: The Heat Flux Analog

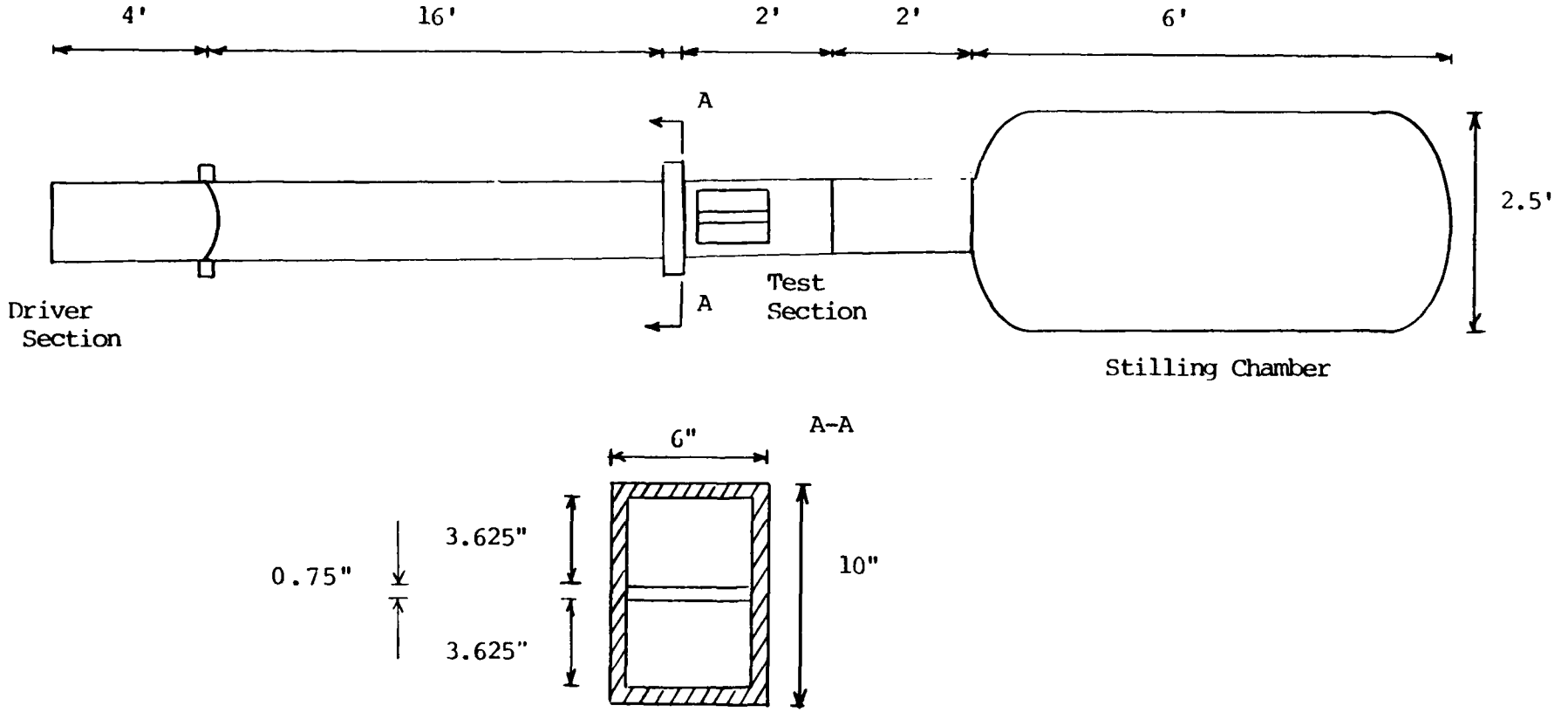

Figure 3.1: The AFIT Low Pressure Shock Tube

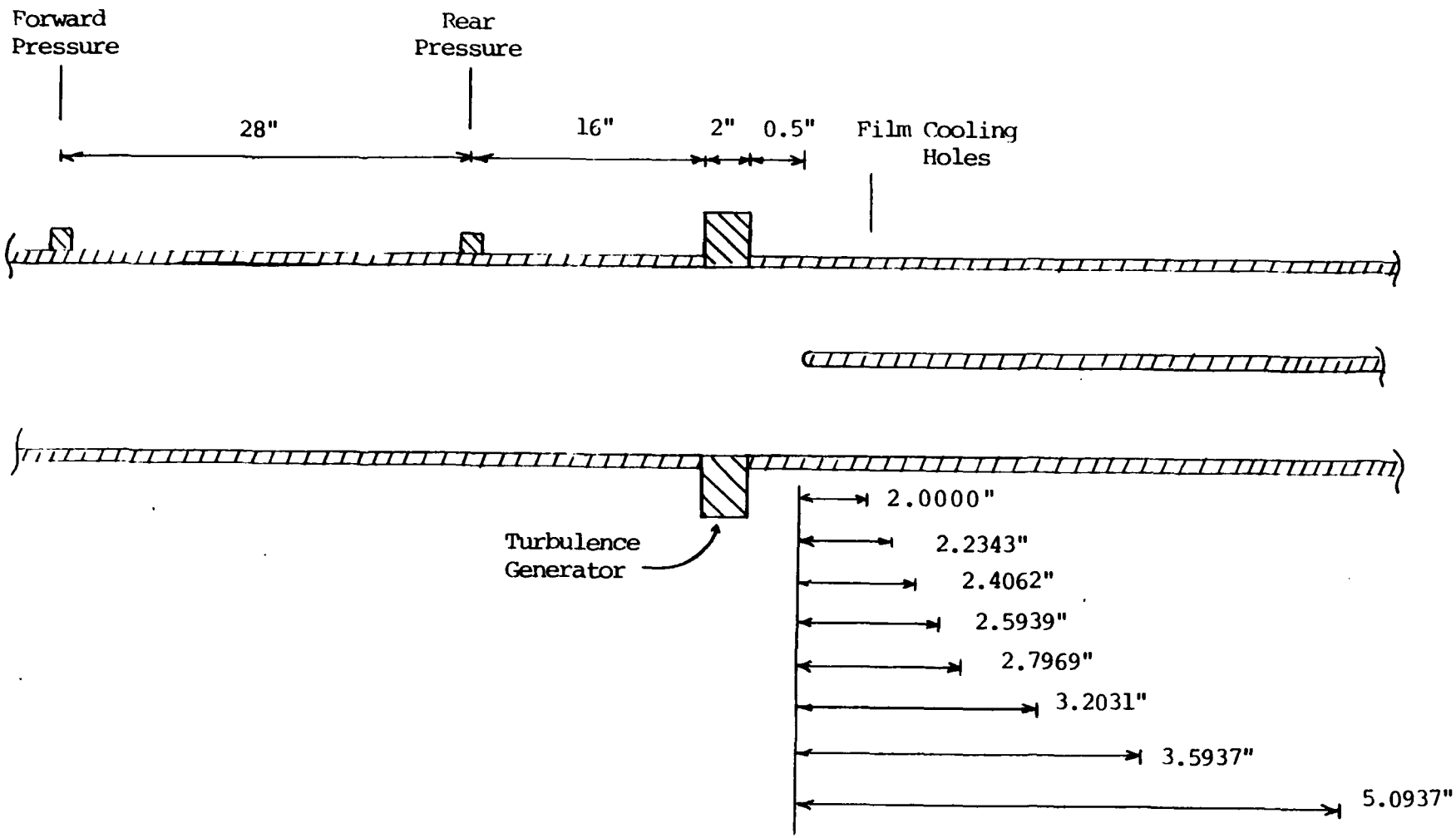

Figure 3.2: Shock Tube Sensor Locations

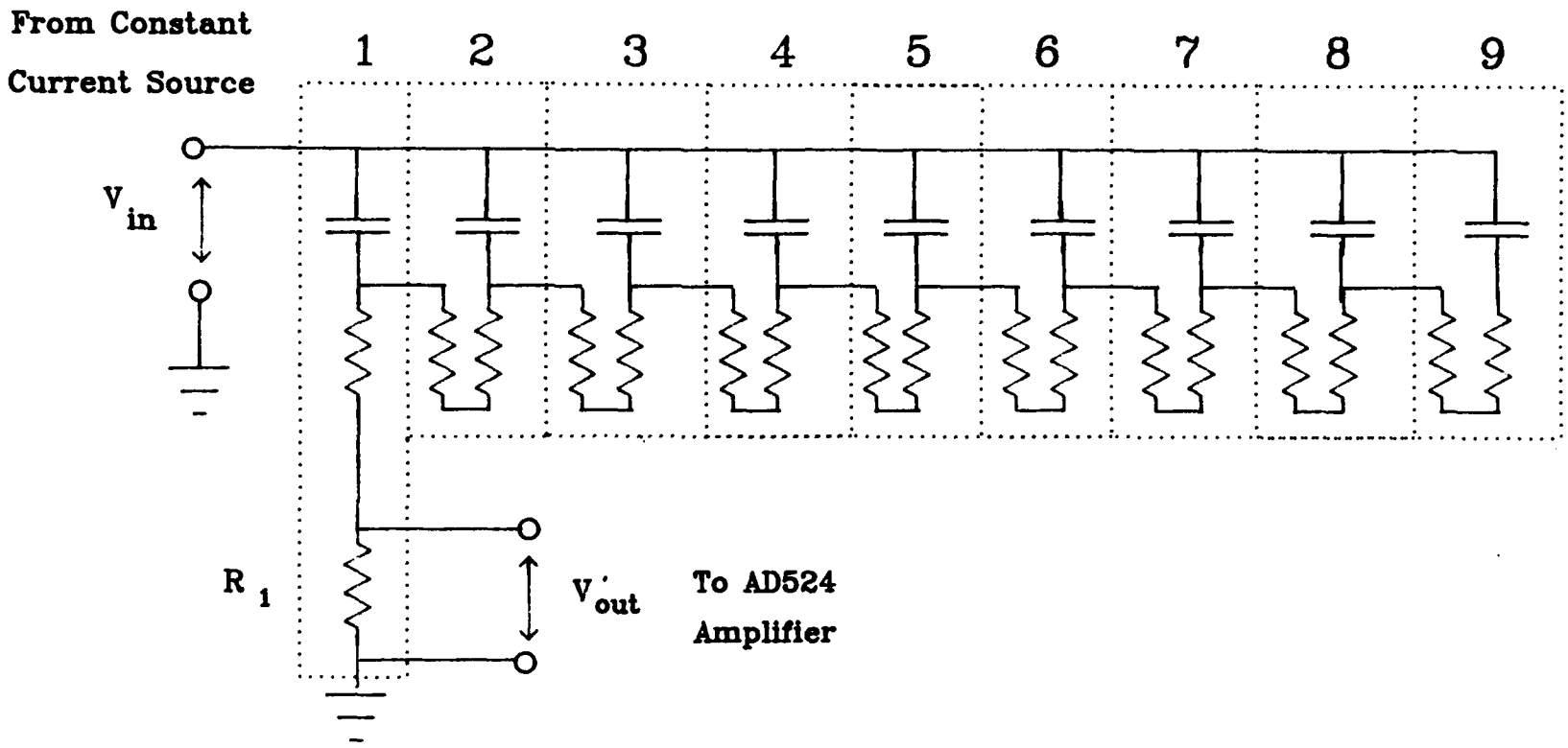

Figure 3.3: The Heat Flux Analog R–C Network

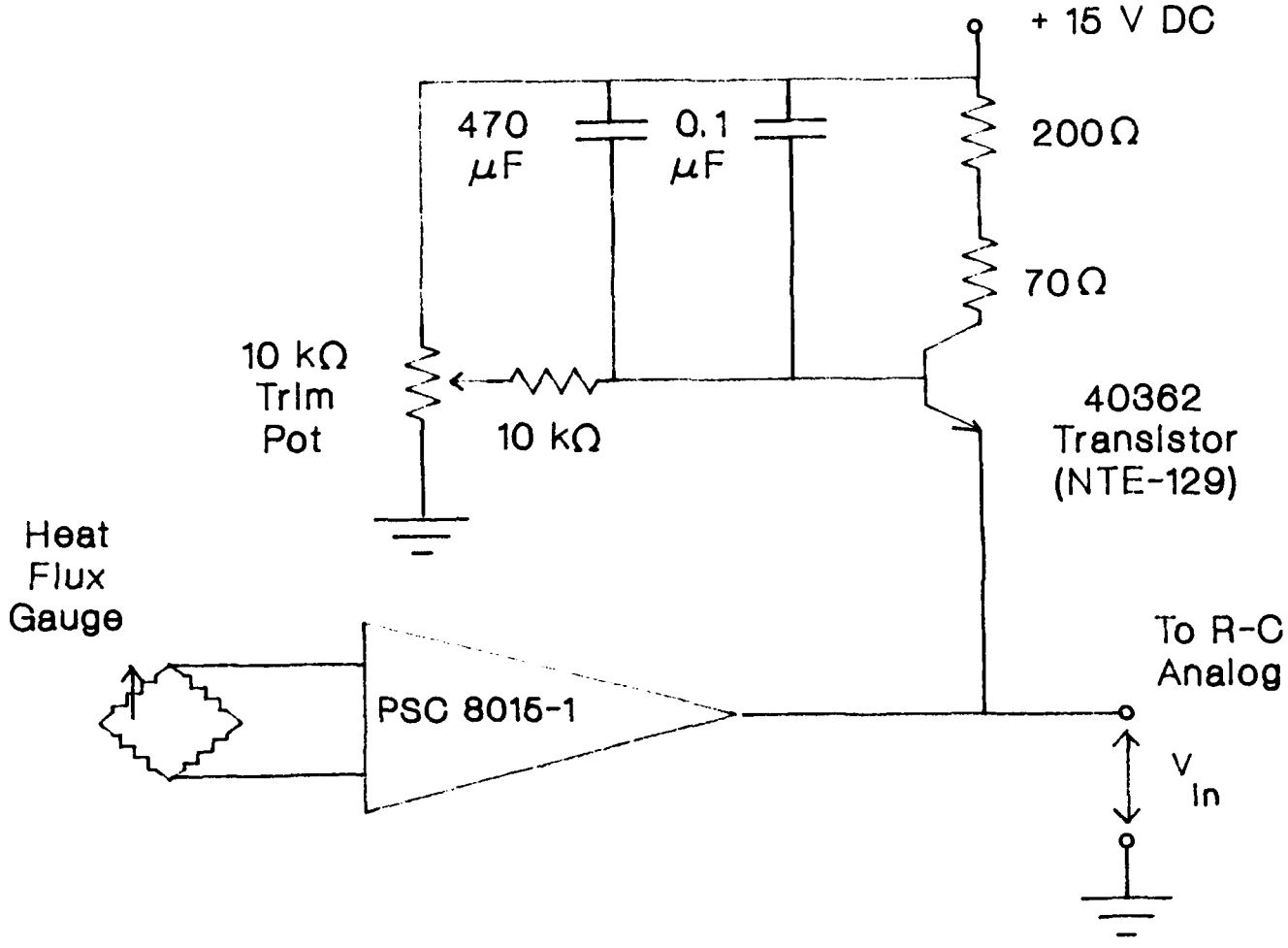

Figure 3.4: Heat Flux Analog Constant Current Source

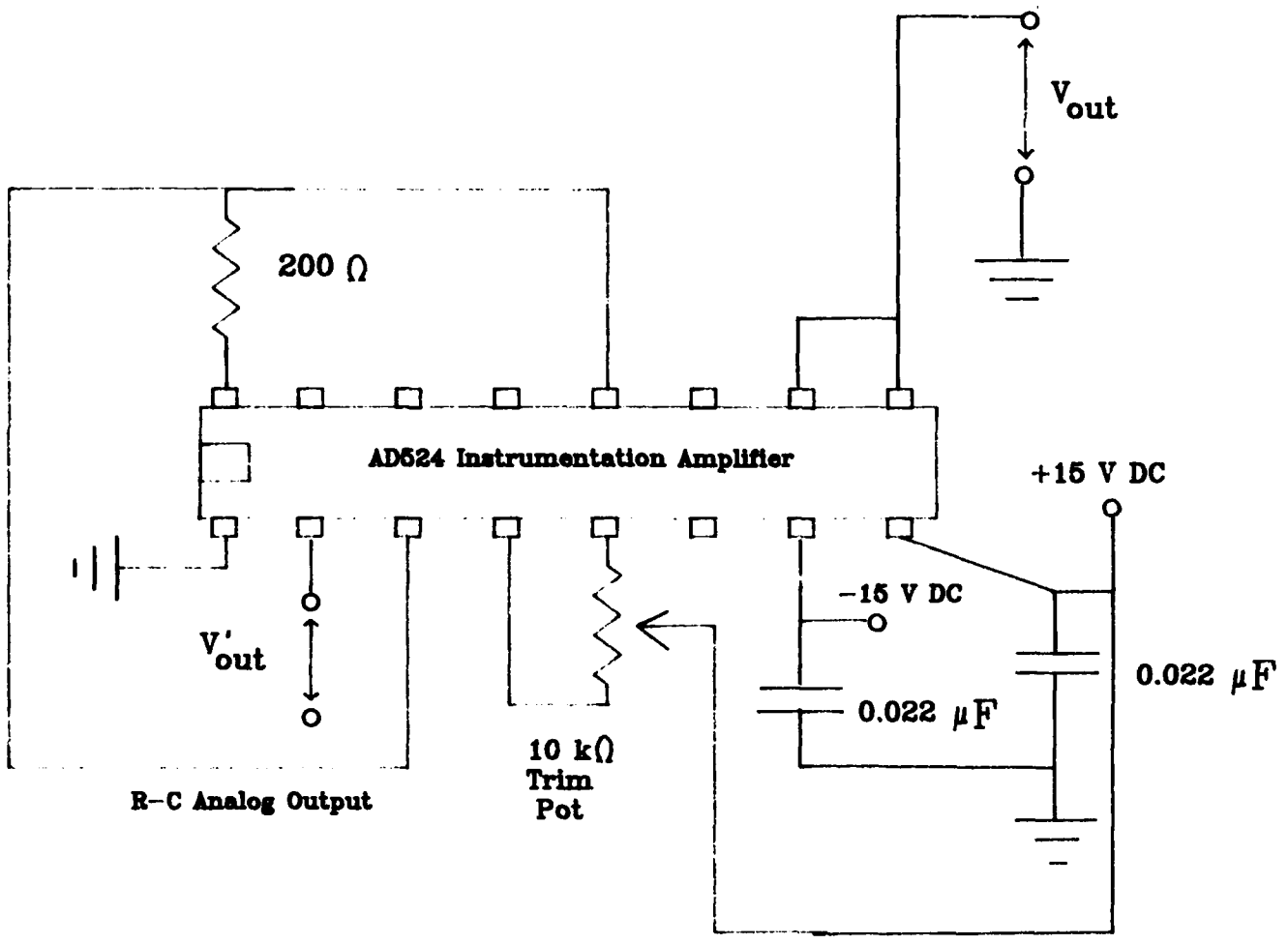

Figure 3.5: Heat Flux Analog Instrumentation Amplifier

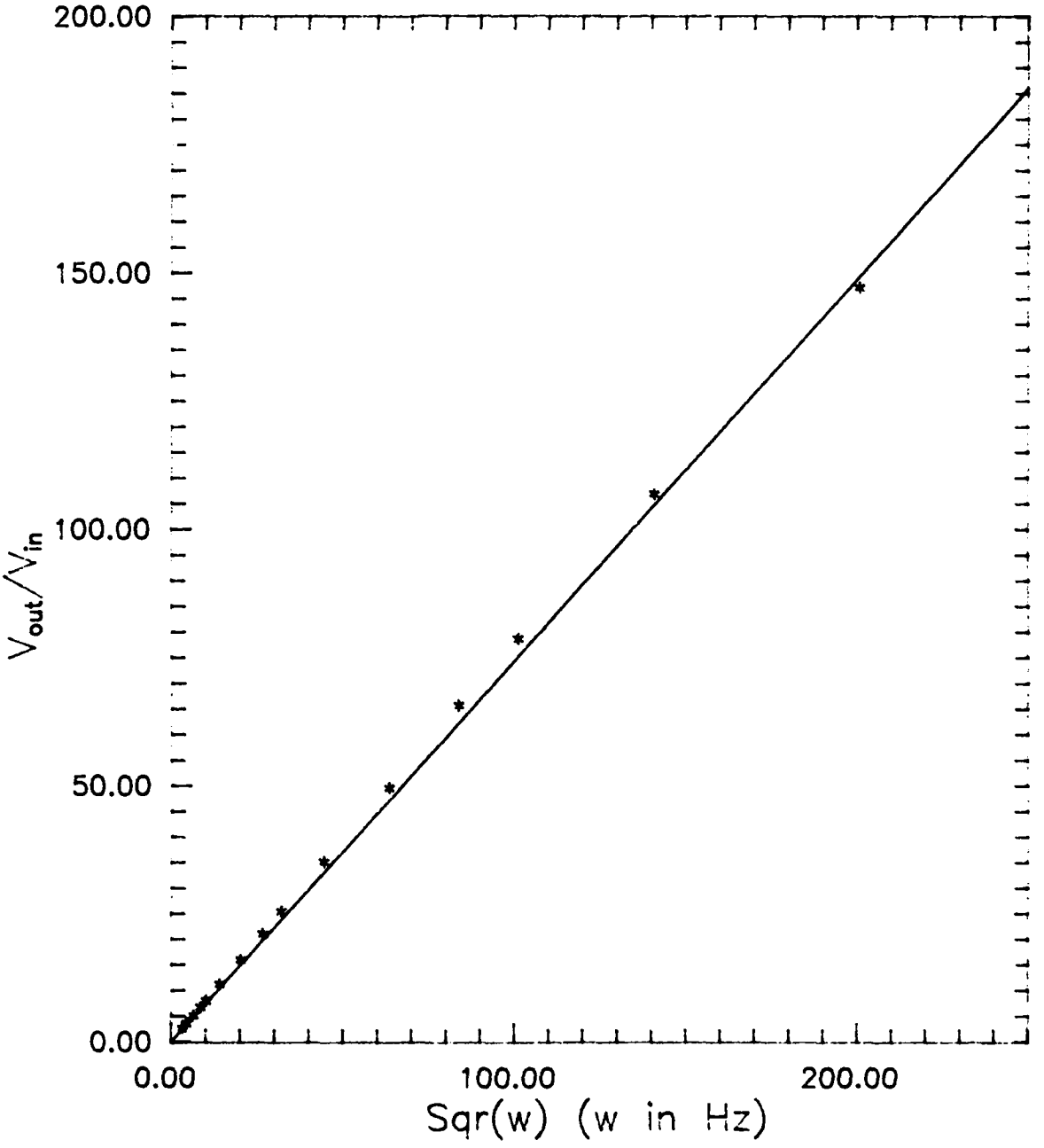

Figure 3.6: Calibration of Heat Flux Circuit 31-105

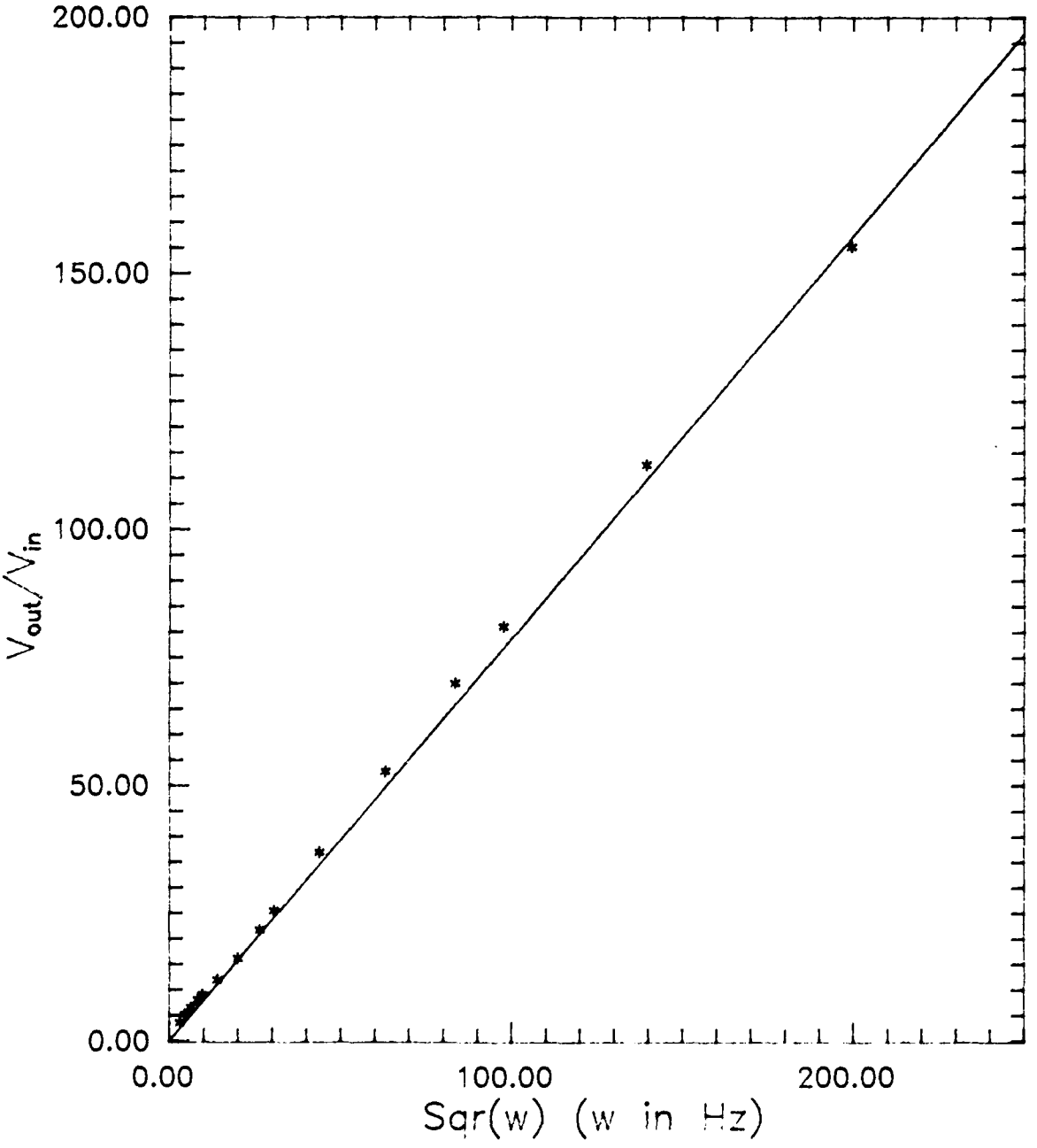

Figure 3.7: Calibration of Heat Flux Circuit 31-790

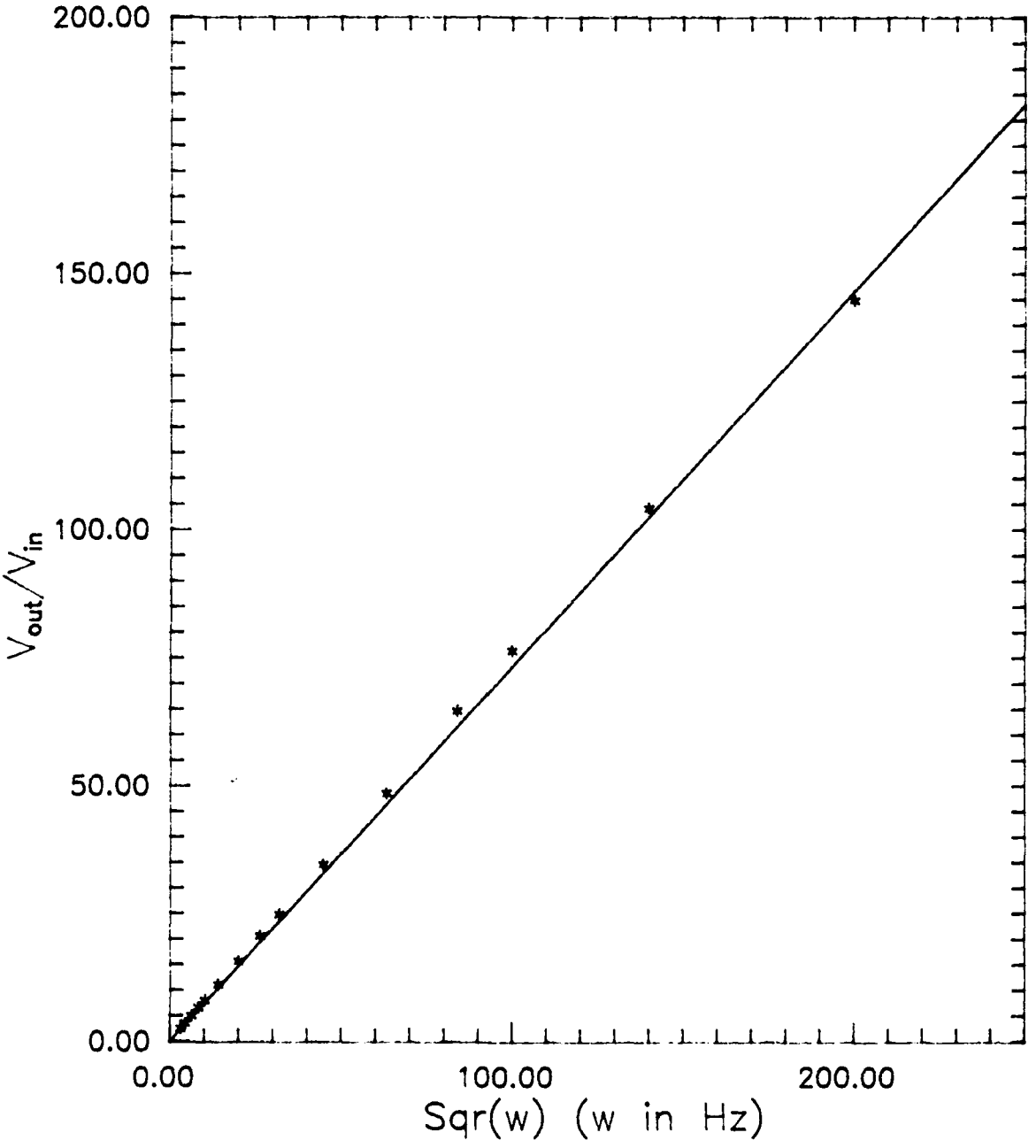

Figure 3.8: Calibration of Heat Flux Circuit 31–820

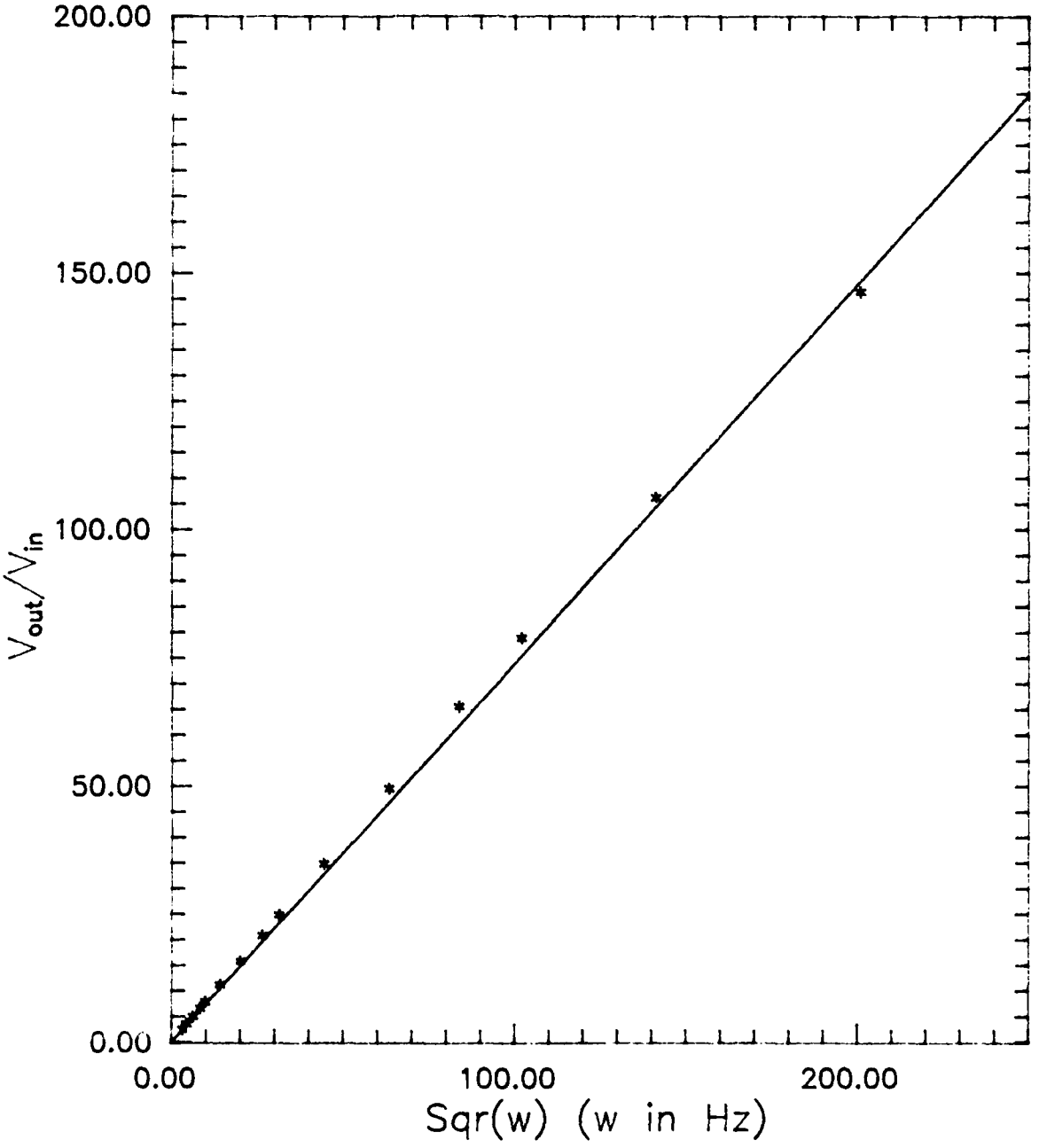

Figure 3.9: Calibration of Heat Flux Circuit 31-850

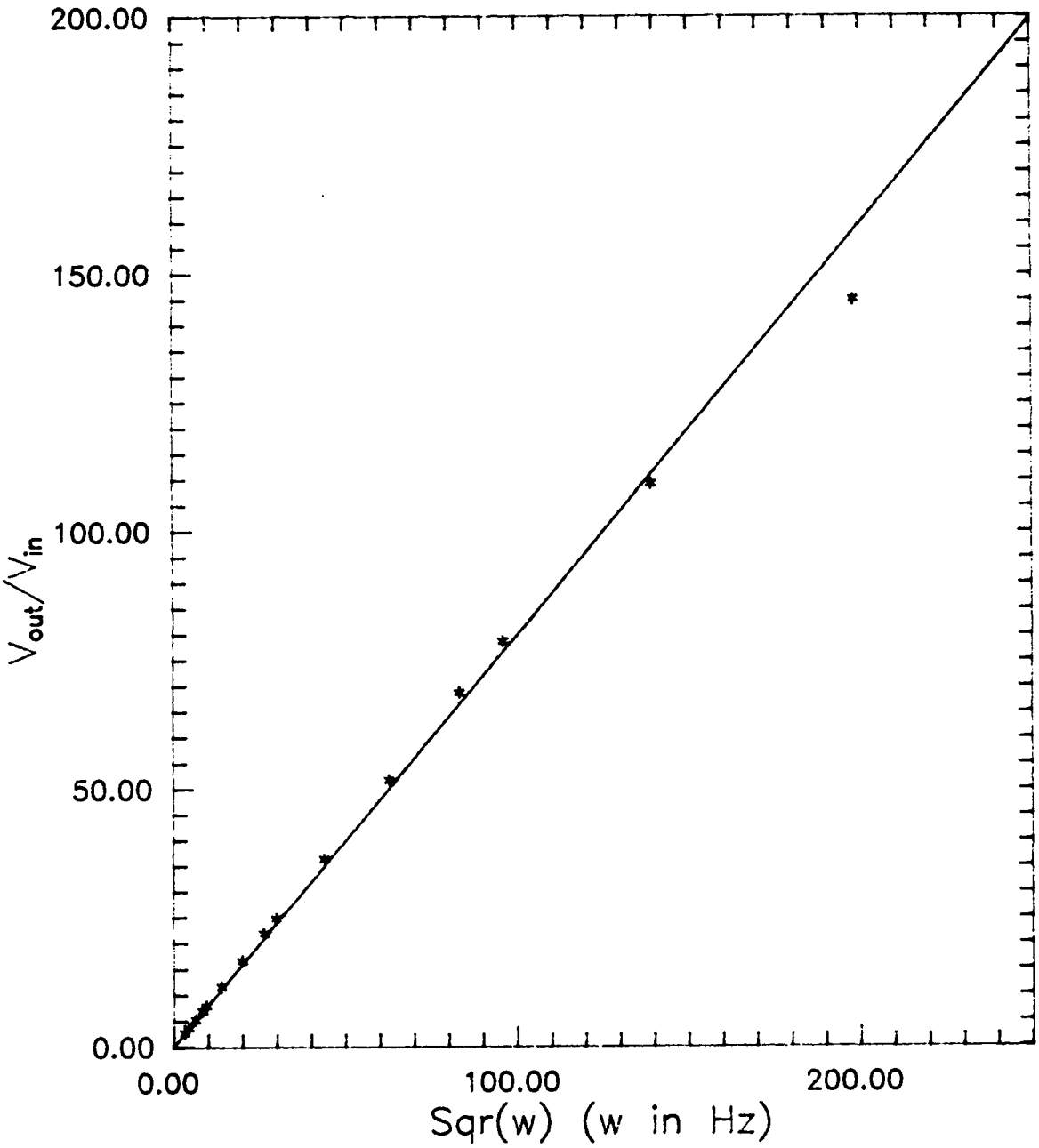

Figure 3.10: Calibration of Heat Flux Circuit 31-87

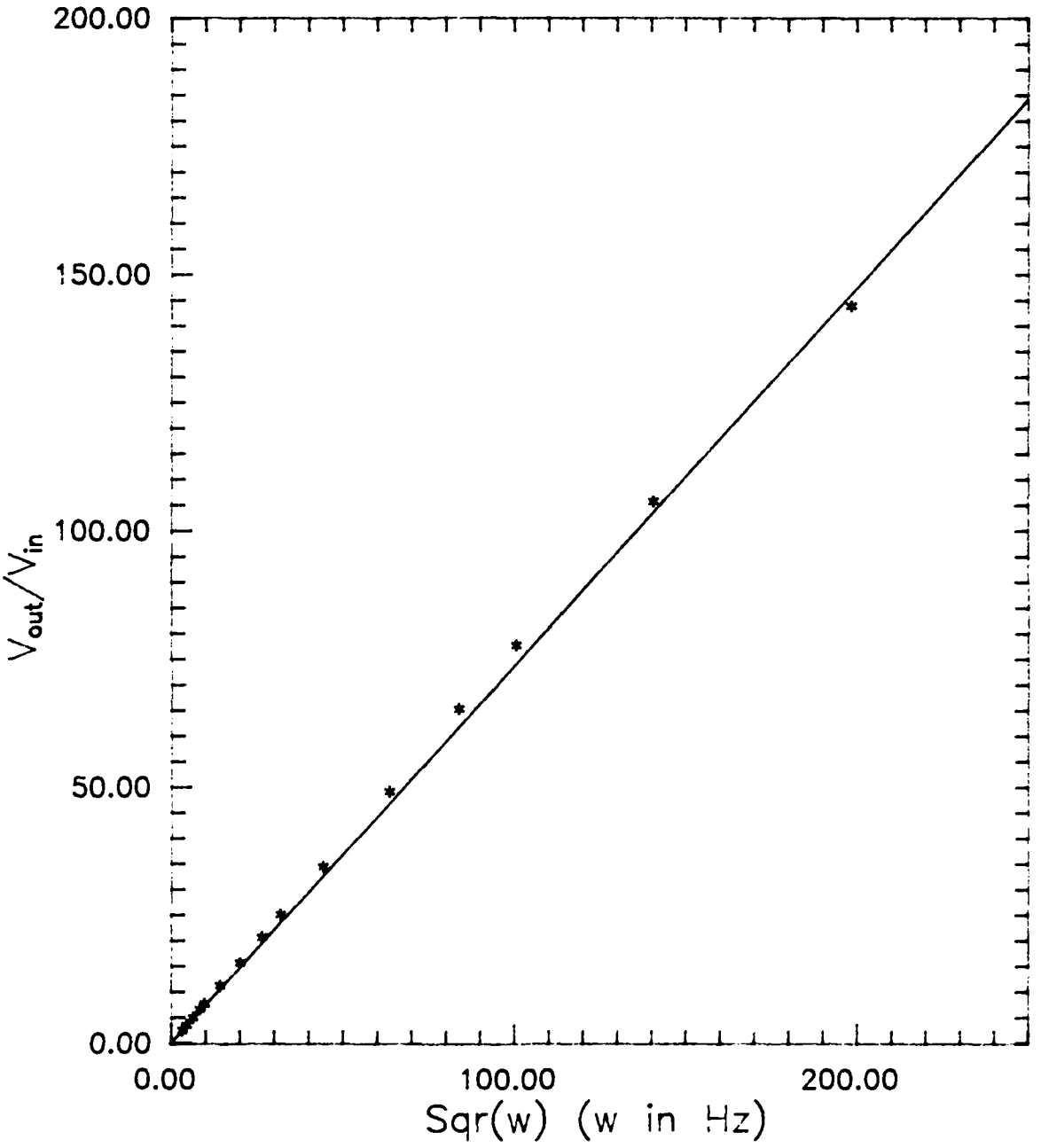

Figure 3.11: Calibration of Heat Flux Circuit 32–10

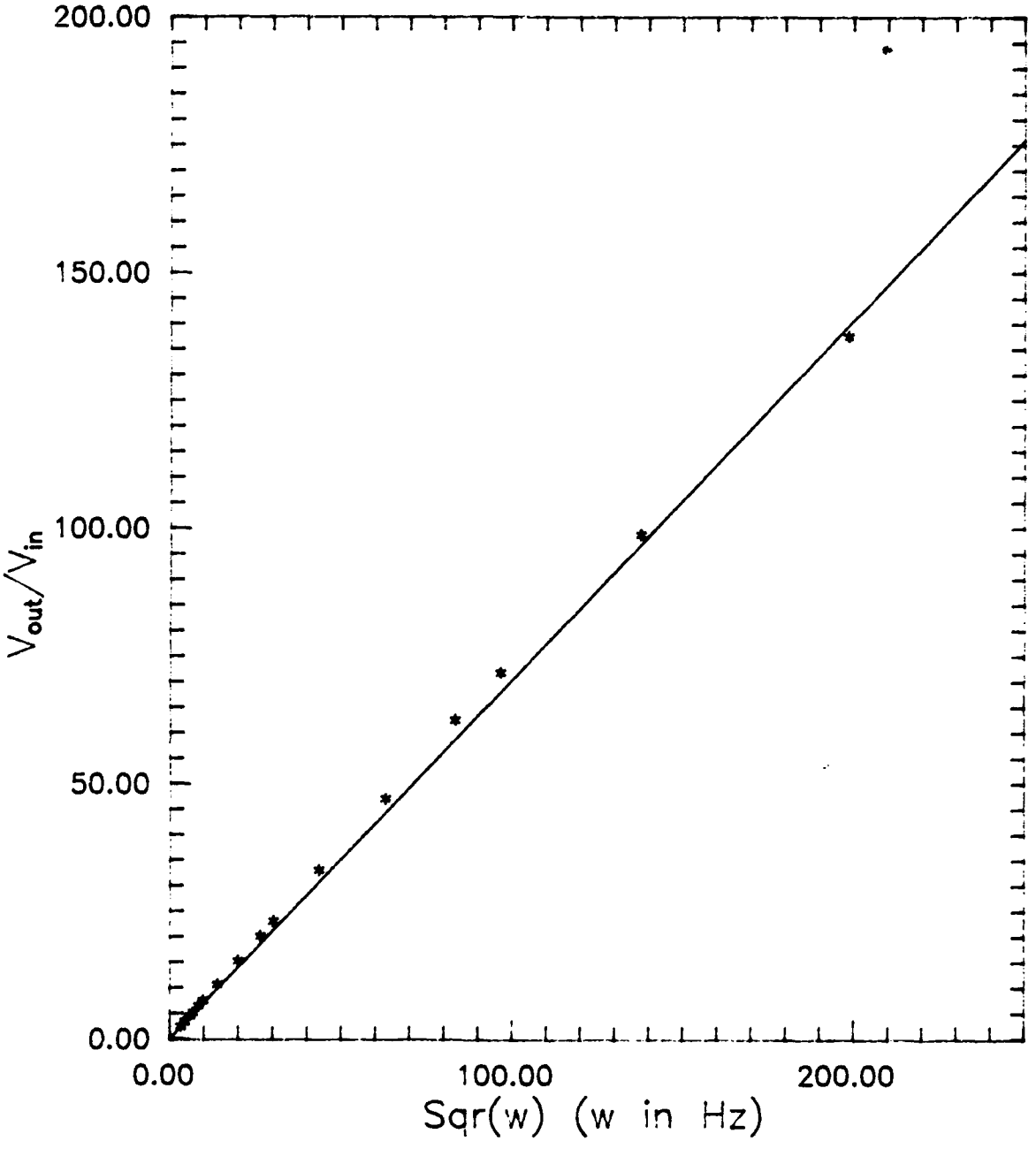

Figure 3.12: Calibration of Heat Flux Circuit 32–20

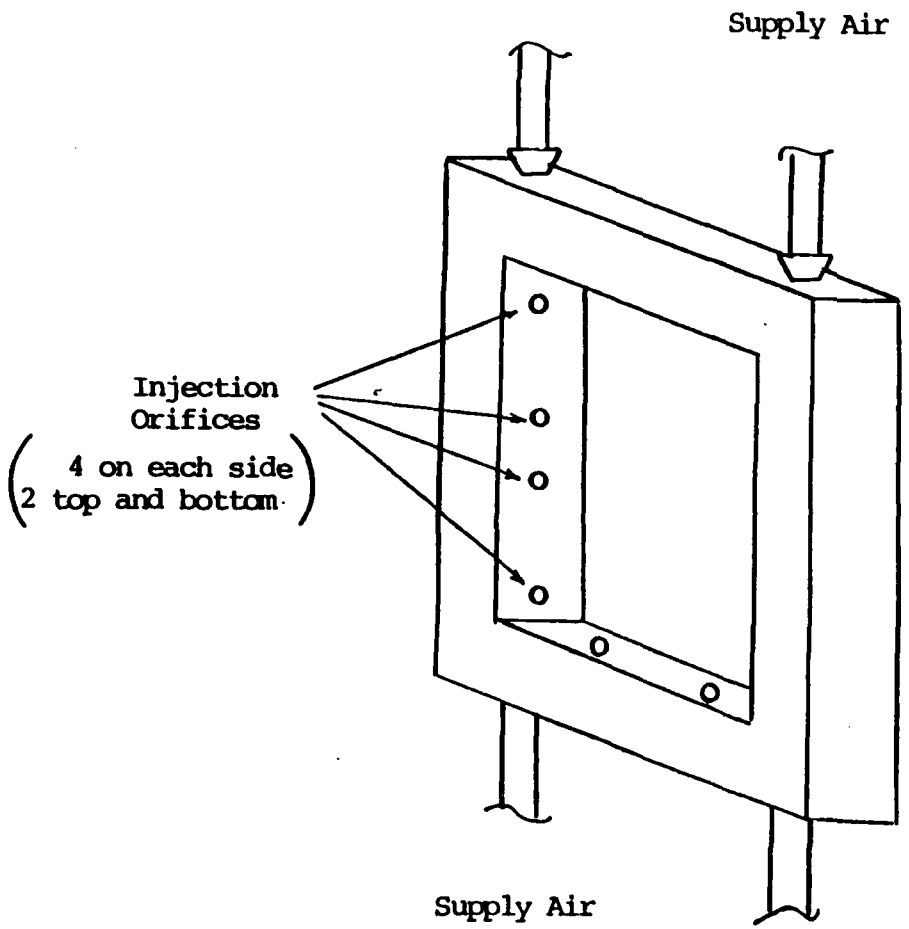

Figure 3.13: Free-Stream Turbulence Generator

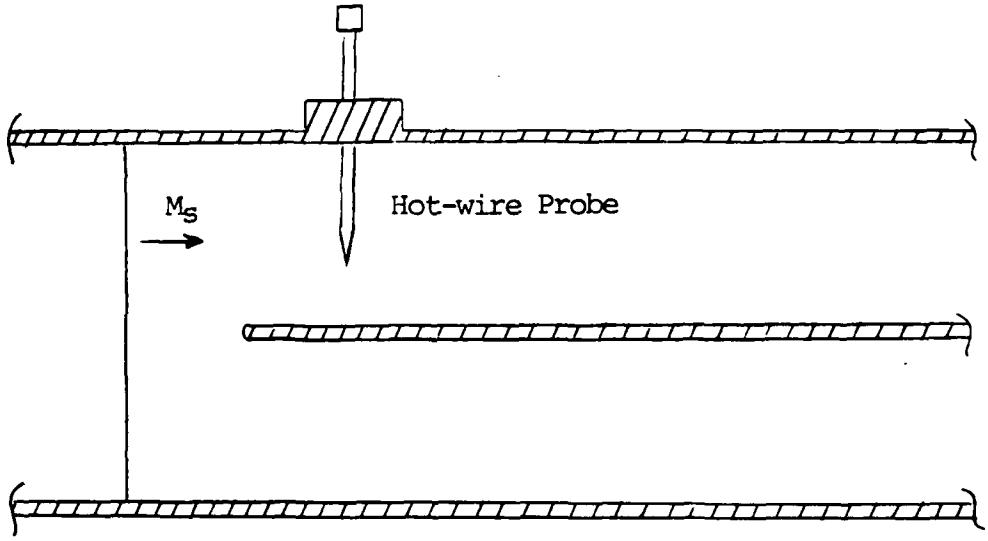

Configuration 1

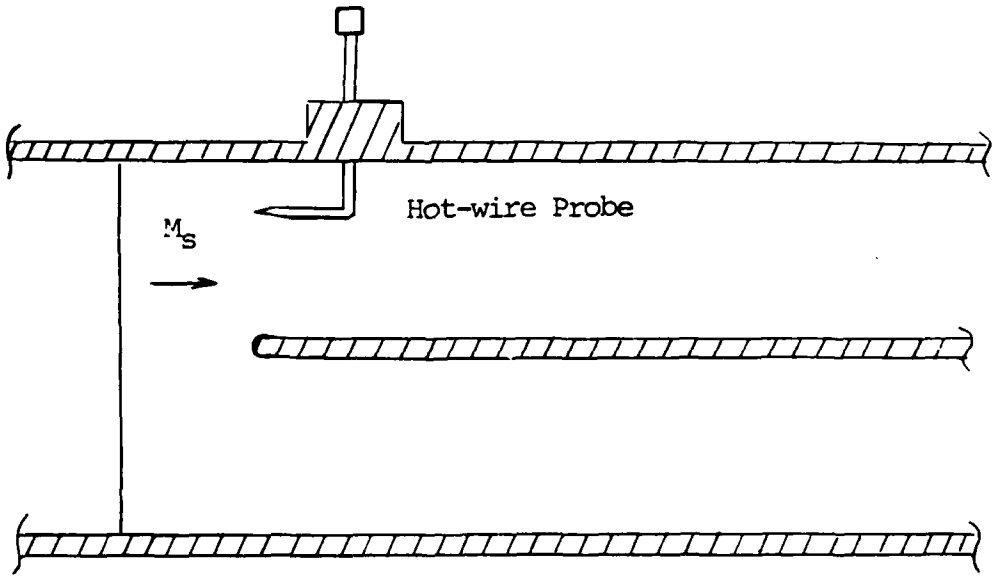

Configuration 2

Figure 3.14: Hot-wire Mounting Configurations

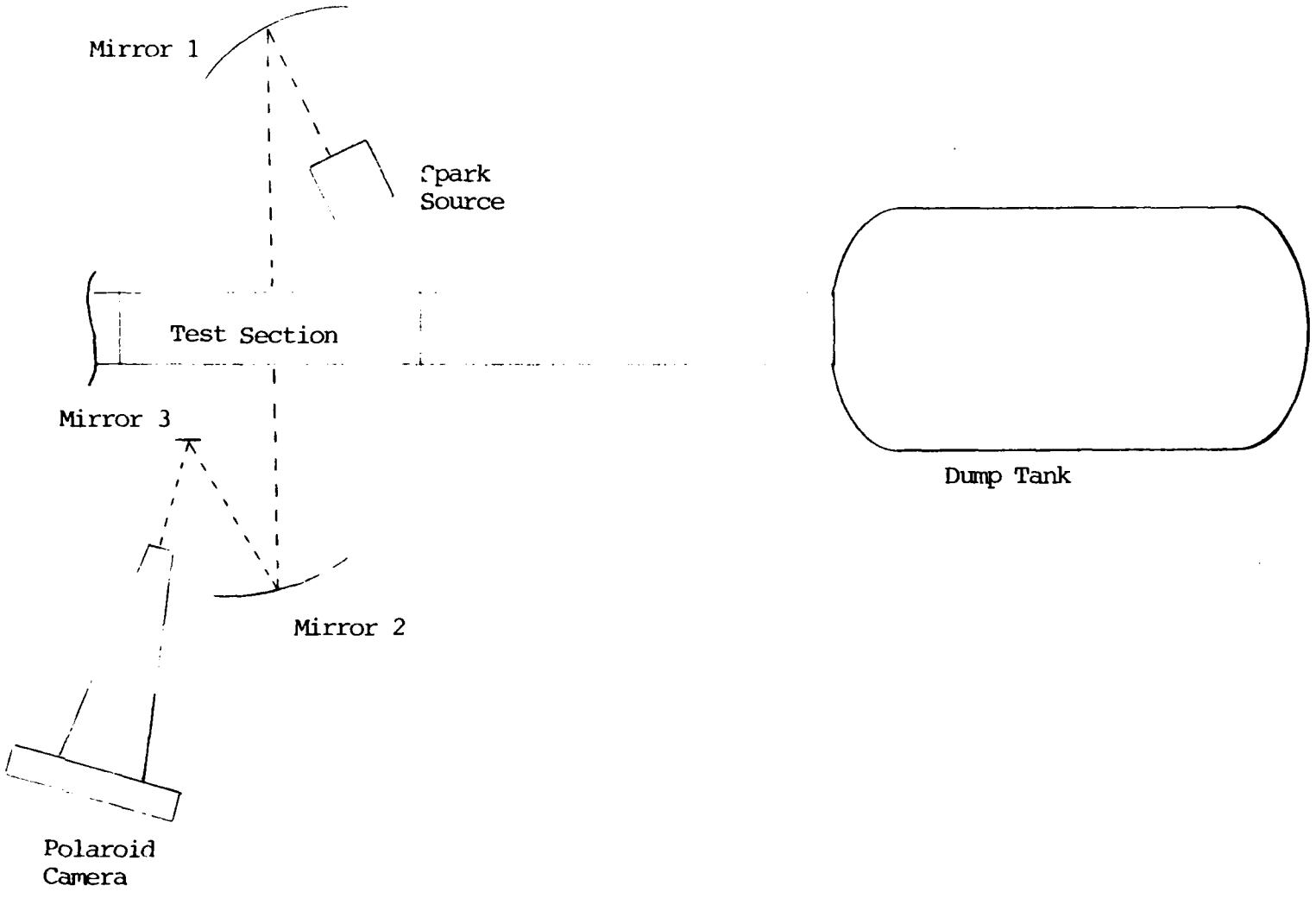

Figure 3.15: Schlieren Instrumentation

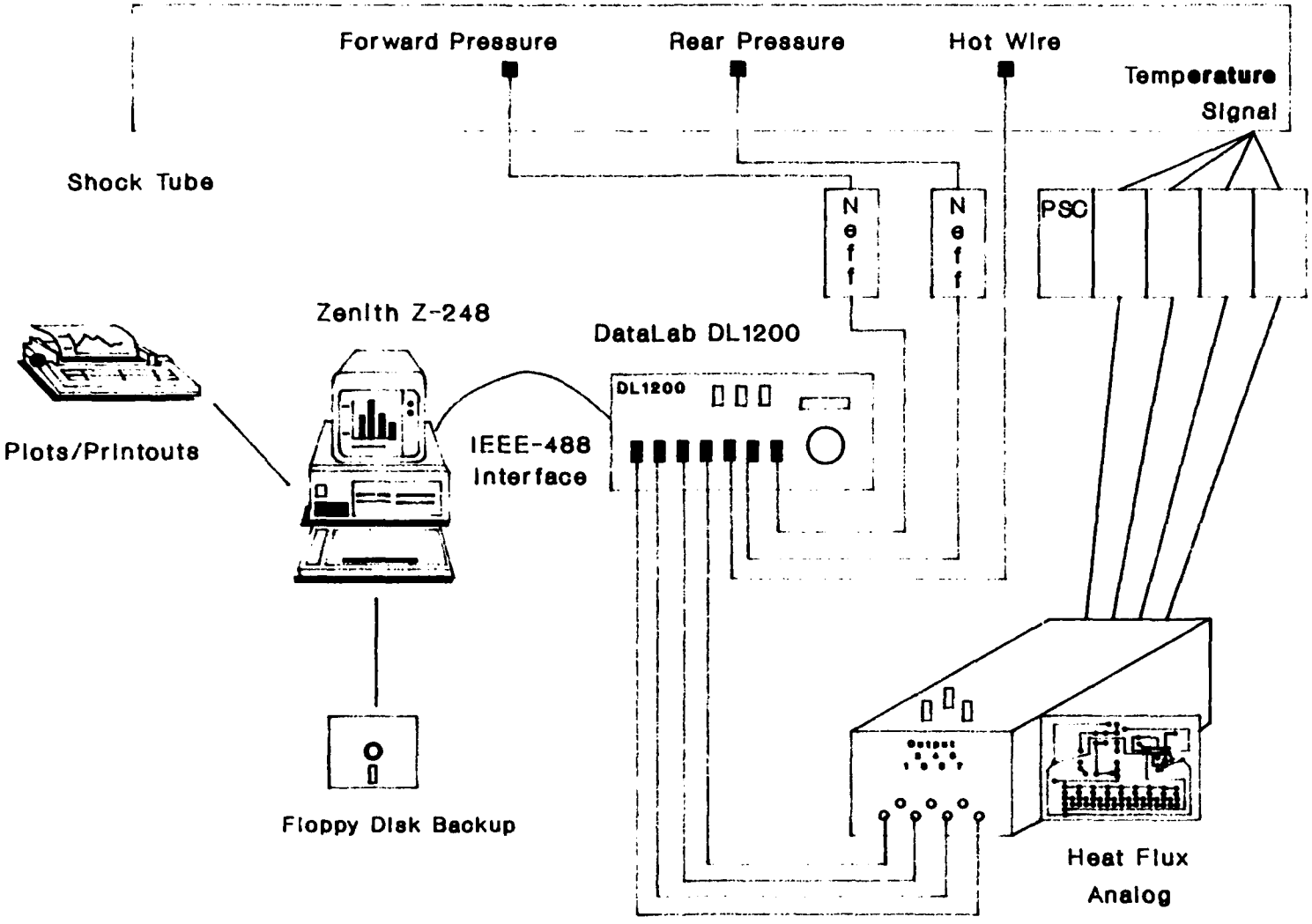

Figure 4.1: Instrumentation-Hardware Interface

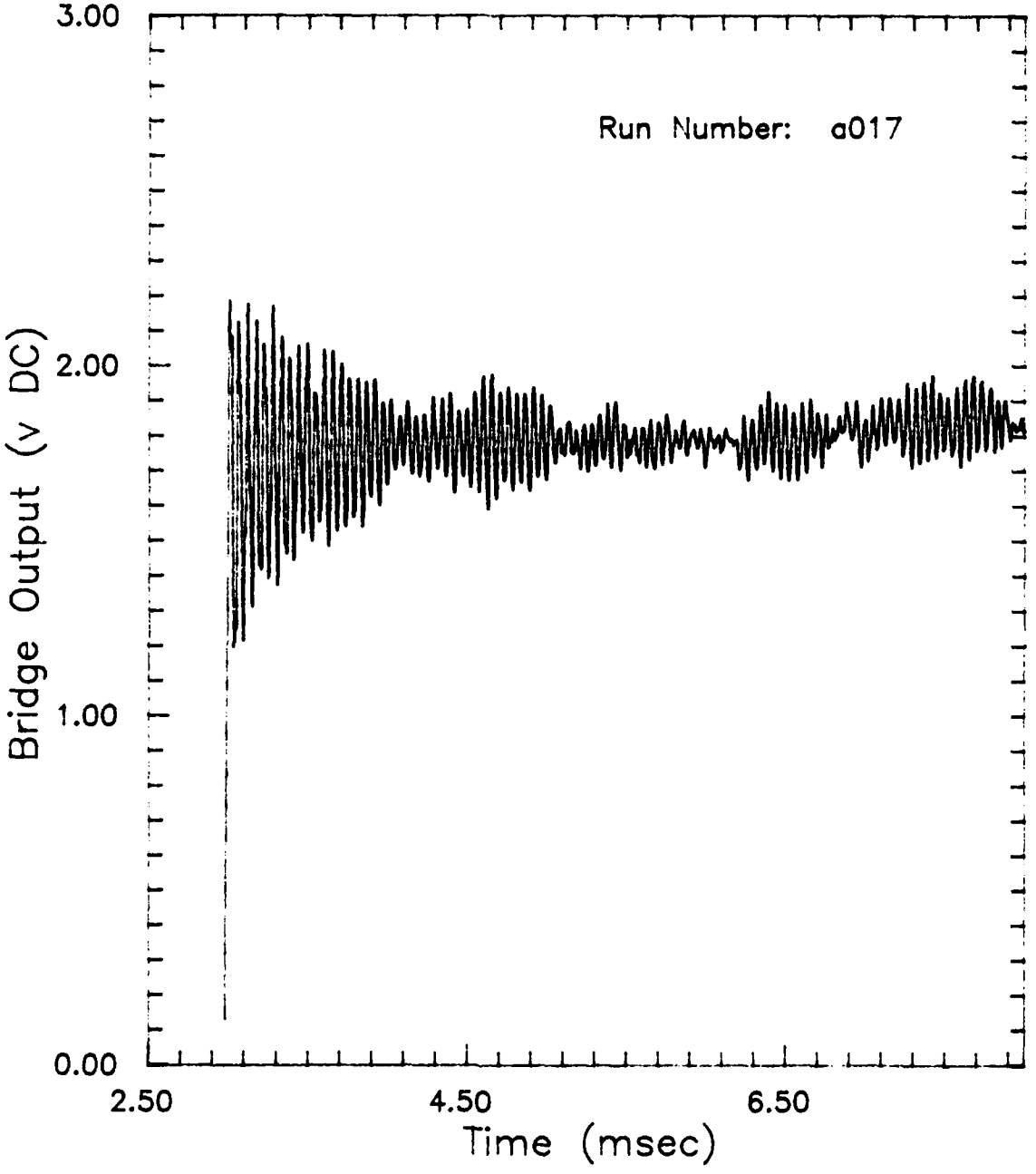

Figure 4.2: Hot–Wire Bridge Output using Configuration 1

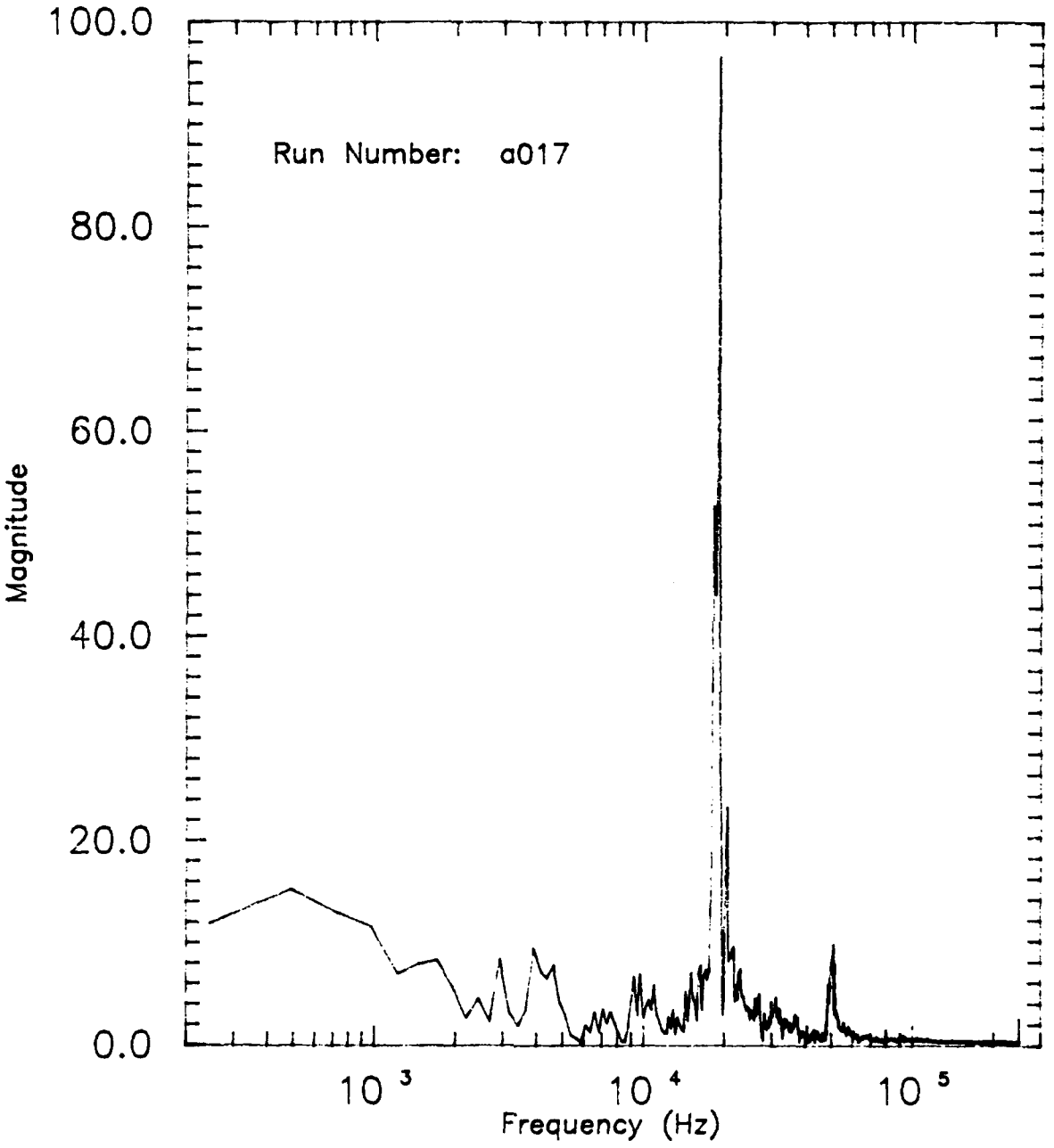

Figure 4.3: Fast Fourier Transform of Figure 4.2 data

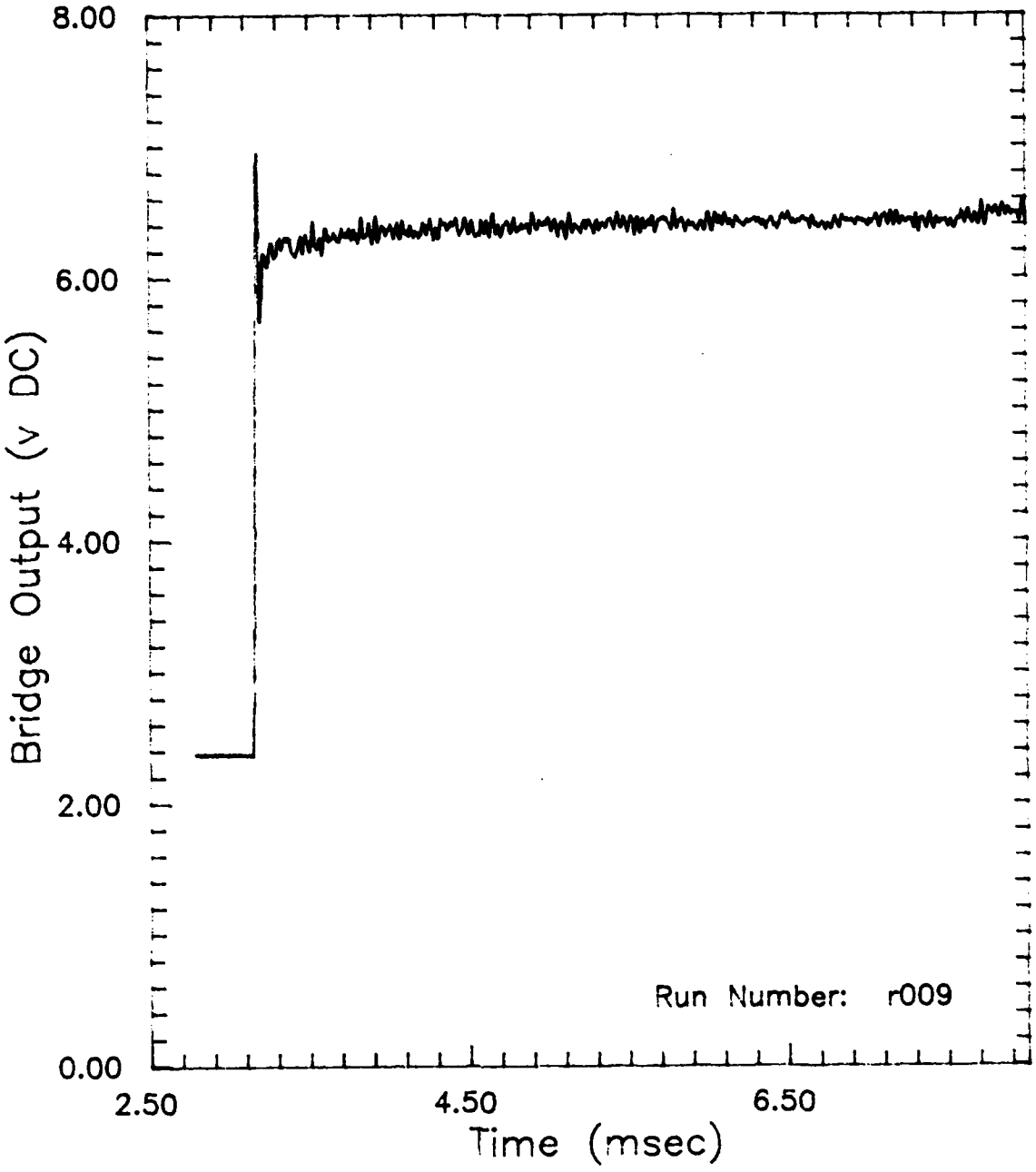

Figure 4.4: Hot-Wire Bridge Output using Configuration 2

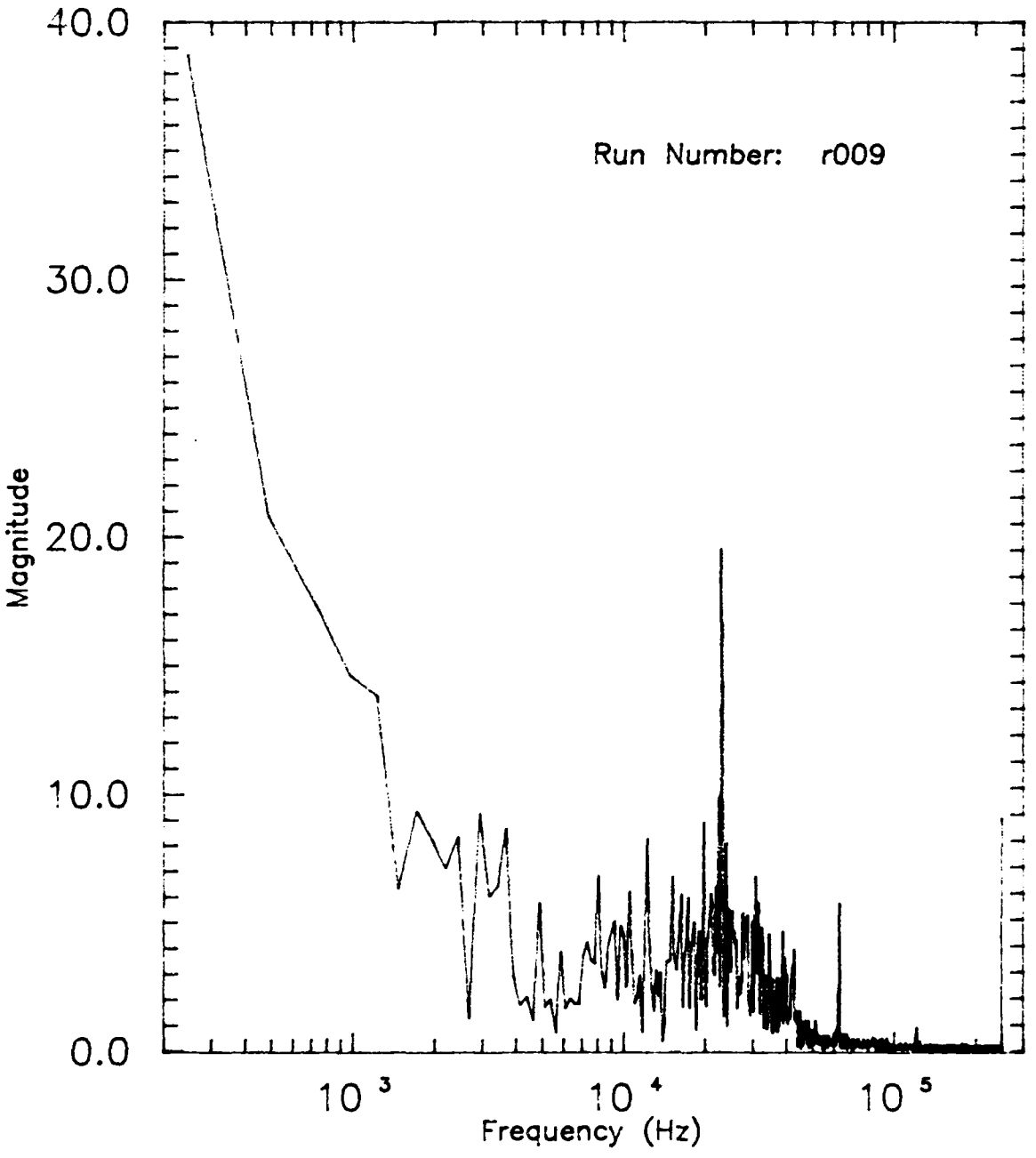

Figure 4.5: Fast Fourier Transform of Figure 4.4 data

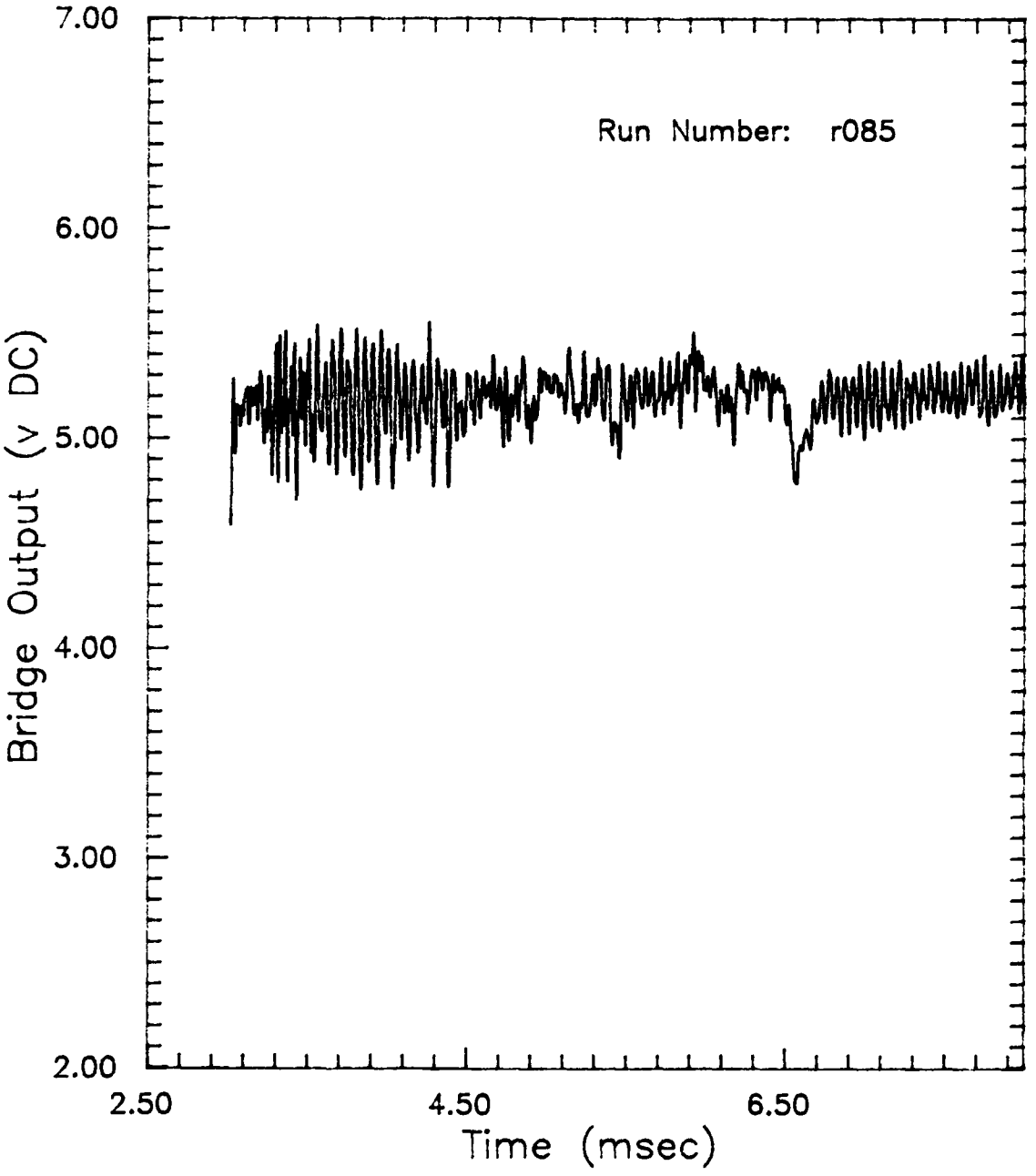

Figure 4.6: Hot-Wire Bridge Output Prior to Filtering

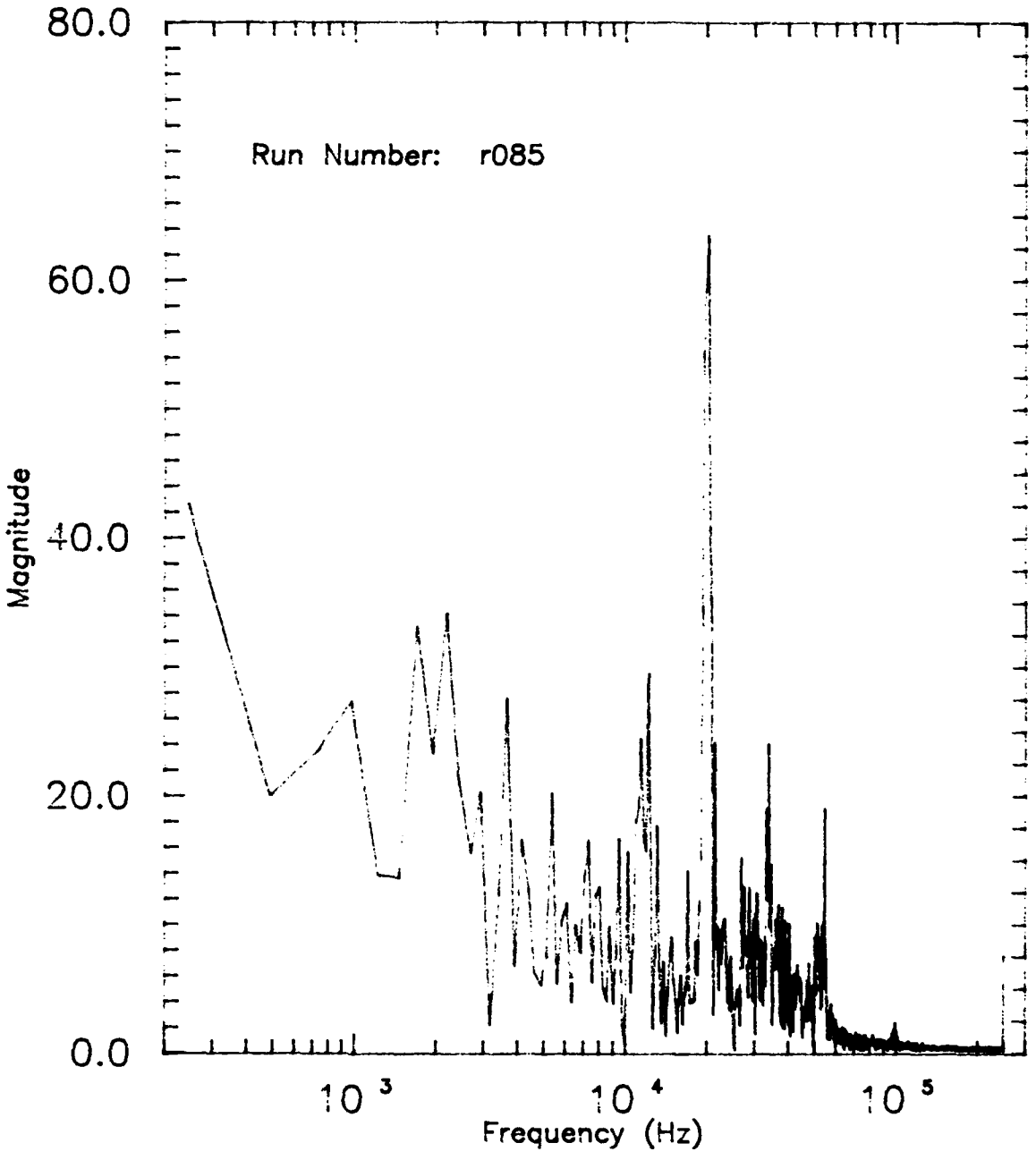

Figure 4.7: Fast Fourier Transform of Figure 4.6 Data

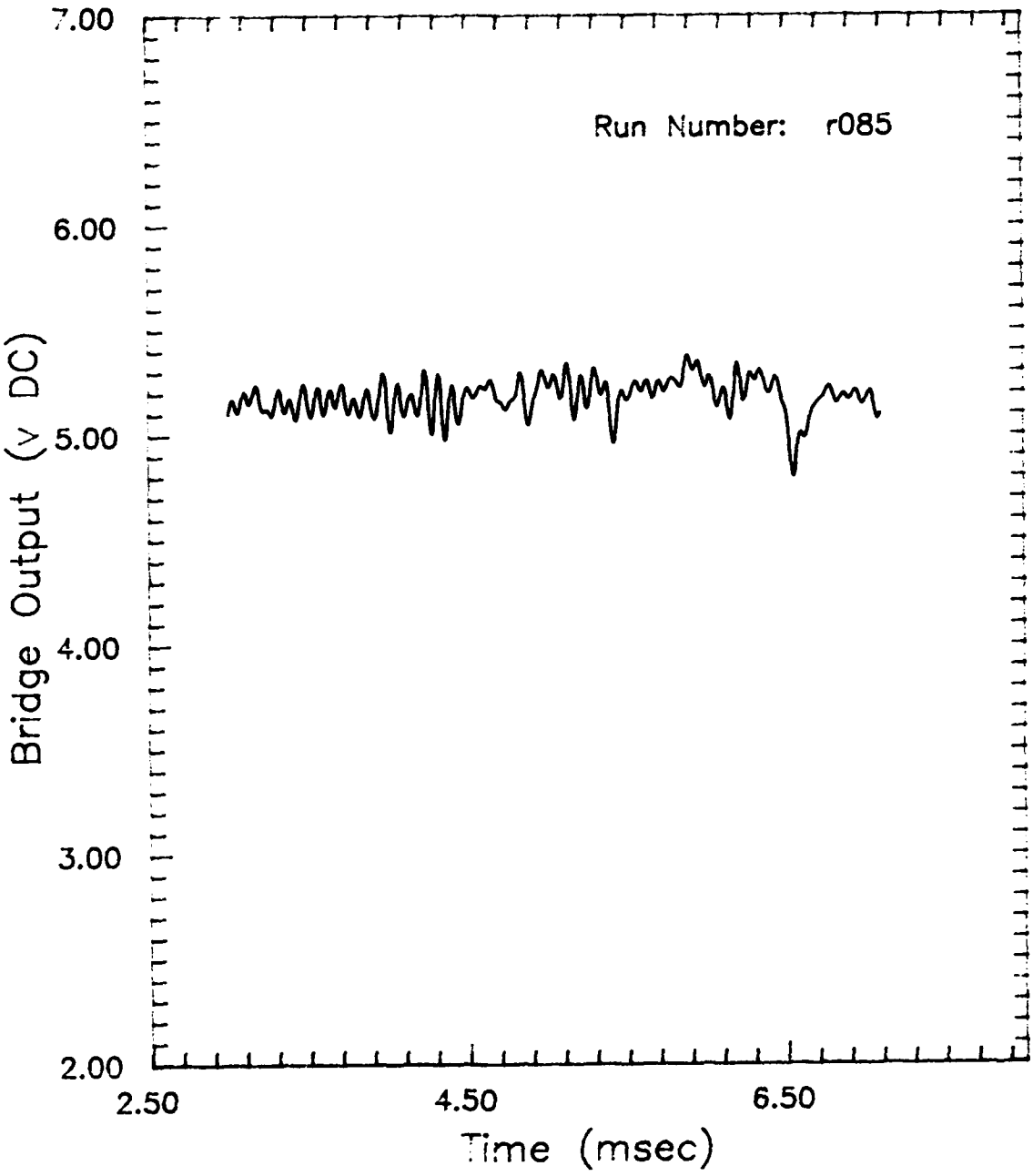

Figure 4.8: Hot-Wire Bridge Output After Filtering

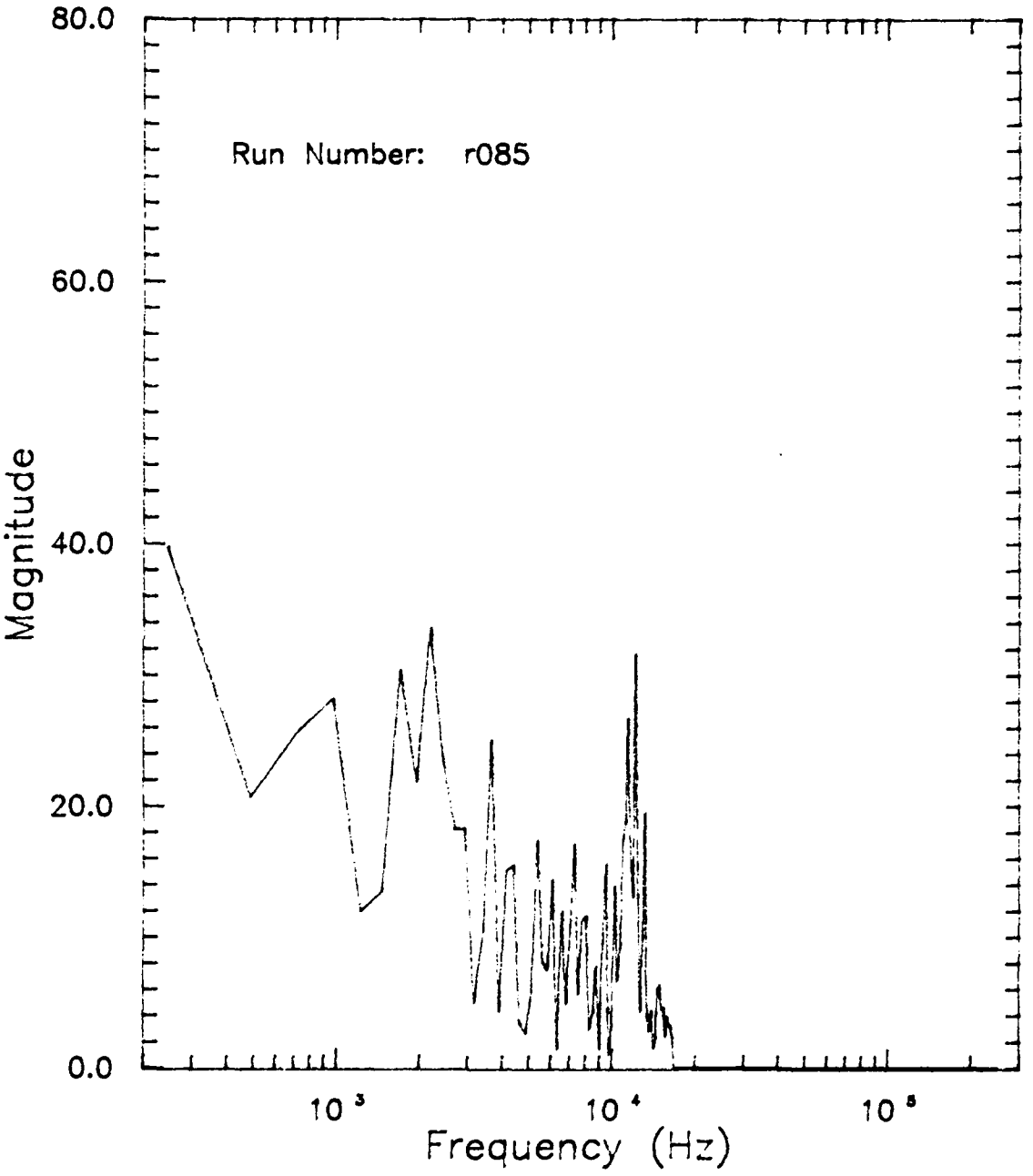

Figure 4.9: Fast Fourier Transform of Figure 4.8 Data

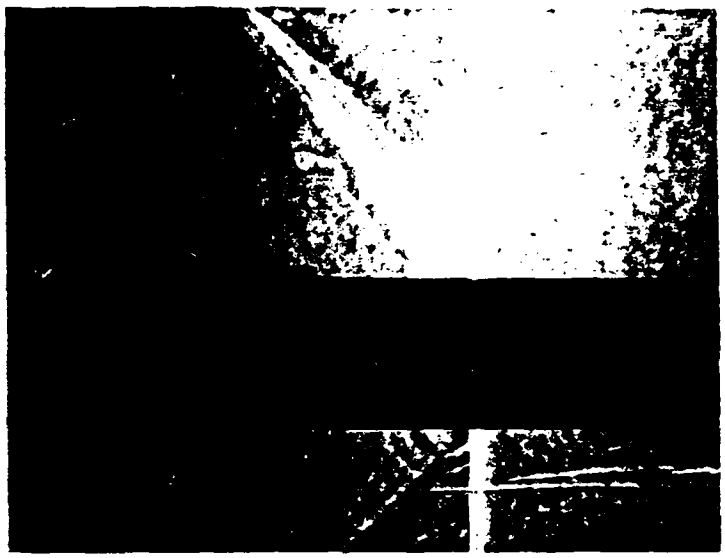

Figure 5.1 (a) Schileran photograph, spark lamp triggered 3 msec after shock passage (of the forward pressure transducer). No turbulence injection

Figure 5.1 (b) Spark lamp triggered 3.06 msec after shock passage. Turbulence injection present.

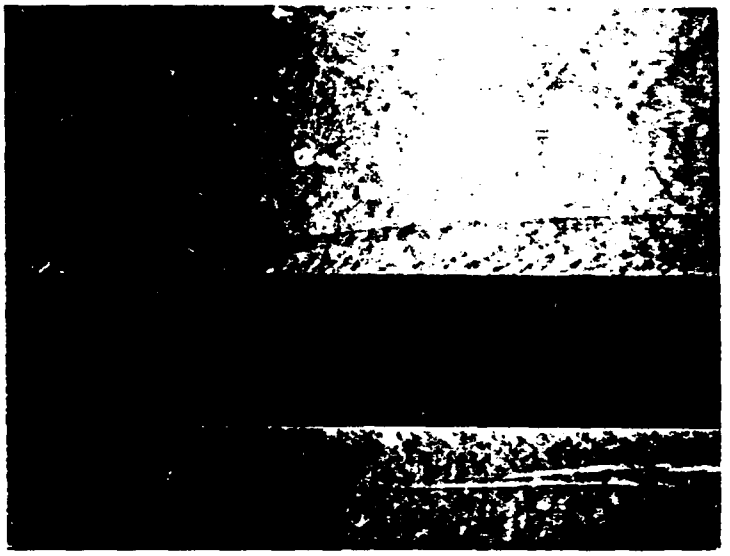

Figure 5.1 (c) 4 msec after shock passage, No turbulence injection

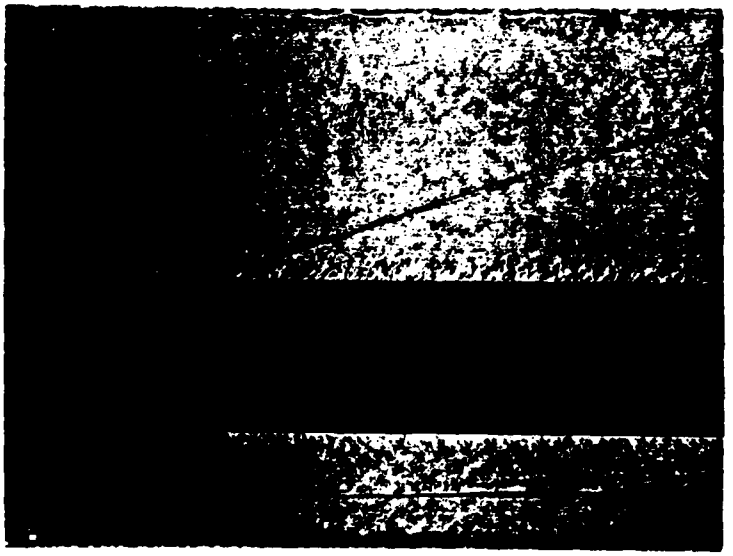

Figure 5.1 (d) 6 msec after shock passage, No turbulence injection

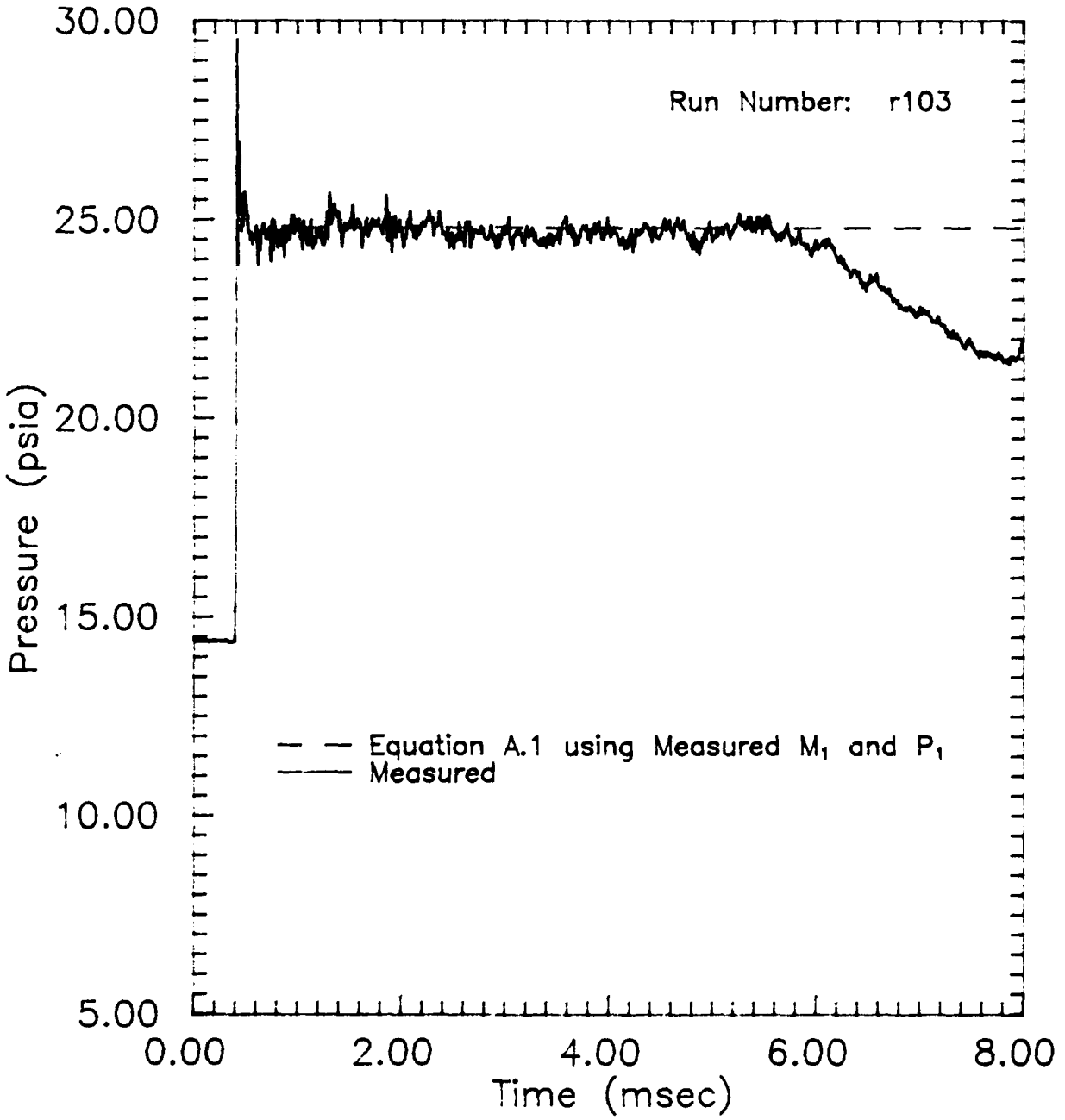

Figure 5.2: Theoretical and Measured Pressure Behind the Normal Shock as a Function of Time

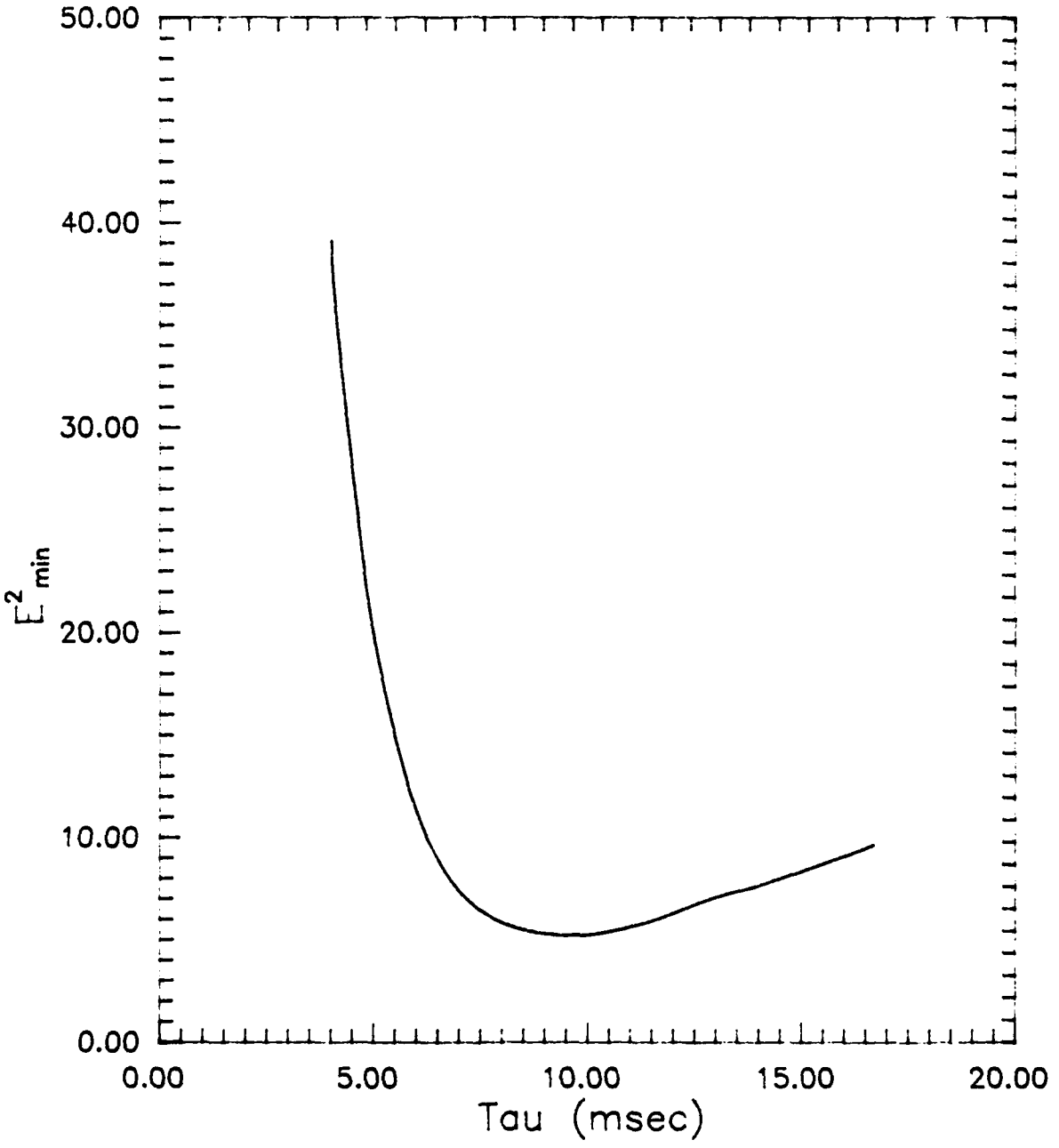

Figure 5.3: Minimum Curve Fit Error as a Function of Time Constant Tau

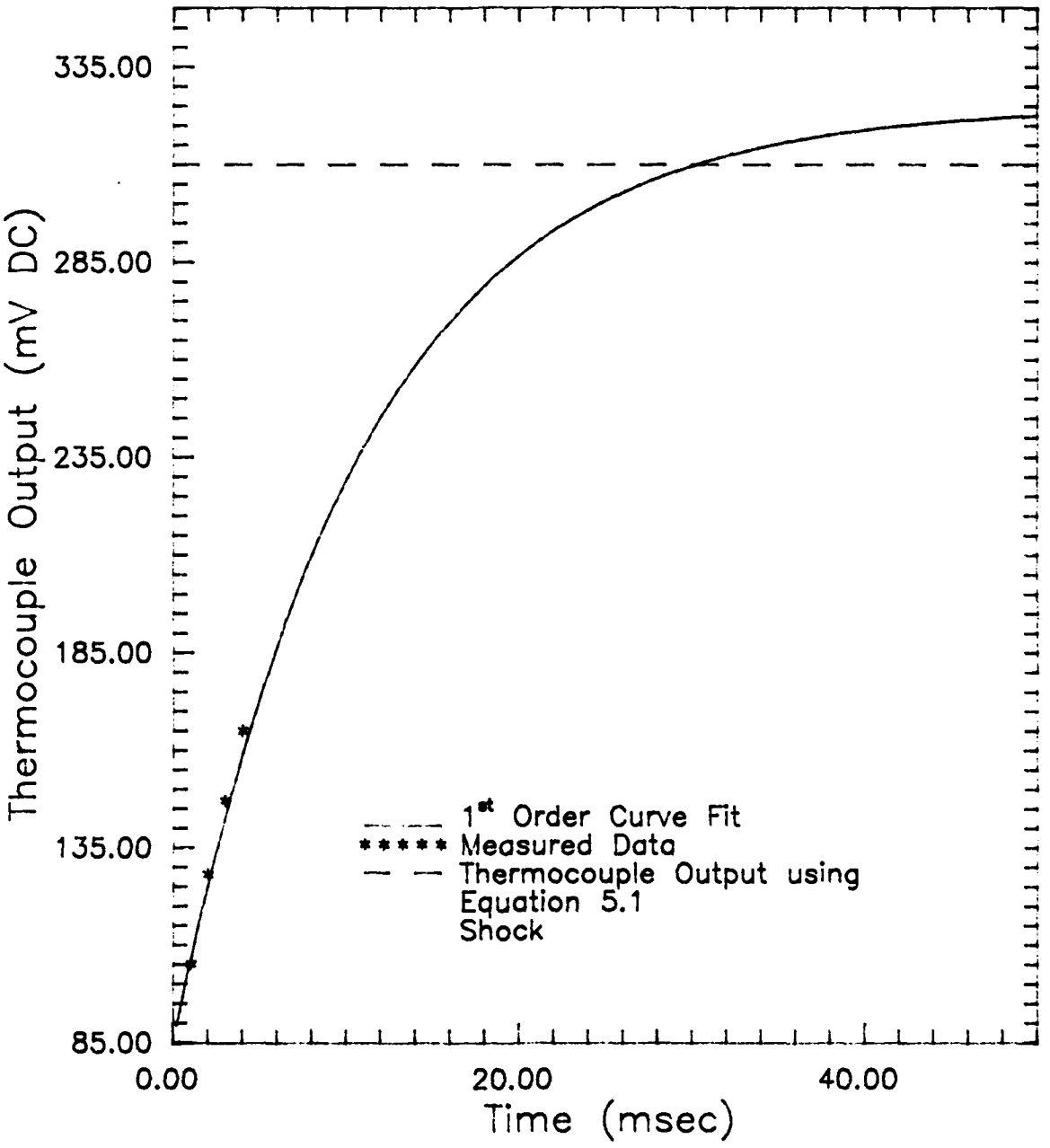

Figure 5.4: Measured and Theoretical Thermocouple Voltage Levels

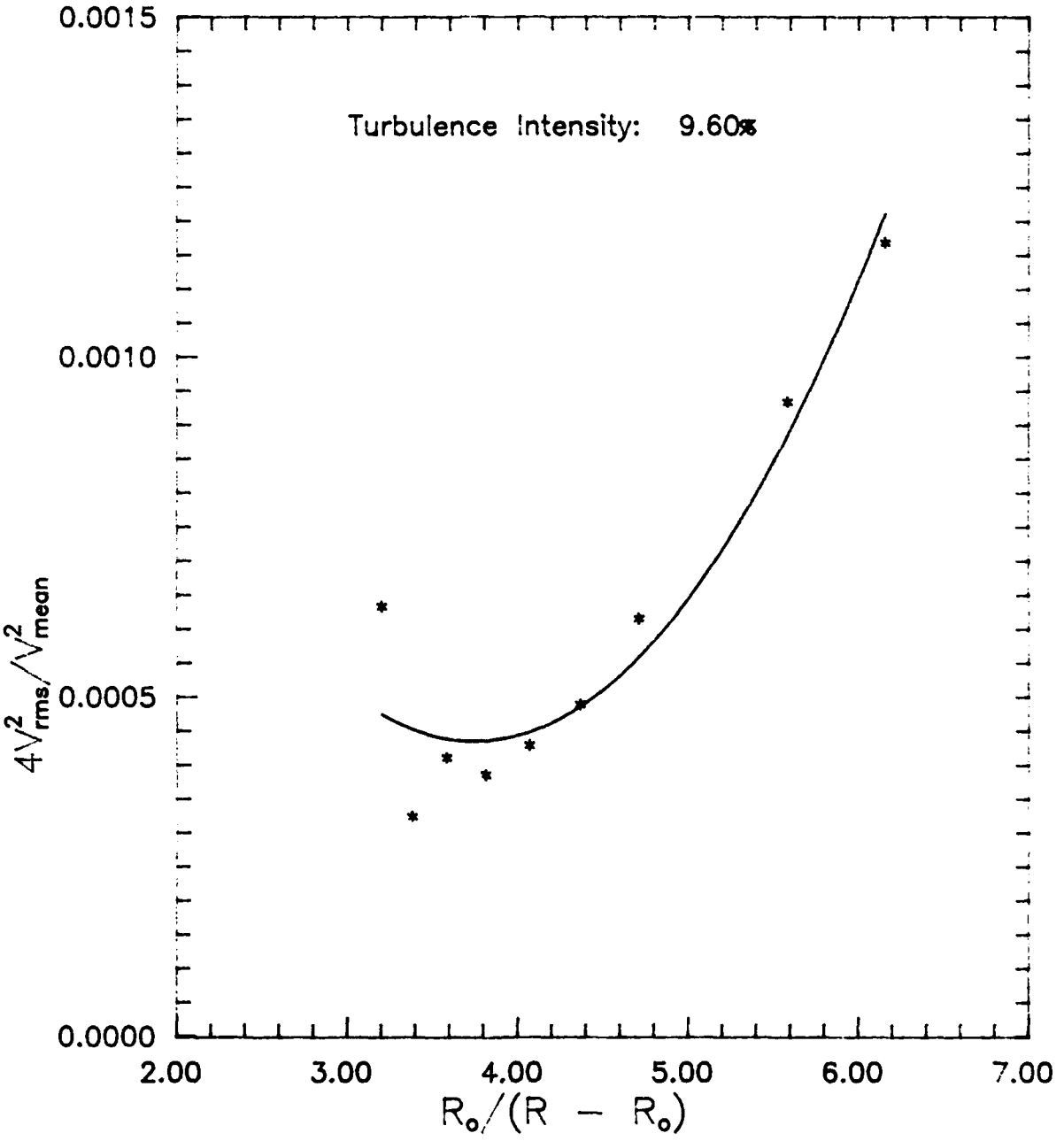

Figure 5.5: Hot-Wire Power Output as a Function of Overheat Parameter, No Turbulence Injection

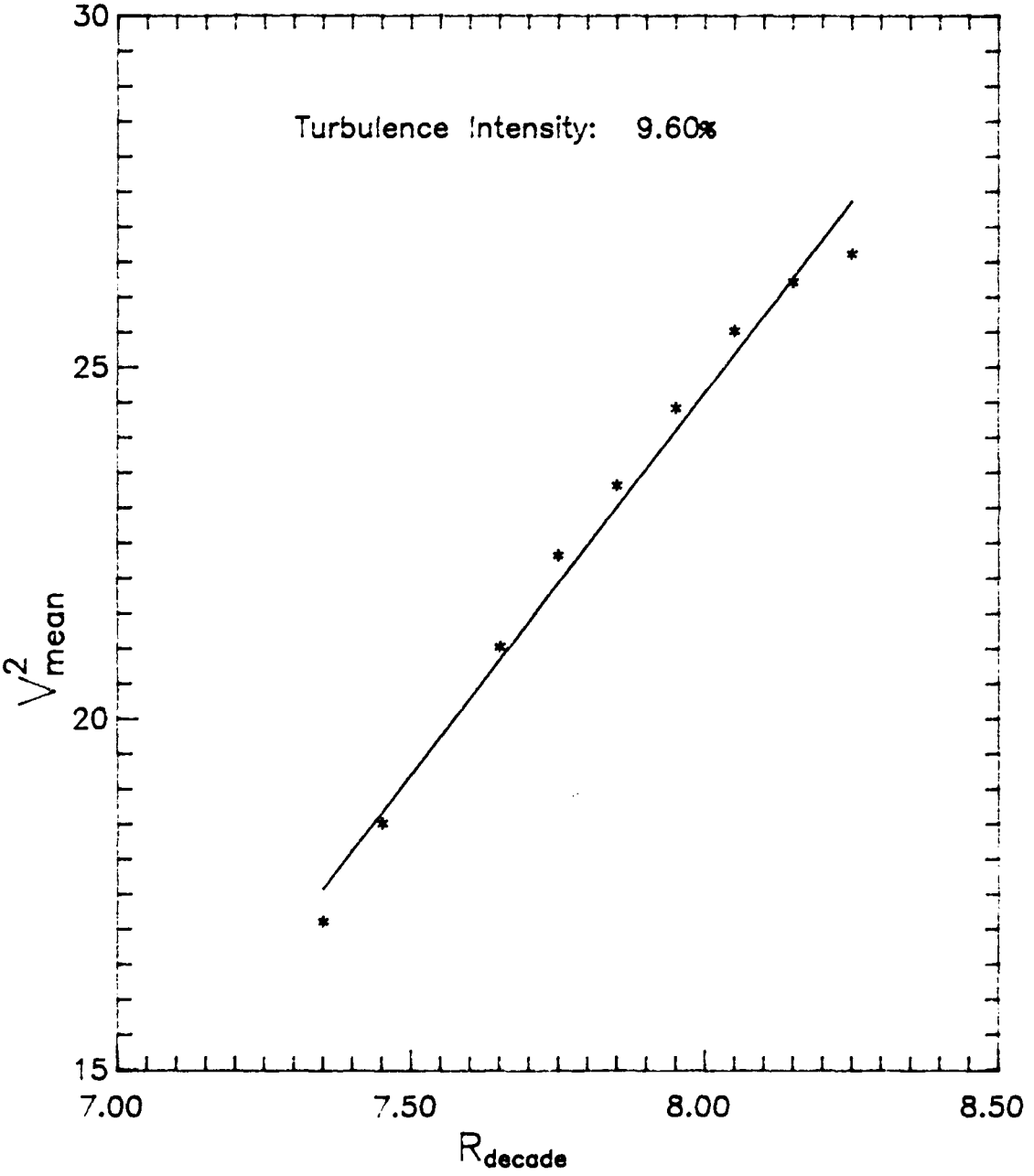

Figure 5.6: Hot-Wire Mean Power Output as a Function of Decade Resistance, No Turbulence Injection

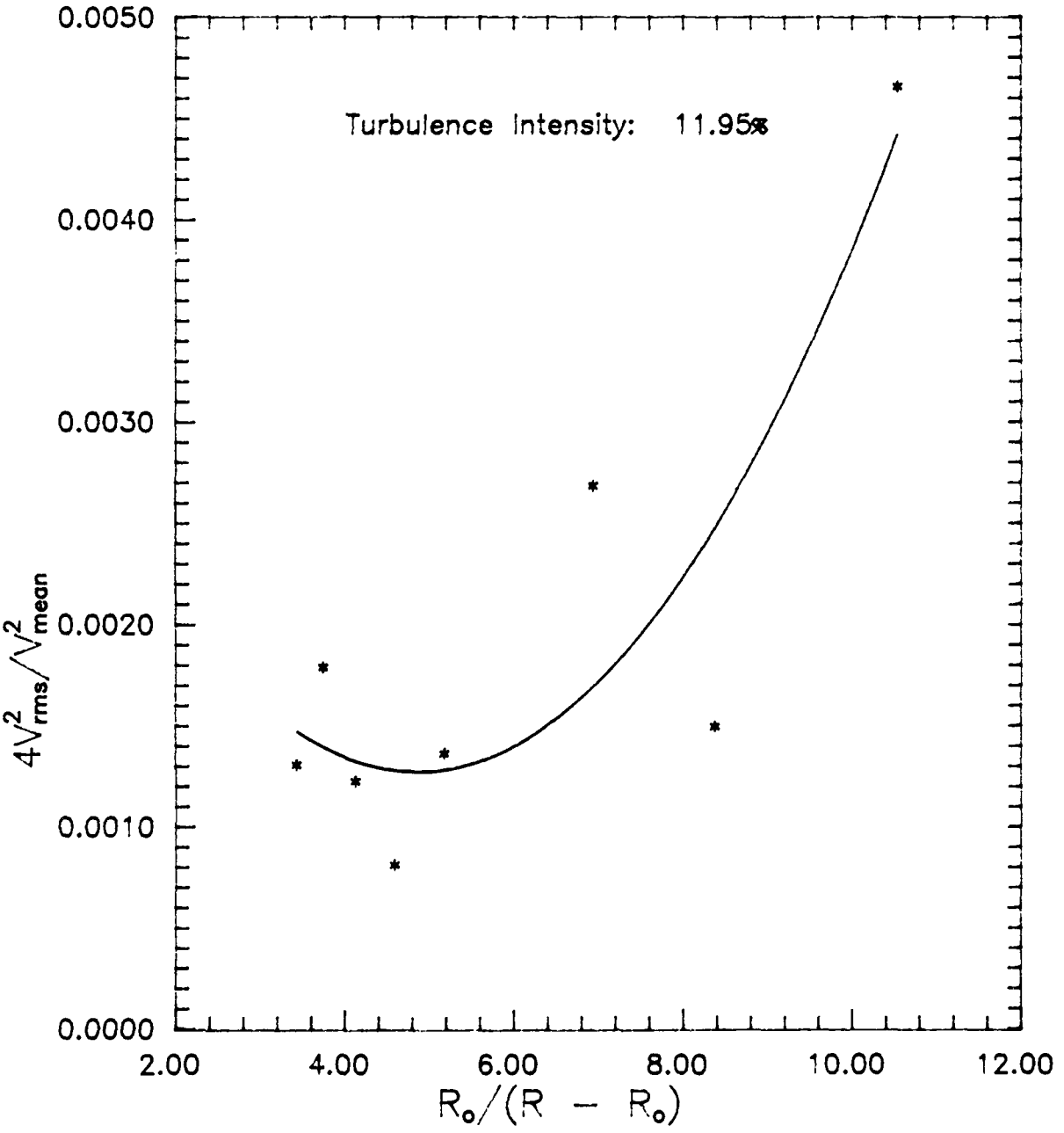

Figure 5.7: Hot-Wire Power Output as a Function of Overheat Parameter, With Turbulence Injection

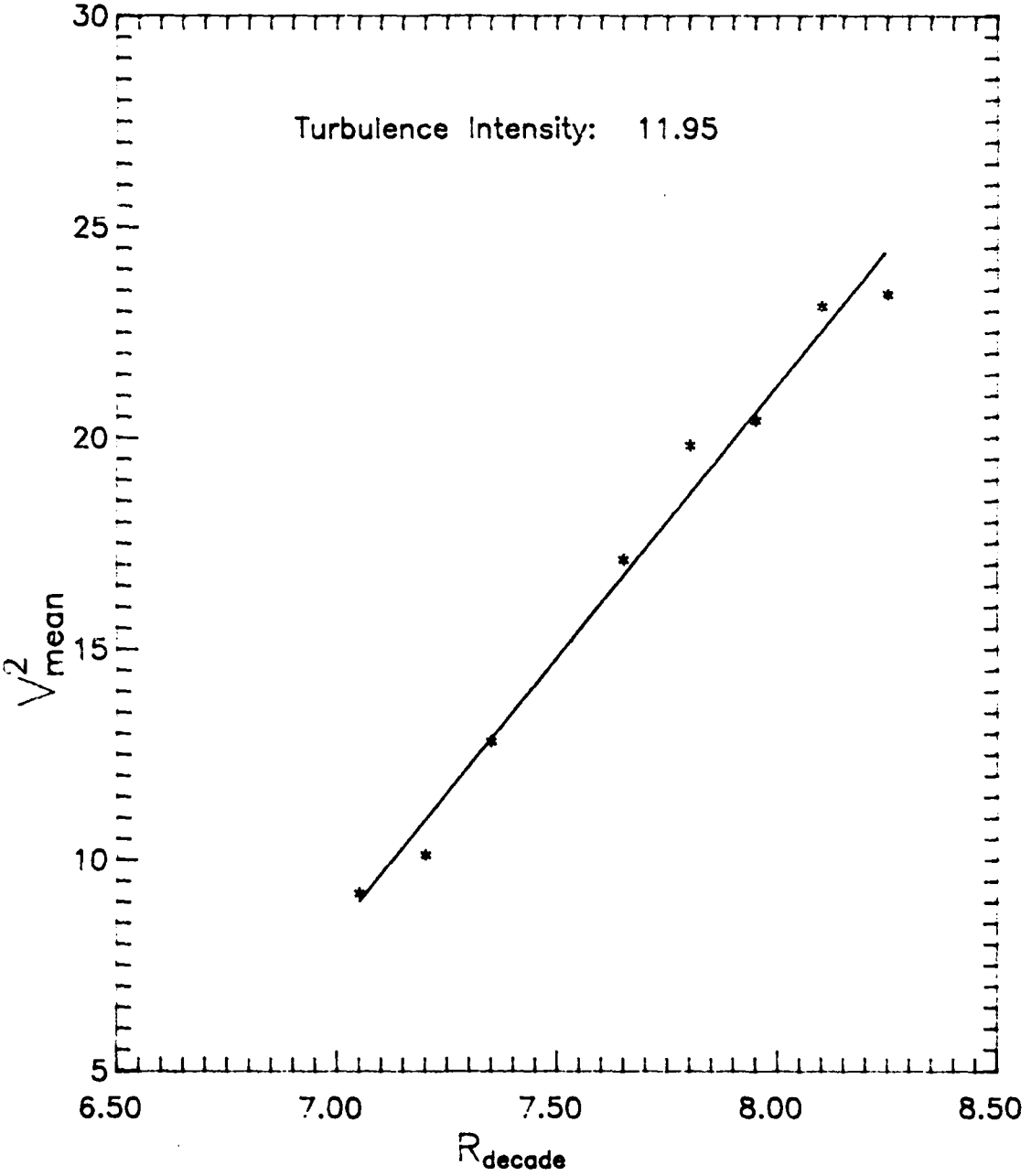

Figure 5.8: Hot-Wire Mean Power Output as a Function of Decade Resistance, With Turbulence Injection

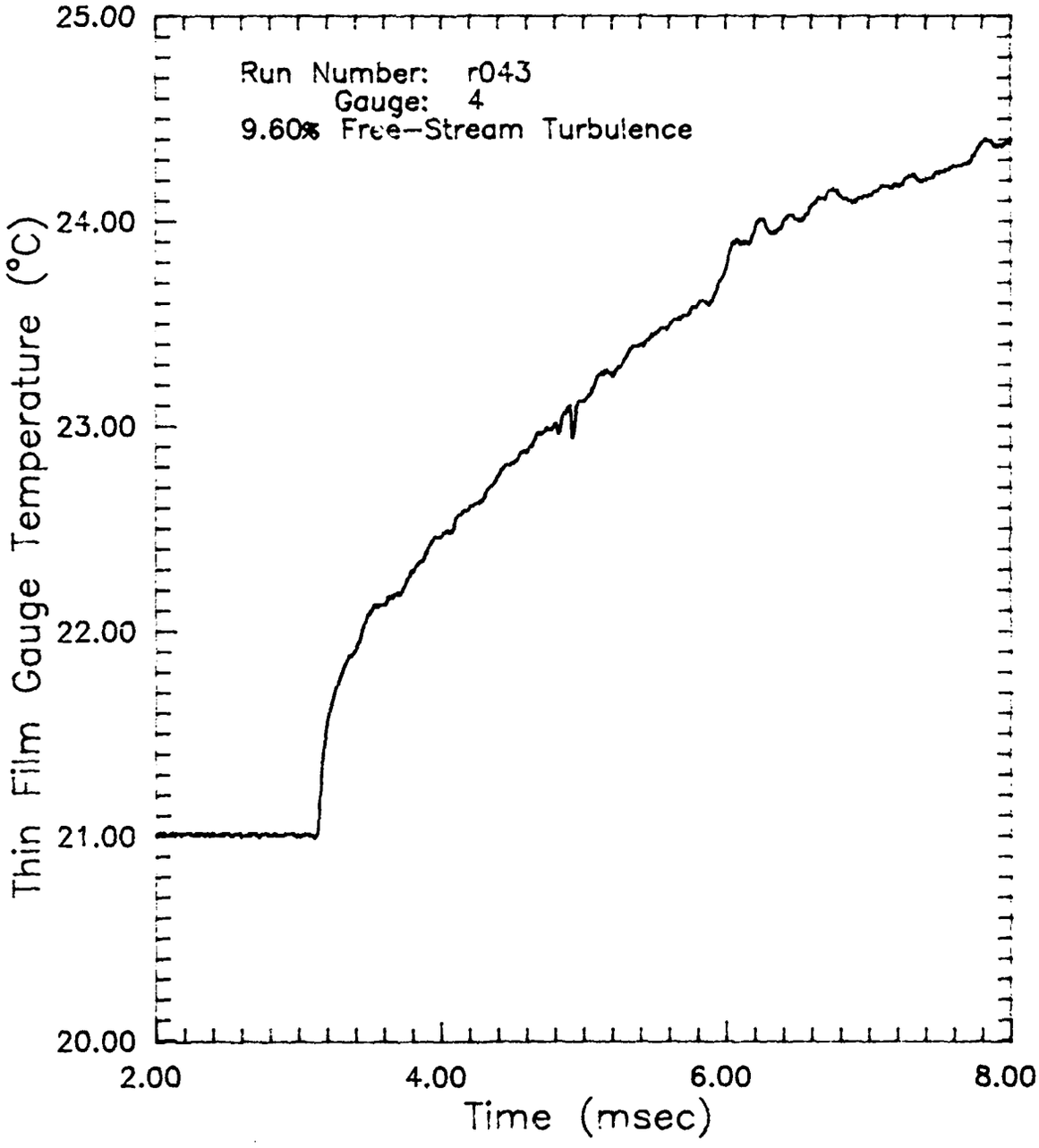

Figure 5.9: Temperature as a function of Time
No Turbulence Injection

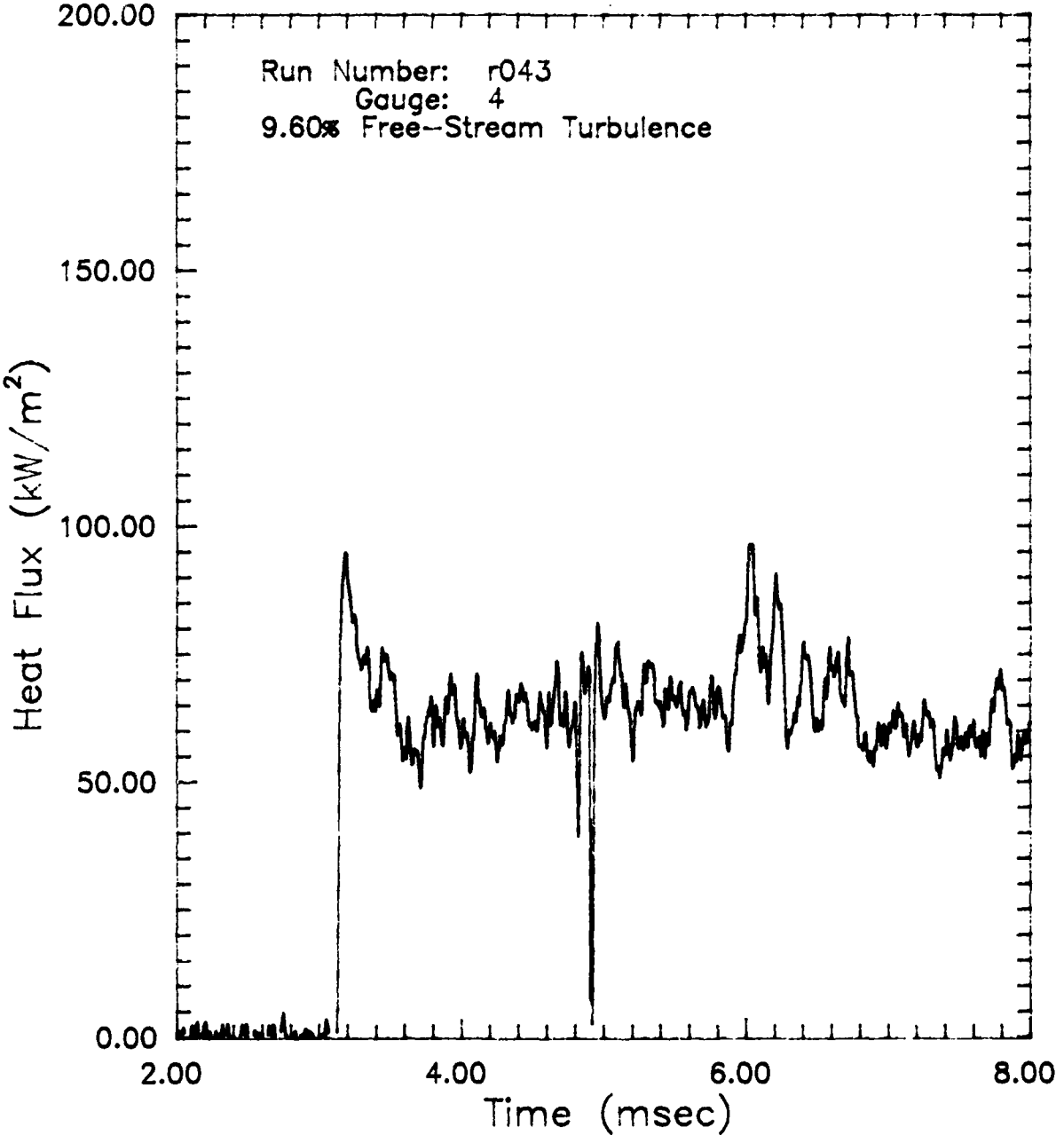

Figure 5.10: Heat Flux as a function of Time
No Turbulence Injection

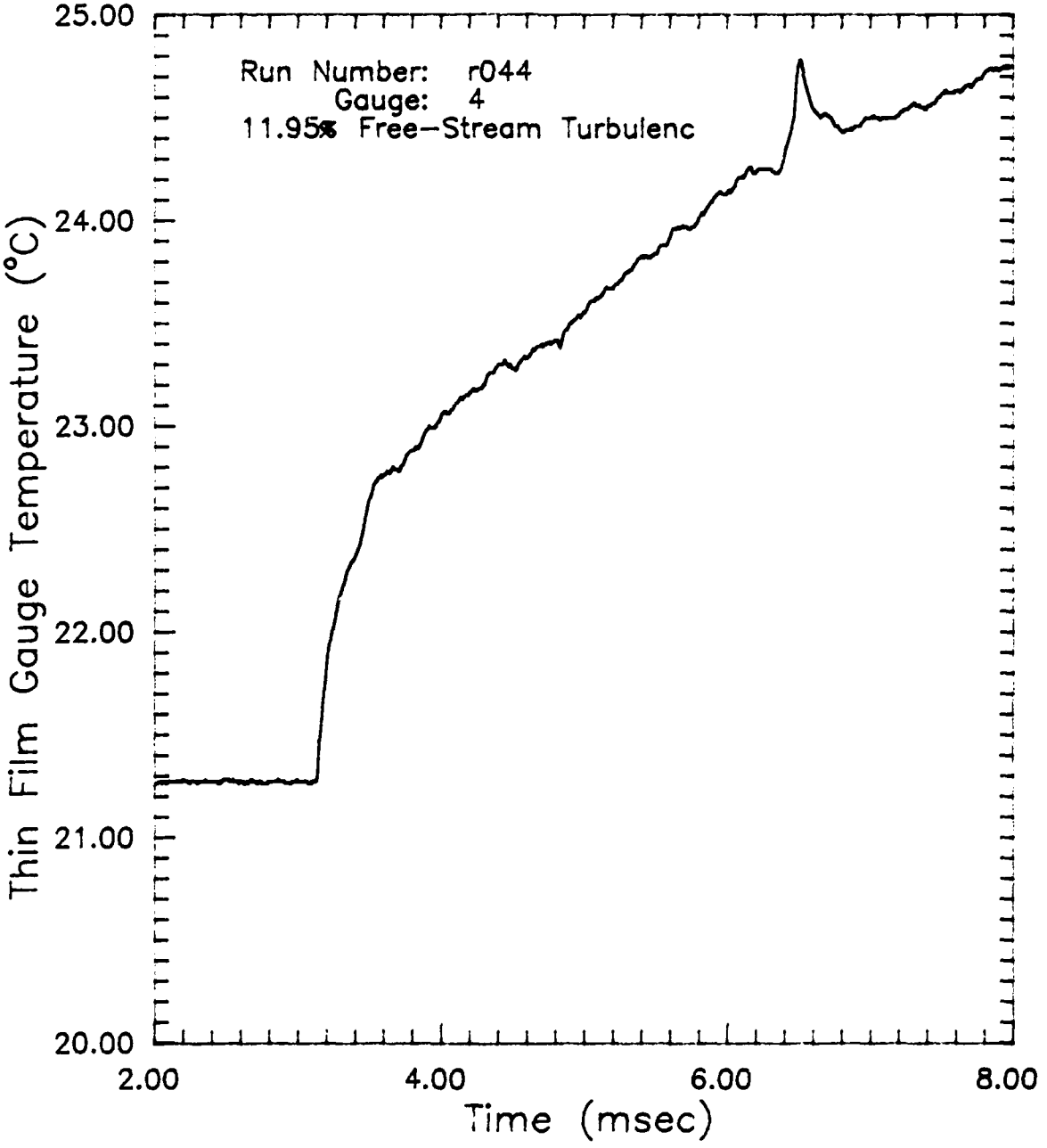

Figure 5.11: Temperature as a function of Time With Turbulence Injection

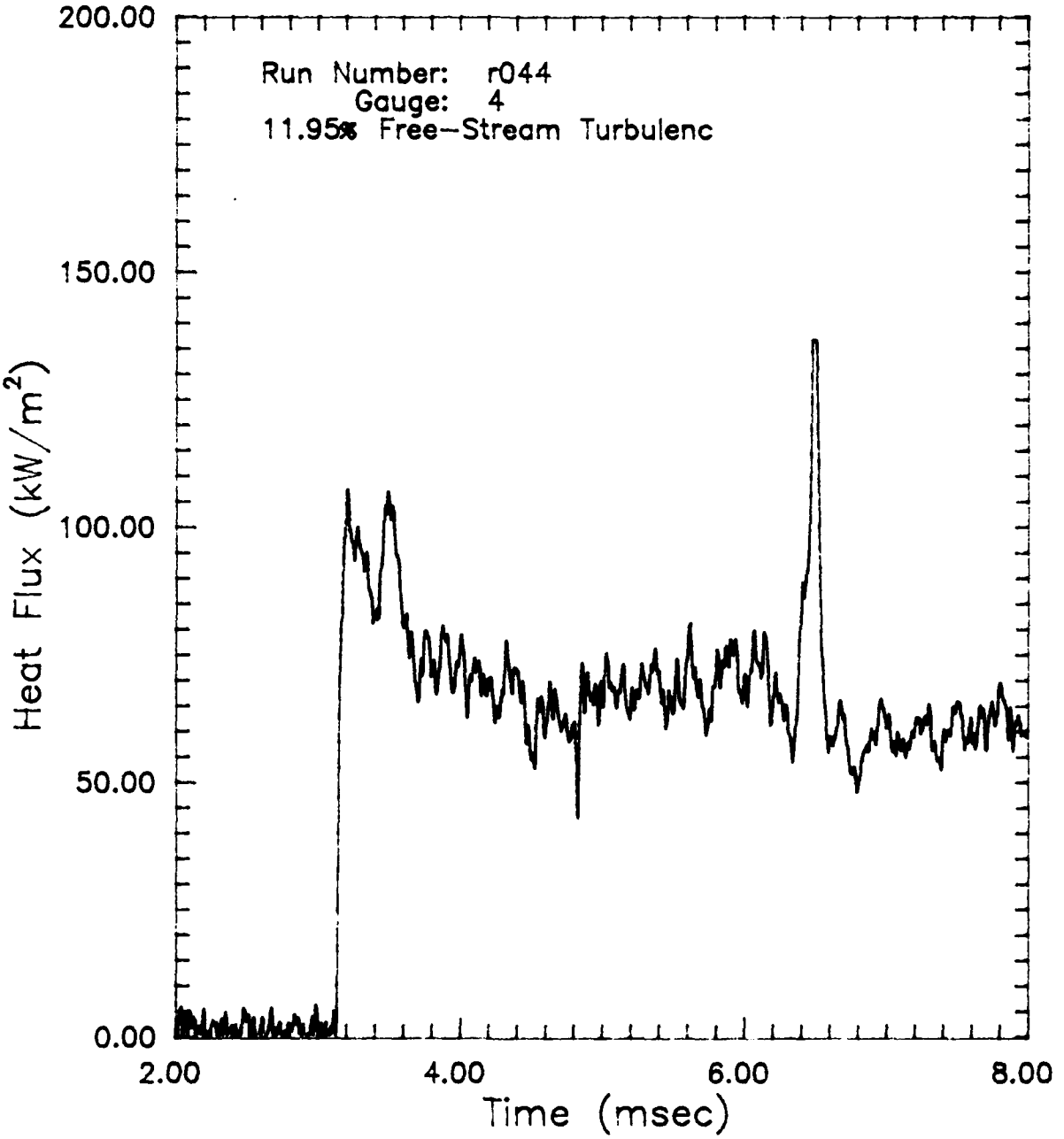

Figure 5.12: Heat Flux as a function of Time With Turbulence Injection

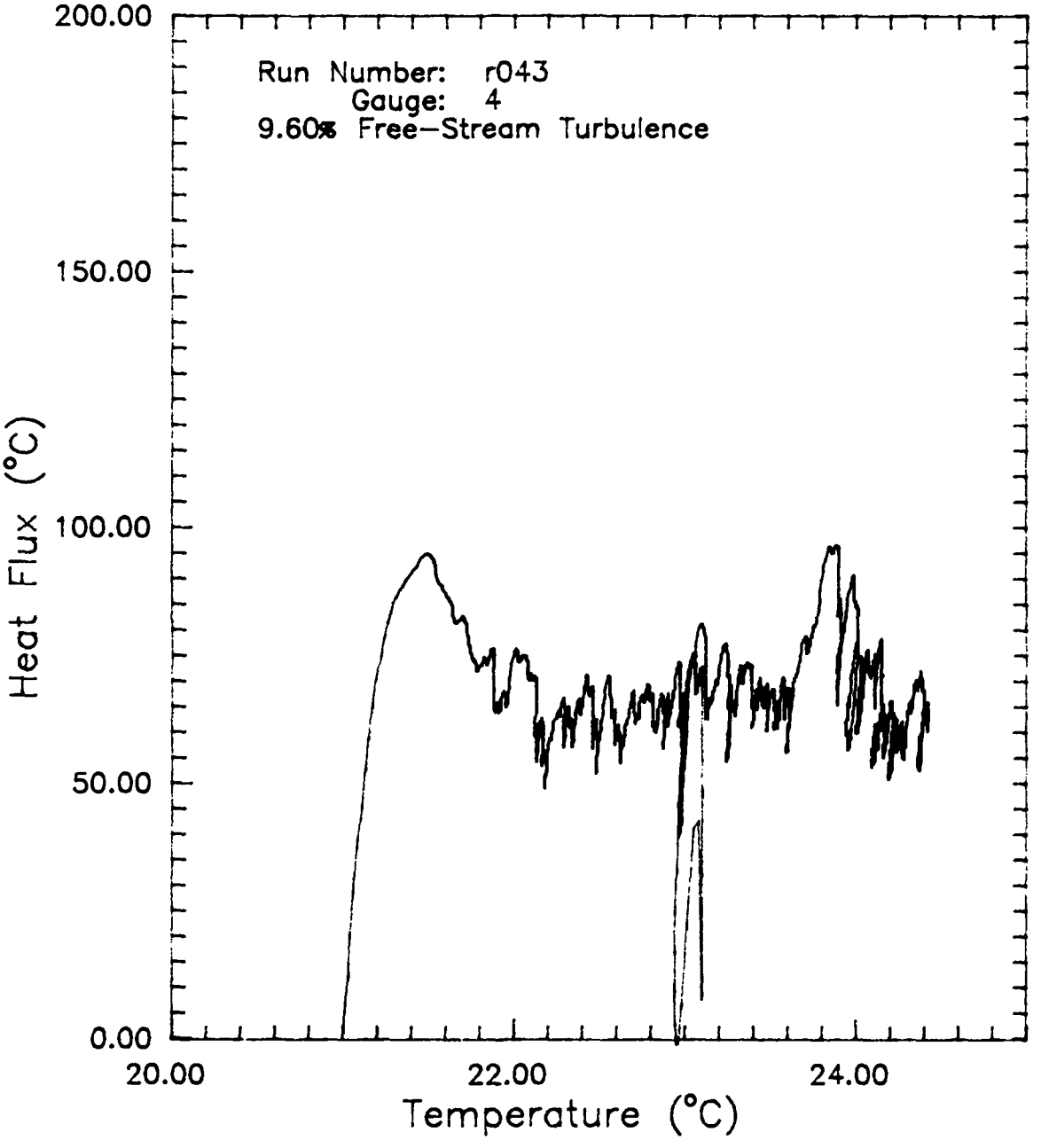

Figure 5.13: Heat Flux as a Function of Thin Film Gauge Temperature, No Turbulence Injection

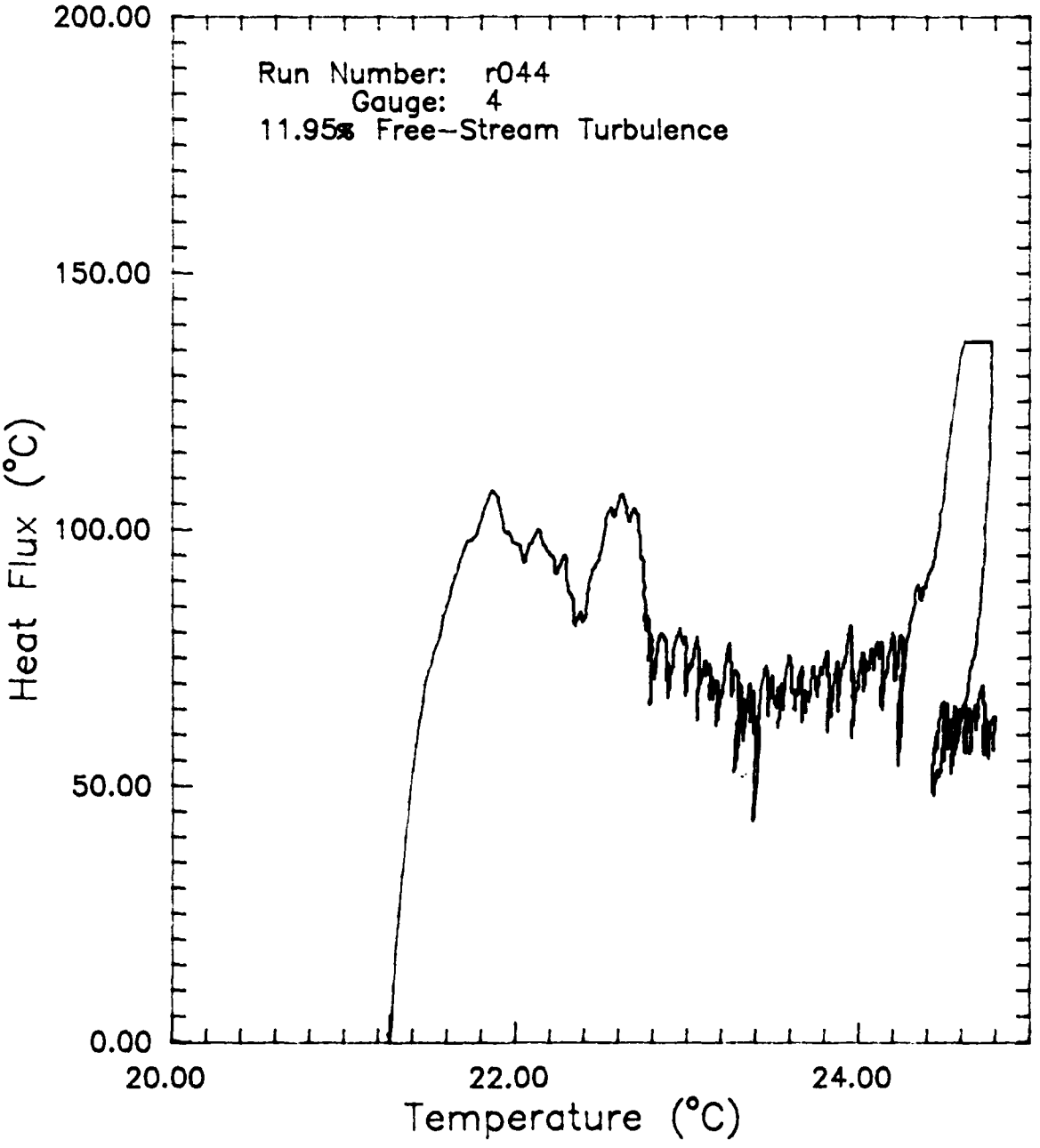

Figure 5.14: Heat Flux as a Function of Thin Film Gauge Temperature, With Turbulence Injection

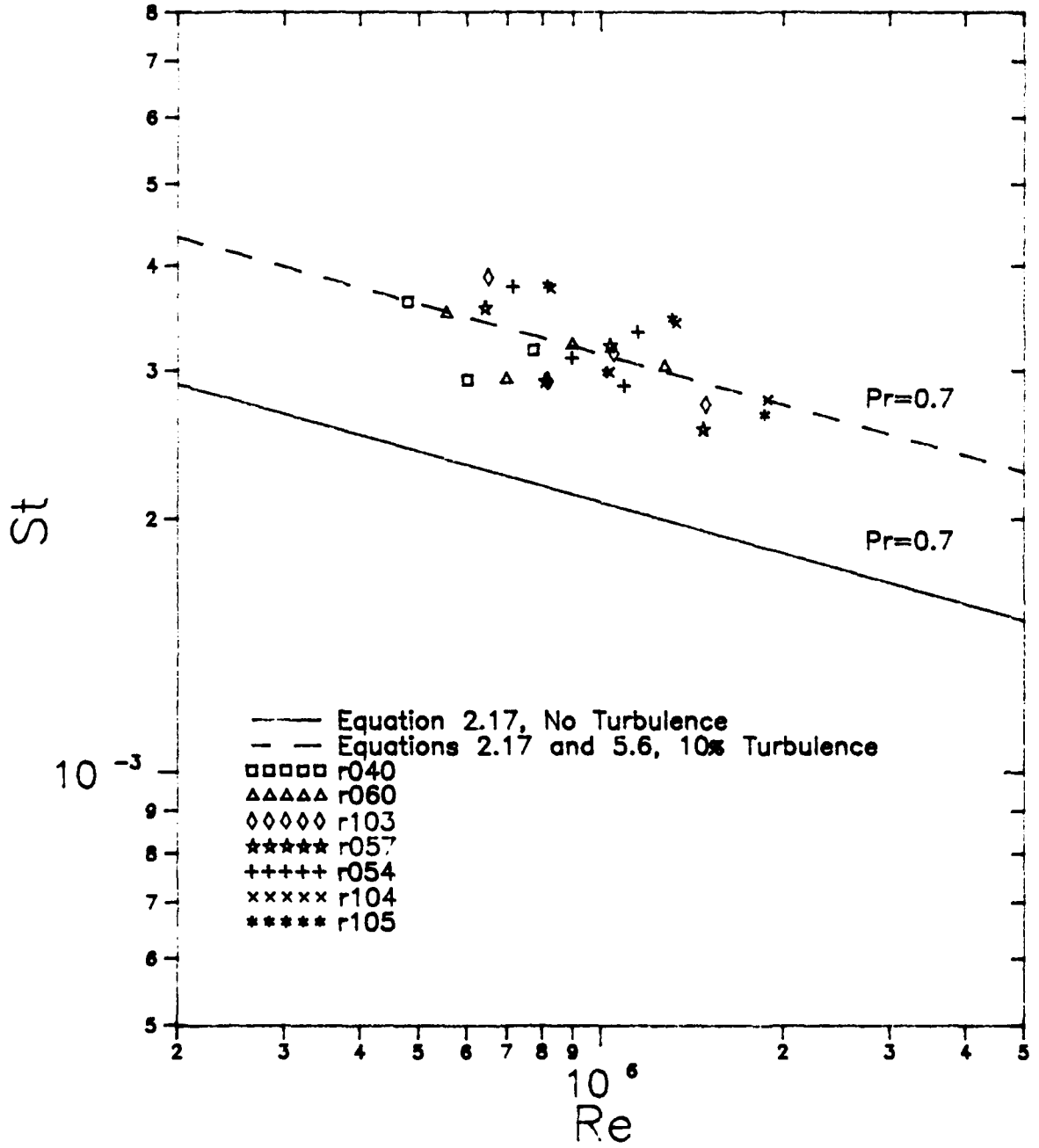

Figure 5.15: Stanton Number as a Function Reynolds Number, No Turbulence Generation

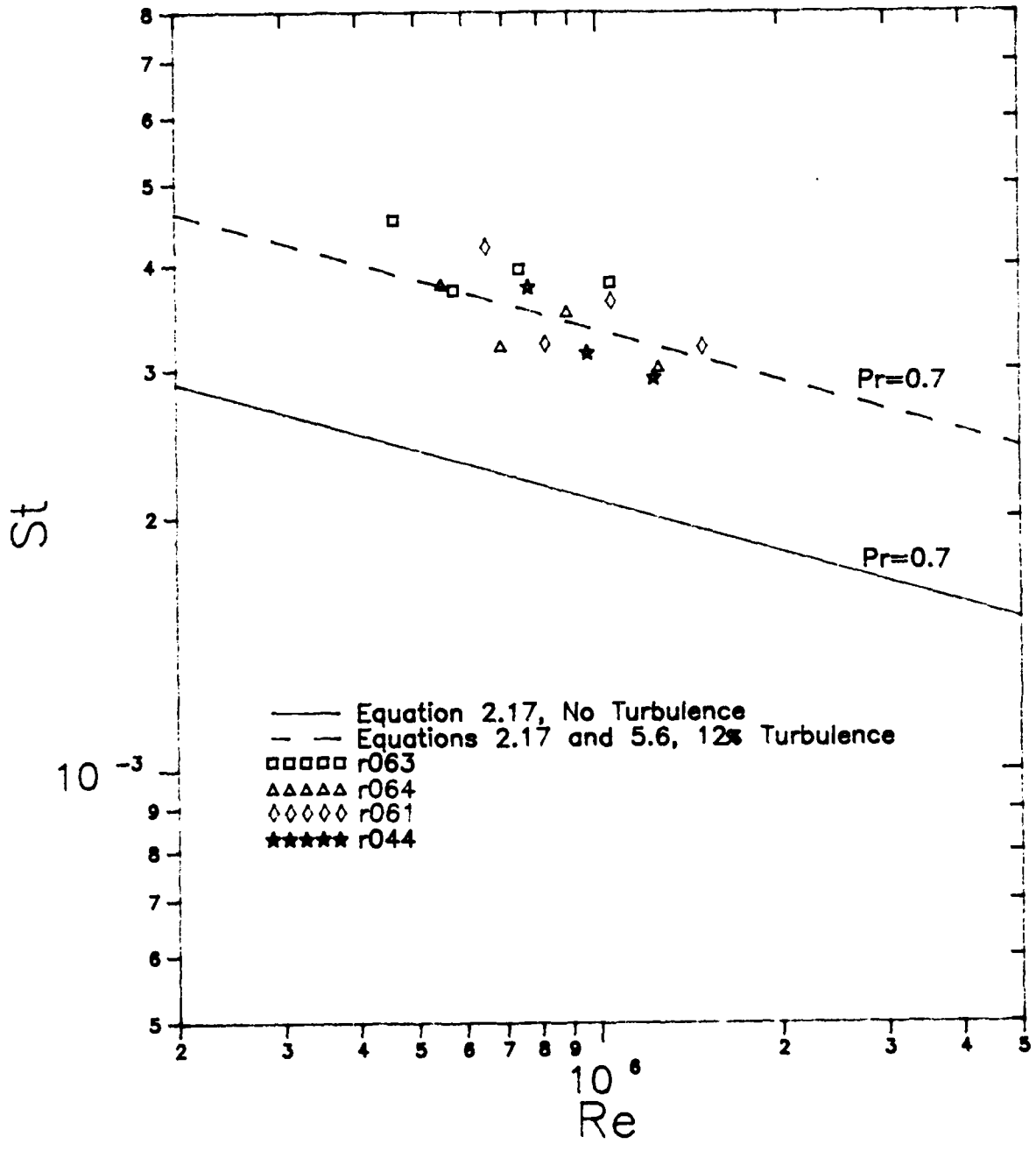

Figure 5.16: Stanton Number as a Function of Reynolds Number, with Turbulence Generation

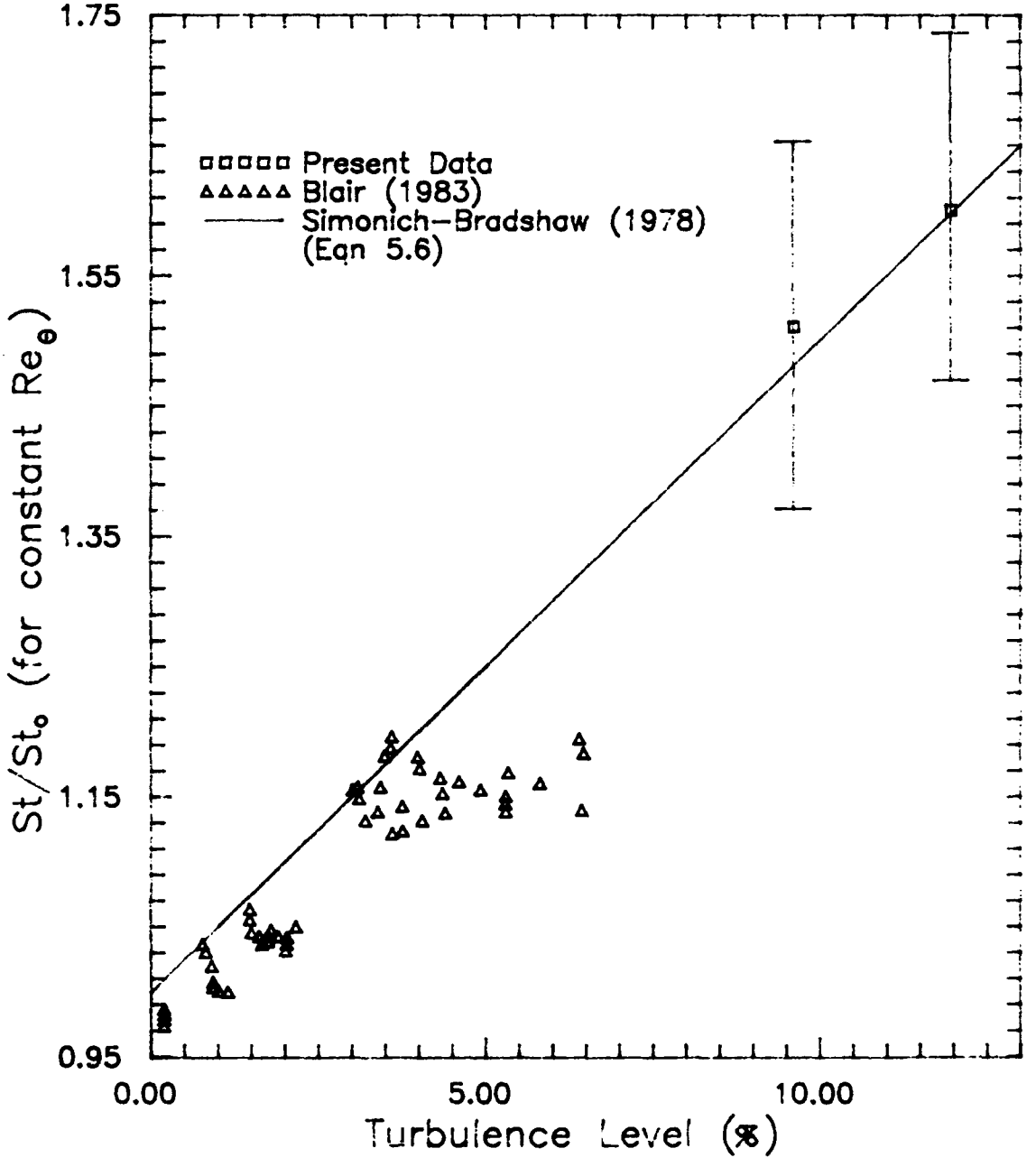

Figure 5.17: St/St$_o$ as a Function of Turbulence Intensity, comparing the Present Data to Blair and Simonich

Appendix A: Shock Tube Performance

Equations relating to shock tube operation and performance from Gaydon [1963: 16-25].

Variable Definitions

- P = Pressure
- T = Temperature
- a = speed of sound
- U = gas speed
- M = Mach number
- γ = ratio of specific heats
- $( )_1$ = Driven section, prior to shock passage
- $( )_2$ = Driven section, after shock passage
- $( )_4$ = Driver section

$$\frac{P_2}{P_1} = \frac{2\gamma M_1^2 - \gamma + 1}{\gamma + 1} \tag{A.1}$$

$$\frac{T_2}{T_1} = \frac{\left(\gamma M_1^2 - \frac{\gamma - 1}{2}\right)\left(\frac{\gamma - 1}{2} M_1^2 + 1\right)}{\left(\frac{\gamma - 1}{2}\right)^2 M_1^2} \tag{A.2}$$

$$\frac{P_4}{P_1} = \frac{P_2}{P_1}\left\{1 - \frac{\gamma_1 - 1}{\gamma_1 + 1}\,\frac{a_1}{a_4}\left(M_1 - \frac{1}{M_1}\right)\right\}^{\frac{2\gamma_4}{\gamma_4 - 1}} \tag{A.3}$$

$$U_2 = \frac{2a_1}{\gamma_1 + 1}\left(M_1 - \frac{1}{M_1}\right) \tag{A.4}$$

Appendix B: Heat Transfer Derivation

The purpose of this derivation is to show that the relationship between heat flux and surface temperature is similar to a one-half derivative, eg

$$Q_s = \tau_s \sqrt{s} \sqrt{(\rho\ C_p k)_2}$$

Where Q and τ are the Laplace transforms of heat flux and temperature, respectively. Refer to Schultz [1973], and Figure B.1.

$$\left.\begin{aligned} -\frac{\partial q}{\partial x} &= \left(\rho\ C_p\right)_1 \frac{\partial T_1}{\partial t} \\ -q &= k_1 \frac{\partial T_1}{\partial x} \end{aligned}\right\} \qquad \frac{\partial^2 T_1}{\partial x^2} = \left(\frac{\rho\ C_p}{k}\right)_1 \frac{\partial T_1}{\partial t} \qquad \text{(B.1)}$$

$$\left.\begin{aligned} -\frac{\partial q}{\partial x} &= \left(\rho\ C_p\right)_2 \frac{\partial T_2}{\partial t} \\ -q &= k_2 \frac{\partial T_2}{\partial x} \end{aligned}\right\} \qquad \frac{\partial^2 T_2}{\partial x^2} = \left(\frac{\rho\ C_p}{k}\right)_2 \frac{\partial T_2}{\partial t} \qquad \text{(B.2)}$$

In general,

$$\alpha \equiv \frac{k}{\rho\ C_p}$$

So, we have

$$\frac{\partial^2 T_1}{\partial x^2} = \frac{1}{\alpha_1} \frac{\partial T_1}{\partial t} \qquad \text{(B.3)}$$

$$\frac{\partial^2 T_2}{\partial x^2} = \frac{1}{\alpha_2} \frac{\partial T_2}{\partial t} \qquad \text{(B.4)}$$

Perform Laplace transform and get,

$$\frac{\partial^2 \tau_1}{\partial x^2} = \frac{1}{\alpha_1} \left(s\tau_1 - T_1(0) \right) \qquad \text{(B.5)}$$

$$\frac{\partial^2 \tau_2}{\partial x^2} = \frac{1}{\alpha_2} \left(s\tau_2 - T_2(0) \right) \qquad \text{(B.6)}$$

From boundary conditions we have

$$T_1(0) = T_2(0) = 0$$

So, we get

$$\frac{\partial^2 \tau_1}{\partial x^2} = \frac{s\tau_1}{\alpha_1} \qquad \text{(B.7)}$$

$$\frac{\partial^2 \tau_2}{\partial x^2} = \frac{s\tau_2}{\alpha_2} \qquad \text{(B.8)}$$

Re-writing,

$$\frac{\partial^2 \tau_1}{\partial x^2} - \frac{s}{\alpha_1} \tau_1 = 0 \qquad \text{(B.9)}$$

$$\frac{\partial^2 \tau_2}{\partial x^2} - \frac{s}{\alpha_2} \tau_2 = 0 \qquad \text{(B.10)}$$

The above equations are recognized as Laplace's equation, the solution of which is well known.

Boundary Conditions:

In the time domain:

$$\text{At the surface,} \quad -k_1 \frac{\partial T_1}{\partial x} = q_s , \qquad x = 0 \tag{B.11}$$

$$\text{Gauge/substrate interface,} \quad -k_1 \frac{\partial T_1}{\partial x} = -k_2 \frac{\partial T_2}{\partial x} , \; T_1 = T_2, \quad x = \ell \tag{B.12}$$

$$\text{Far field conditions,} \quad T_2 \longrightarrow 0 \quad \text{as} \quad x \longrightarrow \infty \tag{B.13}$$

In the Laplace domain:

$$\text{At the surface,} \quad -k_1 \frac{\partial \tau_1}{\partial x} = Q_s , \qquad x = 0 \tag{B.14}$$

$$\text{Gauge/substrate interface,} \quad -k_1 \frac{\partial \tau_1}{\partial x} = -k_2 \frac{\partial \tau_2}{\partial x}, \; \tau_1 = \tau_2, \quad x = \ell \tag{B.15}$$

$$\text{Far field conditions,} \quad \tau_2 \longrightarrow 0 \quad \text{as} \quad x \longrightarrow \infty \tag{B.16}$$

The general solution is:

$$\tau_1 = A\, e^{x\left(\frac{s}{\alpha_1}\right)^{1/2}} + B\, e^{-x\left(\frac{s}{\alpha_1}\right)^{1/2}} \tag{B.17}$$

$$\tau_2 = C\, e^{x\left(\frac{s}{\alpha_2}\right)^{1/2}} + D\, e^{-x\left(\frac{s}{\alpha_2}\right)^{1/2}} \tag{B.18}$$

Since $\tau_2 \longrightarrow 0$ as $x \longrightarrow \infty$, we get

$$C = 0$$

From the surface boundary condition we get

$$Q_s = -k_1 \sqrt{\frac{s}{\alpha_1}} \left(A - B \right) \qquad \text{(B.19)}$$

From the interface boundary condition we get

$$D\, e^{-\ell\left(\frac{s}{\alpha_2}\right)^{1/2}} = A\, e^{\ell\left(\frac{s}{\alpha_1}\right)^{1/2}} + B\, e^{-\ell\left(\frac{s}{\alpha_1}\right)^{1/2}} \qquad \text{(B.20)}$$

and

$$Dk_2\left(\frac{s}{\alpha_2}\right)^{1/2} e^{-\ell\left(\frac{s}{\alpha_2}\right)^{1/2}} = -Ak_1\left(\frac{s}{\alpha_1}\right)^{1/2} e^{\ell\left(\frac{s}{\alpha_1}\right)^{1/2}} + Bk_1\left(\frac{s}{\alpha_1}\right)^{1/2} e^{-\ell\left(\frac{s}{\alpha_1}\right)^{1/2}} \qquad \text{(B.21)}$$

Solve for D from (A.20) to get

$$D = A\, e^{\left\{\ell\left(\frac{s}{\alpha_1}\right)^{1/2} + \ell\left(\frac{s}{\alpha_2}\right)^{1/2}\right\}} + B\, e^{-\left\{\ell\left(\frac{s}{\alpha_1}\right)^{1/2} + \ell\left(\frac{s}{\alpha_2}\right)^{1/2}\right\}} \qquad \text{(B.22)}$$

Recall

$$\alpha = \frac{k}{\rho\, C_p}$$

So

$$\frac{k_1}{k_2}\left(\frac{\alpha_2}{\alpha_1}\right)^{1/2} = \left\{ \frac{(\rho\, k\, C_p)_1}{(\rho\, k\, C_p)_2} \right\}^{1/2}$$

For convenience, let

$$b = \left(\frac{s}{\alpha_1}\right)^{1/2} + \left(\frac{s}{\alpha_2}\right)^{1/2} \qquad \text{(B.23)}$$

and let

$$a = \left\{ \frac{(\rho\ k\ C_p)_1}{(\rho\ k\ C_p)_2} \right\}^{1/2} \qquad \text{(B.24)}$$

Re-writing (B.21) and combining with (B.23) and (B.24) yields

$$D = a \left\{ -A\ e^{\ell\ b} + B\ e^{-\ell\ b} \right\} \qquad \text{(B.25)}$$

Now, re-write (B.22)

$$D = A\ e^{\ell\ b} + B\ e^{-\ell\ b} \qquad \text{(B.26)}$$

Combining (B.25) and (B.26) yields

$$a \left\{ -A\ e^{\ell\ b} + B\ e^{-\ell\ b} \right\} = A\ e^{\ell\ b} + B\ e^{-\ell\ b} \qquad \text{(B.27)}$$

Re-writing, get

$$A\ e^{\ell\ b}(1+a) + B\ e^{-\ell\ b}(1-a) = 0 \qquad \text{(B.28)}$$

Solving for A, get

$$A = -B\ e^{-2\ell\ b}\ \frac{1-a}{1+a} \qquad \text{(B.29)}$$

Substituting (B.29) into (B.19)

$$Q_s = B\ k_1 \left(\frac{s}{\alpha_1}\right)^{1/2} \left(e^{-2\ell\ b}\ \frac{1-a}{1+a} + 1 \right) \qquad \text{(B.30)}$$

Solving for B, get

$$B = \frac{Q_s \Big/ \sqrt{s\ (\rho\ C_p\ k)}_1}{e^{-2\ell\ b\ \frac{1-a}{1+a}} + 1} \qquad (B.31)$$

Substitute into (B.29) and solve for A

$$A = \frac{Q_s \Big/ \sqrt{s\ (\rho\ C_p\ k)}_1}{e^{-2\ell\ b\ \frac{1-a}{1+a}} + 1}\ e^{-2\ell\ b\ \frac{1-a}{1+a}} \qquad (B.32)$$

Substitute (B.31) and (B.32) into (B.22), get

$$D = \frac{Q_s \Big/ \sqrt{s\ (\rho\ C_p\ k)}_1}{e^{-2\ell\ b\ \frac{1-a}{1+a}} + 1} \left\{ e^{-\ell\ b\ \frac{1-a}{1+a}} + e^{-2\ell\ b} \right\} \qquad (B.33)$$

Substitute (B.29) into (B.17) and get the film temperature

$$\tau_1 = B \left\{ -e^{-2\ell\ b\ \frac{1-a}{1+a}}\ e^{x\left(\frac{s}{\alpha_1}\right)^{1/2}} + e^{-x\left(\frac{s}{\alpha_1}\right)^{1/2}} \right\} \qquad (B.34)$$

Set x=0 to get the surface temperature

$$\tau_s = B \left\{ -e^{-2\ell\ b\ \frac{1-a}{1+a}} + 1 \right\} \qquad (B.35)$$

Substitute (B.31) into (B.35) and get

$$\tau_s = \frac{Q_s \Big/ \sqrt{s\ (\rho\ C_p\ k)}_1}{e^{-2\ell\ b\ \frac{1-a}{1+a}} + 1} \left\{ -e^{-2\ell\ b\ \frac{1-a}{1+a}} + 1 \right\} \qquad (B.36)$$

Neglecting the effects of the film is essentially setting ℓ=0. So, get

$$\tau_s = \frac{Q_s \sqrt{s\ (\rho\ C_p\ k)_1}}{\frac{1-a}{1+a} + 1} \left\{ -\frac{1-a}{1+a} + 1 \right\} \qquad \text{(B.37)}$$

Reducing, get

$$\tau_s = \frac{Q_s}{(s\ \rho\ C_p k)_1^{1/2}} \frac{\left(\frac{-1 + a + 1 + a}{1 + a} \right)}{\left(\frac{1 - a + 1 + a}{1 + a} \right)} \qquad \text{(B.38)}$$

$$\tau_s = \frac{Q_s}{(s\ \rho\ C_p k)_1^{1/2}} \frac{2a}{2} \qquad \text{(B.39)}$$

Finally, recalling the definition of a,

$$Q_s = \tau_s \sqrt{s} \sqrt{(\rho\ C_p k)_2} \qquad \text{(B.40)}$$

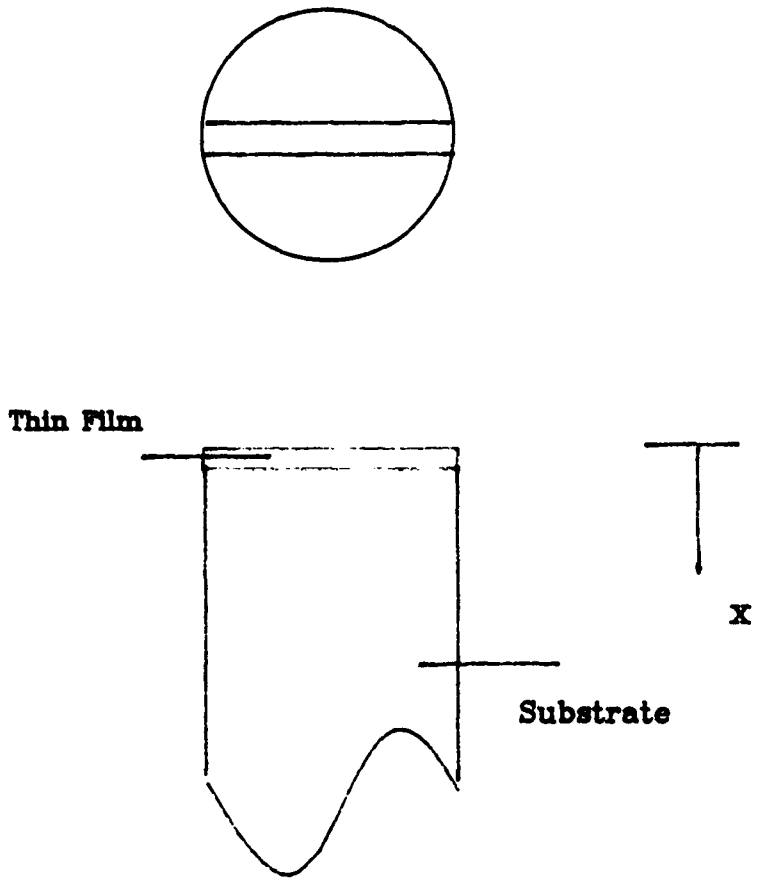

Figure B.1: A Thin Film Gauge

Appendix C: Fluid Properties Curve Fits

A second order polynomial curve fit was performed for the dynamic viscosity and thermal conductivity of air as functions of temperature from 300 K to 400 K. The data was taken from Kays and Crawford [1980: 388]. The curve fits and original data are plotted in Figures C.1 and C.2. The equations for the curve fits are:

$$\mu = -2.82188 \times 10^{-11} T^2 + 6.39988 \times 10^{-8} T + 1.84214 \times 10^{-6}$$

$$k = -3.21349 \times 10^{-4} T^2 + 1.02501 \times 10^{-4} T - 4.77789 \times 10^{-8}$$

Where,

T is in K

μ is in Pa sec

k is in Watt/(m K)

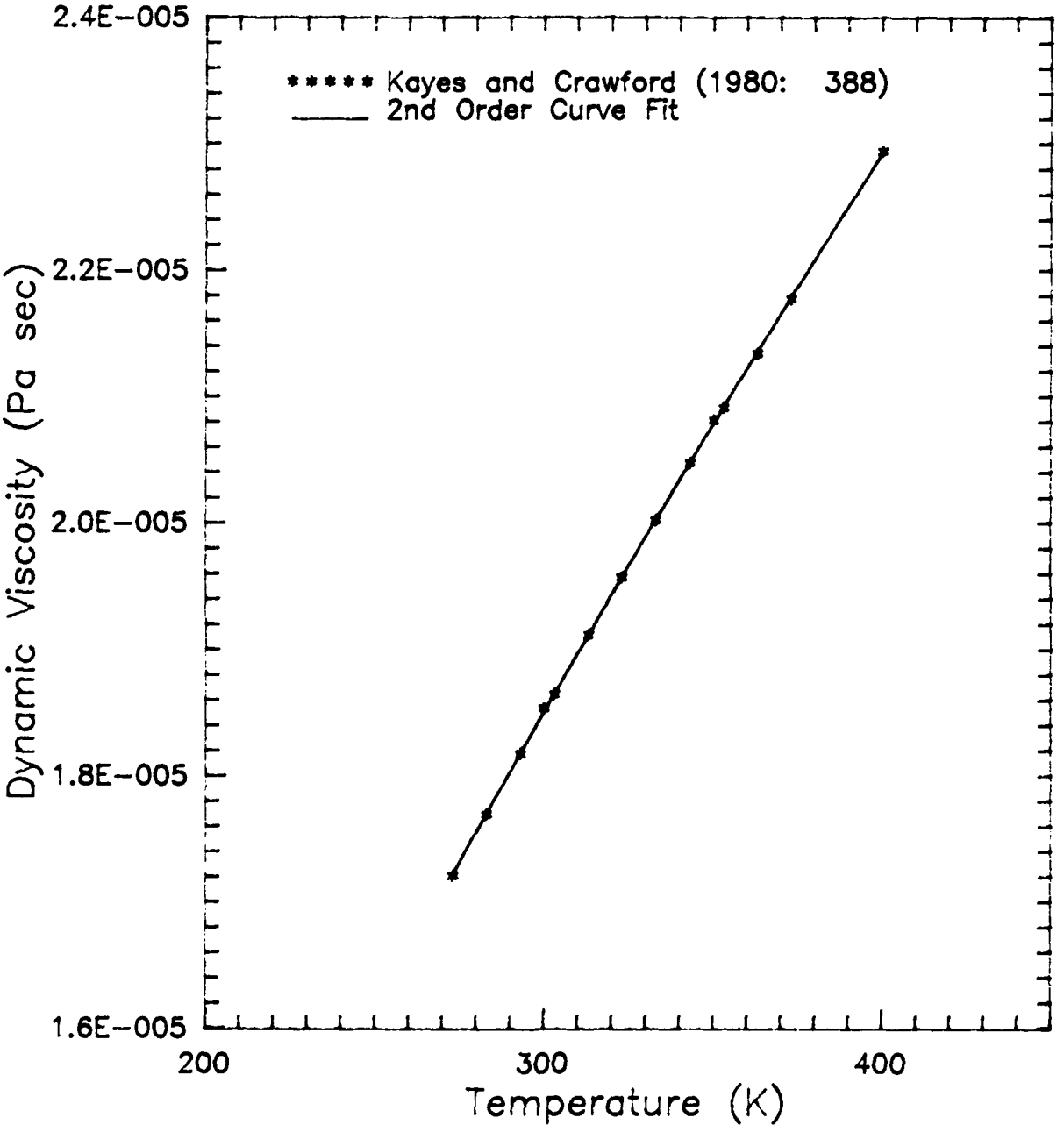

Figure C.1: Dynamic Viscosity as a Function of Temperature

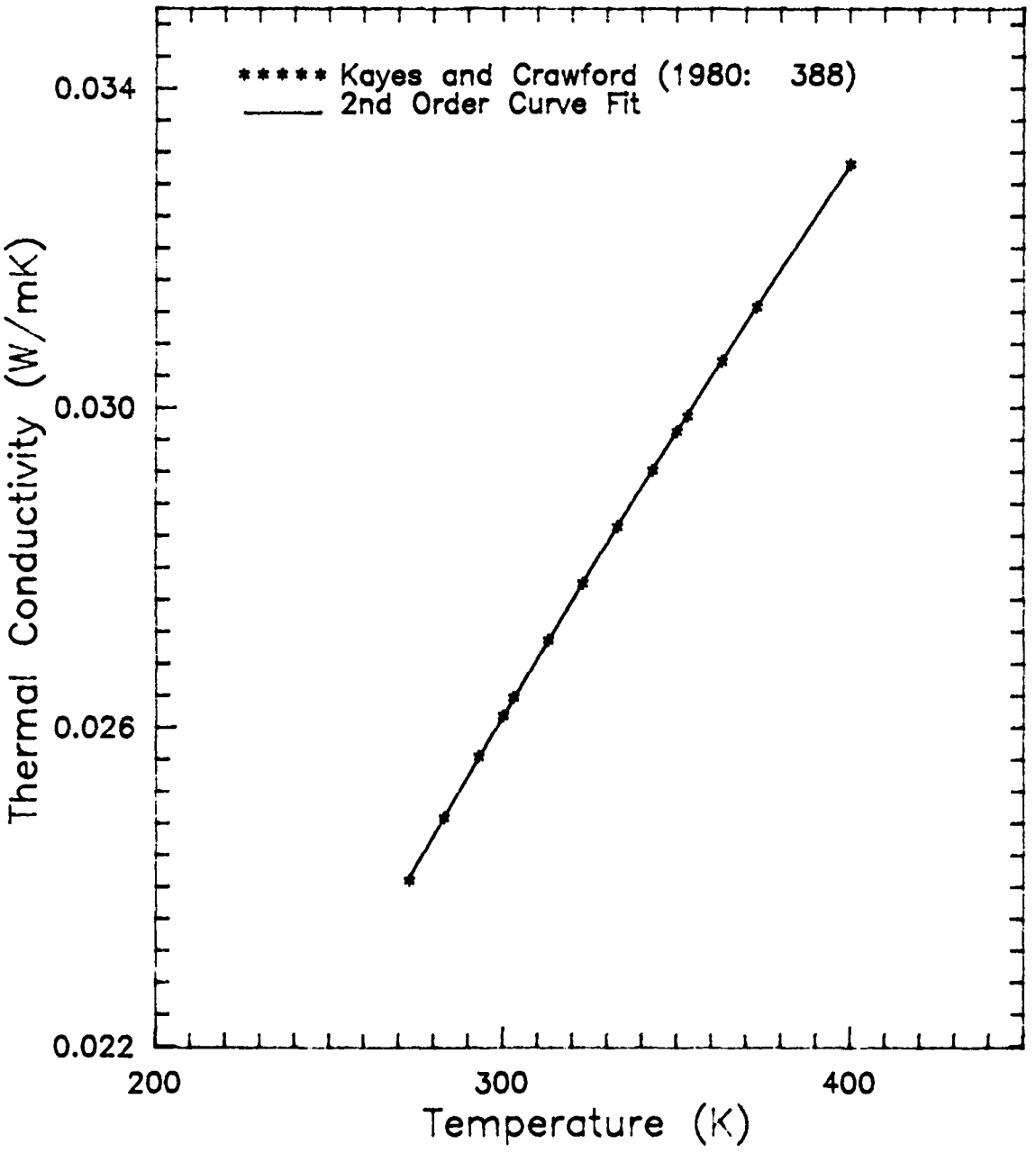

Figure C.2: Thermal Conductivity as a Function of Temperature

APPENDIX D: THIN FILM GAUGE CALIBRATION

The seven thin film gauges used for this heat transfer study were calibrated for output voltage as a function of temperature. The heat flux gauges were connected to the PSC amplifiers, just as the gauges would be used for the heat flux measurements, and the amplifier output was plotted as a function of gauge temperature. The calibration was accomplished by placing each thin film gauge in a plastic bag. The bag was then placed in a water bath, for which the temperature could be easily regulated. The water was constantly stirred, using a magnetic stirring device, to keep the water at uniform temperature. The calibration results are presented in Figures D.1 to D.4.

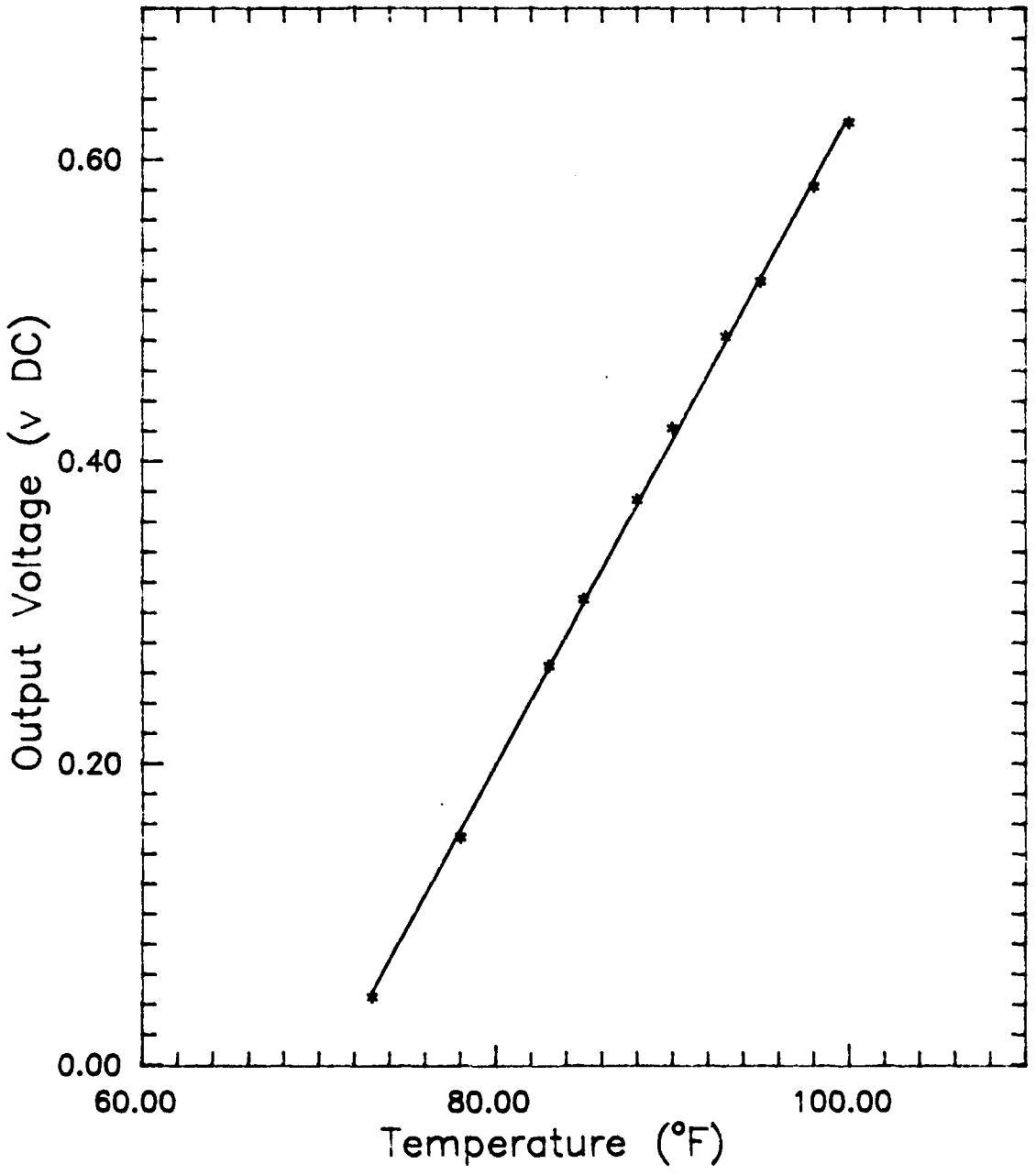

Figure D.1: Heat Flux Gauge 1 Calibration

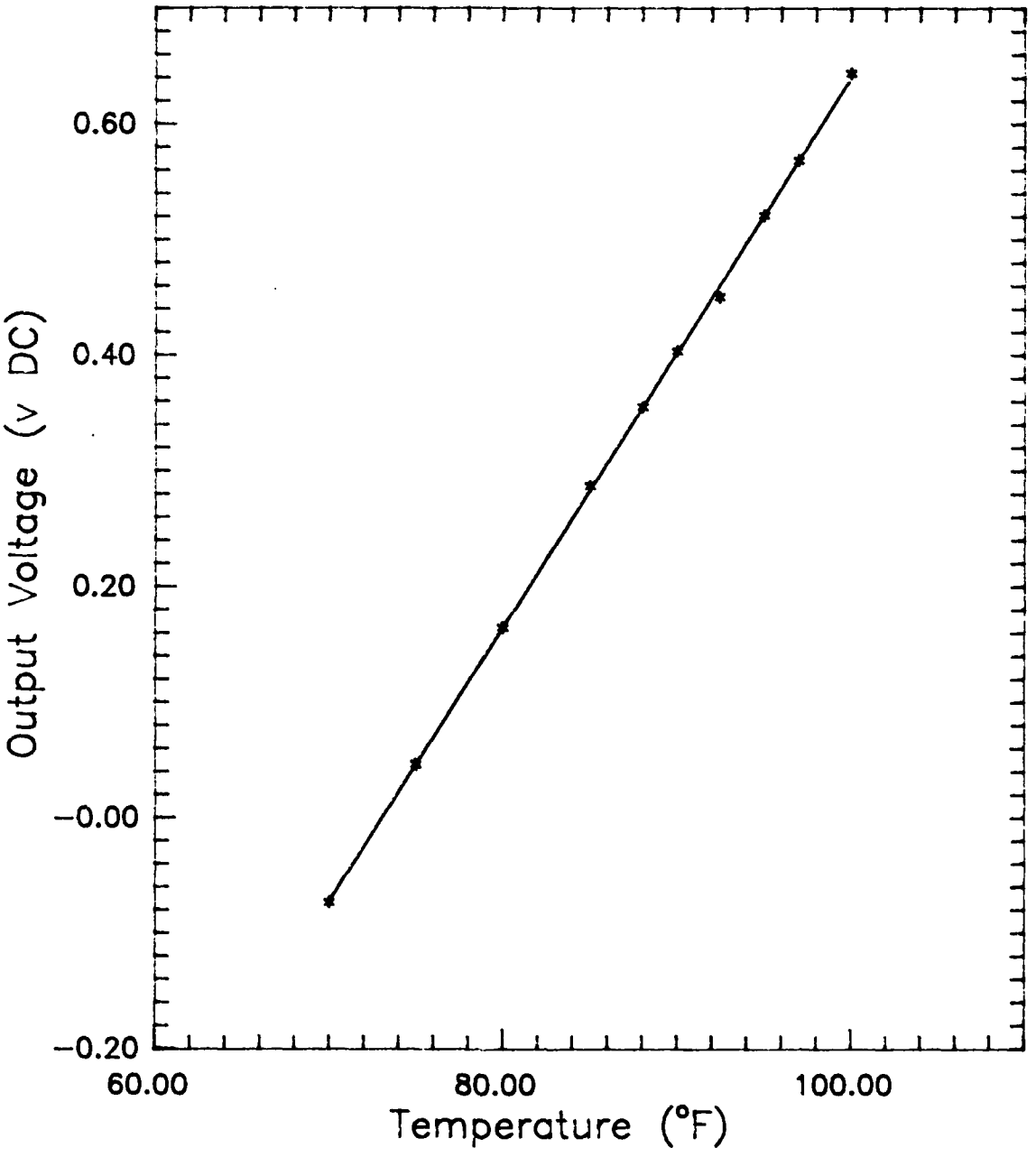

Figure D.2: Heat Flux Gauge 4 Calibration

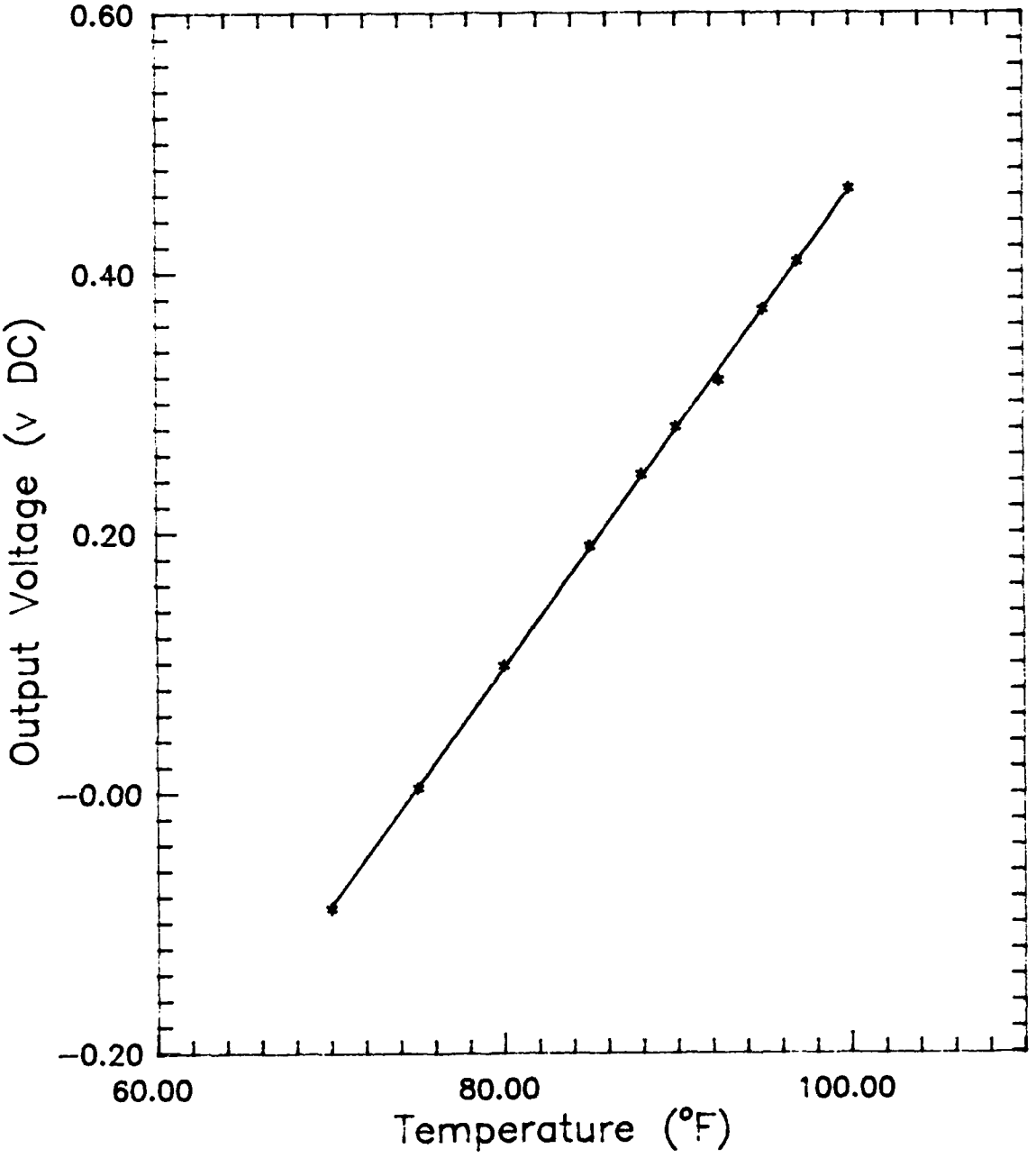

Figure D.3: Heat Flux Gauge 6 Calibration

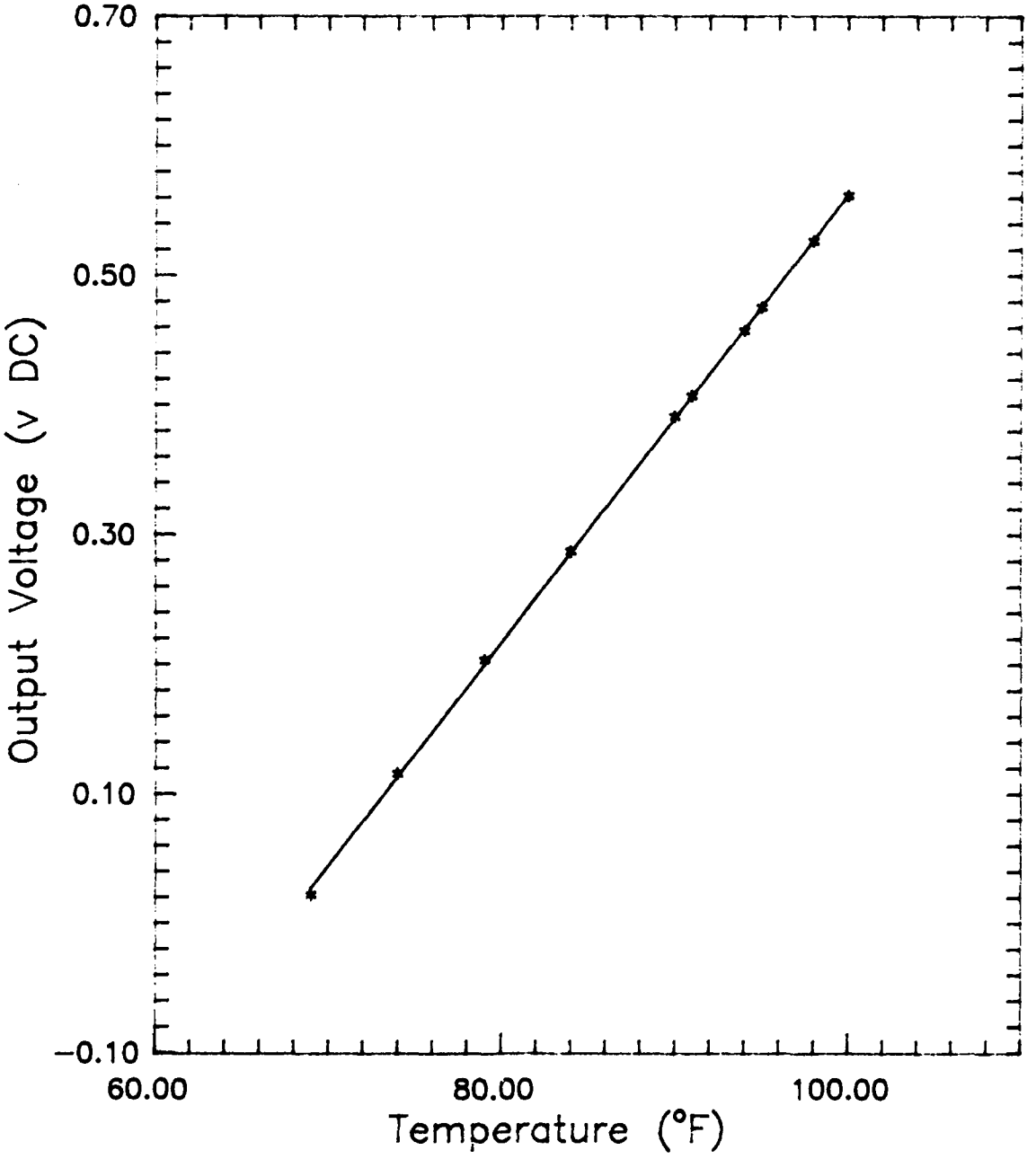

Figure D.4: Heat Flux Gauge 7 Calibration

Appendix E: Pressure Transducer Calibration Results

The pressure transducers were calibrated for output voltage as a function of pressure using the AMETEK Model HK-500 pneumatic dead weight tester. The Neff amplifiers were set for a gain of 10. The transducers were calibrated for pressures ranging form -0.4 psig (14.3 psia) to 60 psig (74.3 psia). The calibration results are shown in Figures E.1 and E.2.

Forward Pressure Transducer

$$p = 37.5272\ V + 2.20402$$

Rear Pressure Transducer

$$p = 27.6524\ V + 0.87726$$

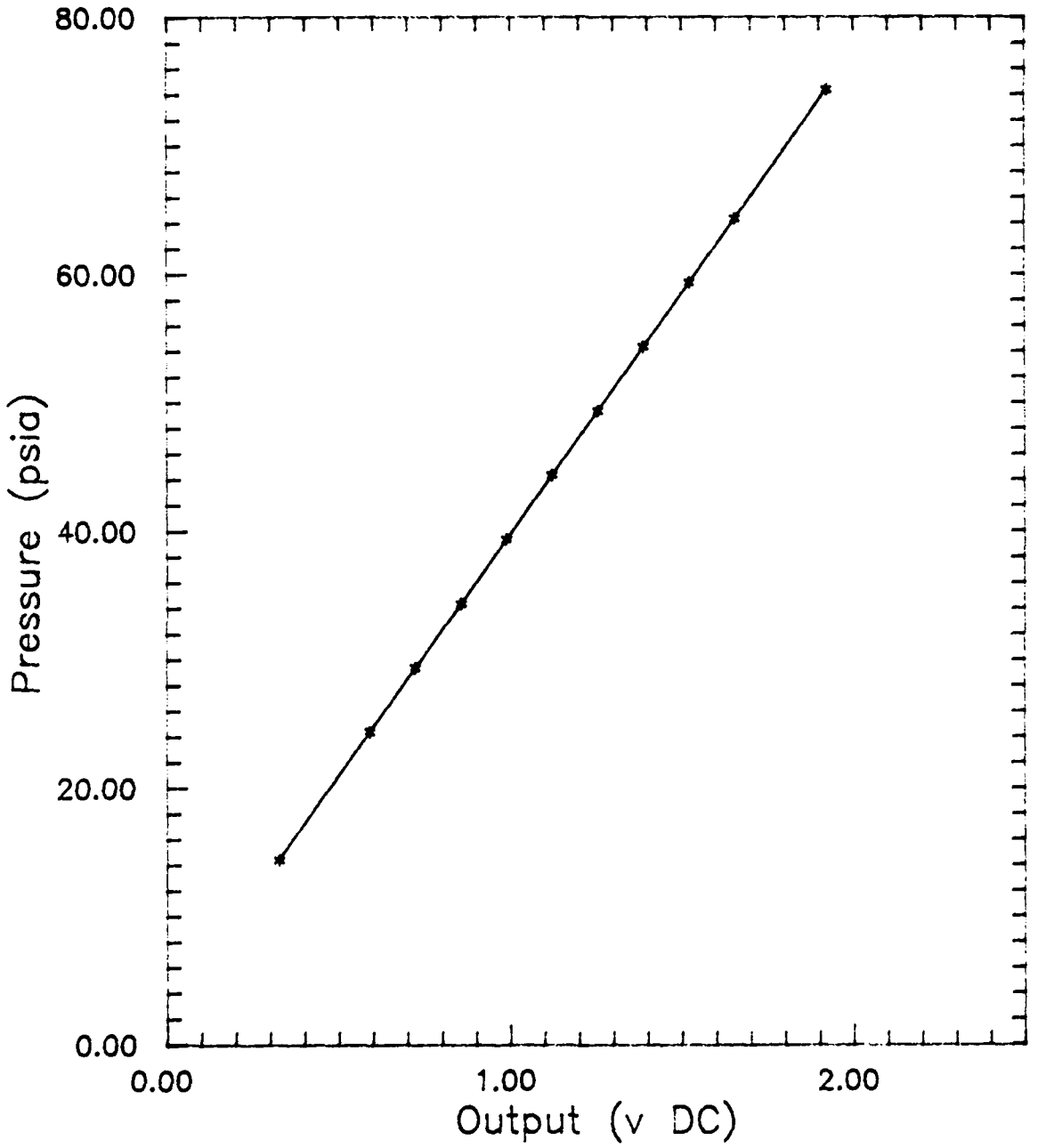

Figure E.1: Calibration Results for the Forward Pressure Transducer

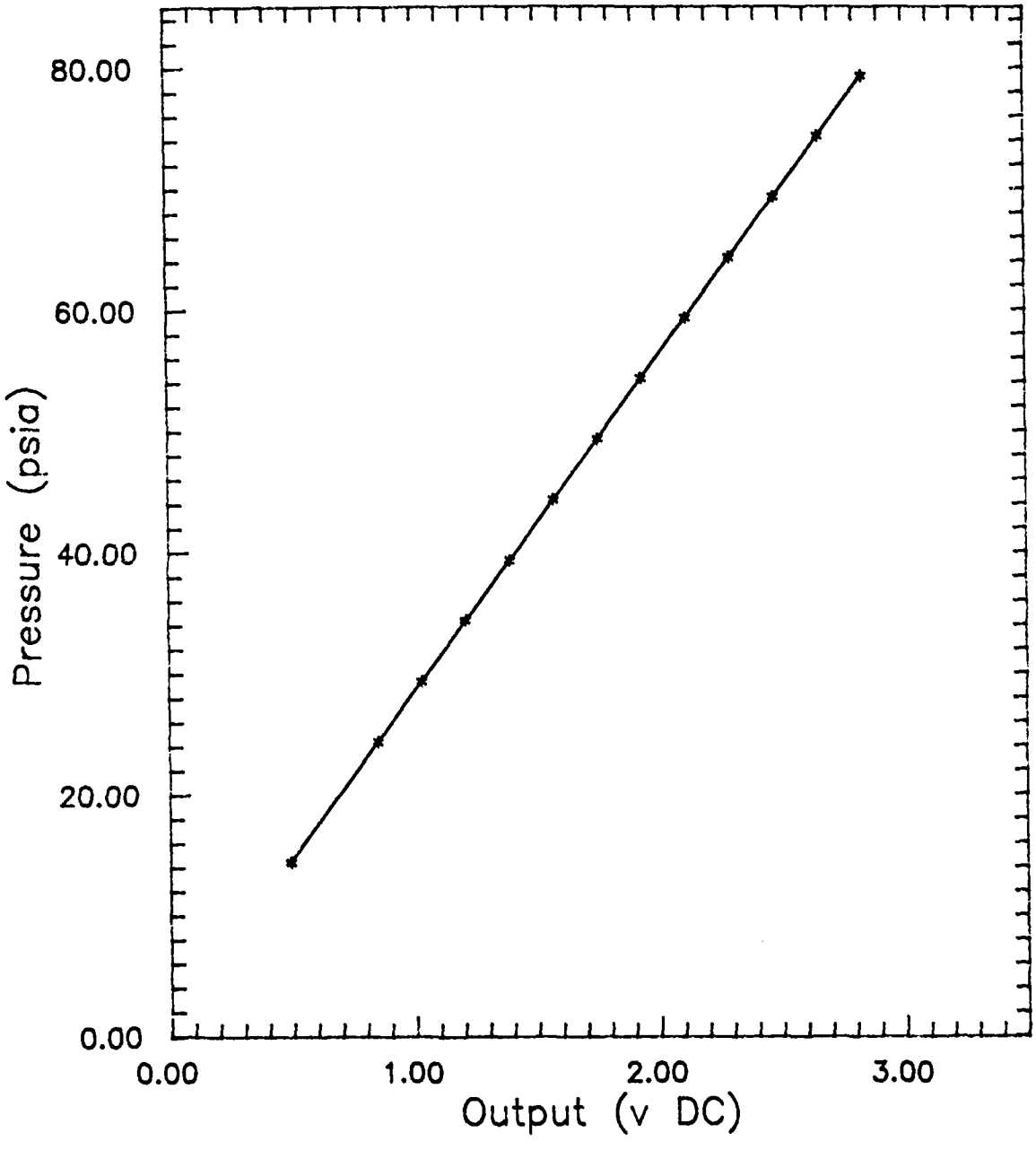

Figure E.2: Calibration Results for the Rear Pressure Transducer

APPENDIX F: DATA SUMMARY BY RUN NUMBER

The following pages give a summary of the data used for heat transfer measurement. The fluid properties based on a measure shock Mach number and the normal shock relations as well as the measured heat flux are displayed.

****
* r040 *
****

Driven Pressure:	29.1000 inches Hg
Driver Pressure:	50.0000 inches Hg, gauge
Pressure behind shock:	44.8221 inches Hg
Driven Temperature:	22.0000 deg C
Temperature behind shock:	61.5320 deg C
Stagnation Temperature:	67.5175 deg C
Driver Temperature:	22.0000 deg C

Measured Shock Mach Number: 1.2096 Theoretical: 1.2370
Shock speed: 443.4942 m/sec

Flow velocity behind shock: 109.8489 m/sec

Adibatic wall temperature:	66.8090 deg C
Reference temperature:	65.6860 deg C
Recovery Factor:	0.8816
Dynamic viscosity:	0.2028E-04
Specific heat:	0.1008E+04
Thermal conductivity:	0.2891E-01
Air density:	1.5613
Prandtl Number:	0.7070E+00

Results based on Theoretical Heat Flux and Measured Mach Number

Re	x (m)	St	Nu	h	q (kW/m^2)
0.480E+06	0.568E-01	0.241E-02	0.818E+03	0.417E+03	0.187E+02
0.517E+06	0.611E-01	0.237E-02	0.867E+03	0.410E+03	0.184E+02
0.557E+06	0.659E-01	0.234E-02	0.921E+03	0.404E+03	0.181E+02
0.601E+06	0.710E-01	0.230E-02	0.978E+03	0.398E+03	0.178E+02
0.688E+06	0.814E-01	0.224E-02	0.109E+04	0.388E+03	0.174E+02
0.772E+06	0.913E-01	0.219E-02	0.120E+04	0.379E+03	0.170E+02
0.109E+07	0.129E+00	0.204E-02	0.158E+04	0.353E+03	0.158E+02

Results based on Measured Heat Flux and Mach Number

x (m)	St	Nu	h	q (kW/m^2)	Qm/Qth
0.568E-01	0.362E-02	0.123E+04	0.627E+03	0.281E+02	0.150E+01
0.710E-01	0.292E-02	0.124E+04	0.505E+03	0.226E+02	0.127E+01
0.913E-01	0.317E-02	0.173E+04	0.548E+03	0.245E+02	0.145E+01

****
* r041 *
****

Driven Pressure: 29.1000 inches Hg
Driver Pressure: 100.0000 inches Hg, gauge
Pressure behind shock: 51.8760 inches Hg

Driven Temperature: 22.0000 deg C

Temperature behind shock: 76.9324 deg C
Stagnation Temperature: 87.9317 deg C

Driver Temperature: 22.0000 deg C

Measured Shock Mach Number: 1.2926 Theoretical: 1.3688
Shock speed: 484.7258 m/sec

Flow velocity behind shock: 148.9116 m/sec

Adibatic wall temperature: 86.6181 deg C
Reference temperature: 84.5654 deg C

Recovery Factor: 0.8814
Dynamic viscosity: 0.2112E-04
Specific heat: 0.1009E+04
Thermal conductivity: 0.3022E-01
Air density: 1.7116
Prandtl Number: 0.7051E+00

Results based on Theoretical Heat Flux and Measured Mach Number

Re	x (m)	St	Nu	h	q (kW/m^2)
0.685E+06	0.568E-01	0.225E-02	0.108E+04	0.578E+03	0.373E+02
0.738E+06	0.611E-01	0.221E-02	0.115E+04	0.569E+03	0.368E+02
0.795E+06	0.659E-01	0.218E-02	0.122E+04	0.561E+03	0.362E+02
0.857E+06	0.710E-01	0.215E-02	0.130E+04	0.552E+03	0.357E+02
0.982E+06	0.814E-01	0.209E-02	0.145E+04	0.538E+03	0.347E+02
0.110E+07	0.913E-01	0.204E-02	0.159E+04	0.525E+03	0.339E+02

Results based on Measured Heat Flux and Mach Number

x (m)	St	Nu	h	q (kW/m^2)	Qm/Qth
0.568E-01	0.356E-02	0.172E+04	0.916E+03	0.592E+02	0.159E+01
0.710E-01	0.287E-02	0.174E+04	0.739E+03	0.477E+02	0.134E+01
0.913E-01	0.309E-02	0.240E+04	0.796E+03	0.514E+02	0.152E+01

****
* r043 *
****

Driven Pressure: 28.9800 inches Hg
Driver Pressure: 115.0000 inches Hg, gauge
Pressure behind shock: 55.3649 inches Hg

Driven Temperature: 21.0000 deg C

Temperature behind shock: 83.5105 deg C
Stagnation Temperature: 97.4313 deg C

Driver Temperature: 21.0000 deg C

Measured Shock Mach Number: 1.3343 Theoretical: 1.4007
Shock speed: 505.0409 m/sec

Flow velocity behind shock: 167.5246 m/sec

Adibatic wall temperature: 95.7664 deg C
Reference temperature: 93.1706 deg C

Recovery Factor: 0.8813
Dynamic viscosity: 0.2149E-04
Specific heat: 0.1009E+04
Thermal conductivity: 0.3081E-01
Air density: 1.7838
Prandtl Number: 0.7040E+00

Results based on Theoretical Heat Flux and Measured Mach Number

Re	x (m)	St	Nu	h	q (kW/m^2)
0.789E+06	0.568E-01	0.218E-02	0.121E+04	0.659E+03	0.493E+02
0.850E+06	0.611E-01	0.215E-02	0.129E+04	0.649E+03	0.485E+02
0.916E+06	0.659E-01	0.212E-02	0.137E+04	0.639E+03	0.478E+02
0.988E+06	0.710E-01	0.209E-02	0.145E+04	0.630E+03	0.471E+02
0.113E+07	0.814E-01	0.203E-02	0.162E+04	0.613E+03	0.458E+02
0.127E+07	0.913E-01	0.199E-02	0.178E+04	0.599E+03	0.448E+02

Results based on Measured Heat Flux and Mach Number

x (m)	St	Nu	h	q (kW/m^2)	Qm/Qth
0.568E-01	0.331E-02	0.184E+04	0.998E+03	0.746E+02	0.151E+01
0.710E-01	0.277E-02	0.192E+04	0.834E+03	0.624E+02	0.132E+01
0.913E-01	0.248E-02	0.222E+04	0.748E+03	0.560E+02	0.125E+01

****
* r044 *
****

Driven Pressure:	28.9800	inches Hg	
Driver Pressure:	115.0000	inches Hg, gauge	
Pressure behind shock:	54.6341	inches Hg	
Driven Temperature:	21.0000	deg C	
Temperature behind shock:	81.9929	deg C	
Stagnation Temperature:	95.3150	deg C	
Driver Temperature:	21.0000	deg C	
Measured Shock Mach Number:	1.3262	Theoretical:	1.4007
Shock speed:	500.8962	m/sec	
Flow velocity behind shock:	163.8823	m/sec	
Adibatic wall temperature:	93.7223	deg C	
Reference temperature:	91.2377	deg C	
Recovery Factor:	0.8813		
Dynamic viscosity:	0.2141E-04		
Specific heat:	0.1009E+04		
Thermal conductivity:	0.3067E-01		
Air density:	1.7696		
Prandtl Number:	0.7042E+00		

Results based on Theoretical Heat Flux and Measured Mach Number

Re	x (m)	St	Nu	h	q (kW/m^2)
0.769E+06	0.568E-01	0.220E-02	0.119E+04	0.643E+03	0.467E+02
0.828E+06	0.611E-01	0.216E-02	0.126E+04	0.633E+03	0.460E+02
0.892E+06	0.659E-01	0.213E-02	0.134E+04	0.624E+03	0.454E+02
0.962E+06	0.710E-01	0.210E-02	0.142E+04	0.614E+03	0.447E+02
0.110E+07	0.814E-01	0.204E-02	0.159E+04	0.598E+03	0.435E+02
0.124E+07	0.913E-01	0.200E-02	0.174E+04	0.584E+03	0.425E+02

Results based on Measured Heat Flux and Mach Number

x (m)	St	Nu	h	q (kW/m^2)	Qm/Qth
0.568E-01	0.376E-02	0.203E+04	0.110E+04	0.799E+02	0.171E+01
0.710E-01	0.314E-02	0.213E+04	0.920E+03	0.669E+02	0.150E+01
0.913E-01	0.293E-02	0.255E+04	0.857E+03	0.623E+02	0.147E+01

****
* r054 *
****

Driven Pressure:	28.9800 inches Hg	
Driver Pressure:	100.0000 inches Hg, gauge	
Pressure behind shock:	52.5149 inches Hg	
Driven Temperature:	19.0000 deg C	
Temperature behind shock:	75.1669 deg C	
Stagnation Temperature:	86.7142 deg C	
Driver Temperature:	19.0000 deg C	
Measured Shock Mach Number:	1.3023	Theoretical: 1.3697
Shock speed:	487.1373 m/sec	
Flow velocity behind shock:	152.5755 m/sec	
Adibatic wall temperature:	85.3434 deg C	
Reference temperature:	83.1806 deg C	
Recovery Factor:	0.8813	
Dynamic viscosity:	0.2106E-04	
Specific heat:	0.1008E+04	
Thermal conductivity:	0.3013E-01	
Air density:	1.7394	
Prandtl Number:	0.7046E+00	

Results based on Theoretical Heat Flux and Measured Mach Number

Re	x (m)	St	Nu	h	q (kW/m^2)
0.715E+06	0.568E-01	0.223E-02	0.112E+04	0.596E+03	0.395E+02
0.770E+06	0.611E-01	0.219E-02	0.119E+04	0.587E+03	0.390E+02
0.830E+06	0.659E-01	0.216E-02	0.126E+04	0.578E+03	0.384E+02
0.895E+06	0.710E-01	0.213E-02	0.134E+04	0.570E+03	0.378E+02
0.103E+07	0.814E-01	0.207E-02	0.150E+04	0.554E+03	0.368E+02
0.115E+07	0.913E-01	0.203E-02	0.164E+04	0.542E+03	0.359E+02

Results based on Measured Heat Flux and Mach Number

x (m)	St	Nu	h	q (kW/m^2)	Qm/Qth
0.568E-01	0.377E-02	0.190E+04	0.101E+04	0.669E+02	0.169E+01
0.710E-01	0.310E-02	0.196E+04	0.829E+03	0.550E+02	0.146E+01
0.913E-01	0.333E-02	0.270E+04	0.890E+03	0.590E+02	0.164E+01
0.129E+00	0.654E-02	0.506E+04	0.113E+04	0.507E+02	0.320E+01

****
* r057 *
****

Driven Pressure:	28.9300 inches Hg		
Driver Pressure:	90.0000 inches Hg, gauge		
Pressure behind shock:	49.8768 inches Hg		
Driven Temperature:	18.0000 deg C		
Temperature behind shock:	68.5941 deg C		
Stagnation Temperature:	78.1676 deg C		
Driver Temperature:	18.0000 deg C		
Measured Shock Mach Number:	1.2730	Theoretical:	1.3477
Shock speed:	471.6590 m/sec		
Flow velocity behind shock:	138.9251 m/sec		
Adibatic wall temperature:	77.0335 deg C		
Reference temperature:	75.2384 deg C		
Recovery Factor:	0.8815		
Dynamic viscosity:	0.2071E-04		
Specific heat:	0.1008E+04		
Thermal conductivity:	0.2958E-01		
Air density:	1.6897		
Prandtl Number:	0.7056E+00		

Results based on Theoretical Heat Flux and Measured Mach Number

Re	x (m)	St	Nu	h	q (kW/m^2)
0.643E+06	0.568E-01	0.227E-02	0.103E+04	0.538E+03	0.318E+02
0.693E+06	0.611E-01	0.224E-02	0.110E+04	0.530E+03	0.313E+02
0.747E+06	0.659E-01	0.221E-02	0.116E+04	0.522E+03	0.308E+02
0.805E+06	0.710E-01	0.217E-02	0.124E+04	0.514E+03	0.304E+02
0.922E+06	0.814E-01	0.212E-02	0.138E+04	0.501E+03	0.296E+02
0.103E+07	0.913E-01	0.207E-02	0.151E+04	0.489E+03	0.289E+02
0.147E+07	0.129E+00	0.193E-02	0.200E+04	0.456E+03	0.269E+02

Results based on Measured Heat Flux and Mach Number

x (m)	St	Nu	h	q (kW/m^2)	Qm/Qth
0.568E-01	0.356E-02	0.162E+04	0.843E+03	0.498E+02	0.157E+01
0.710E-01	0.291E-02	0.165E+04	0.688E+03	0.406E+02	0.134E+01
0.913E-01	0.321E-02	0.234E+04	0.759E+03	0.448E+02	0.155E+01
0.129E+00	0.255E-02	0.264E+04	0.603E+03	0.356E+02	0.132E+01

****
* r059 *
****

Driven Pressure:	28.9300 inches Hg	
Driver Pressure:	70.0000 inches Hg, gauge	
Pressure behind shock:	42.4046 inches Hg	
Driven Temperature:	18.0000 deg C	
Temperature behind shock:	52.1213 deg C	
Stagnation Temperature:	56.7188 deg C	
Driver Temperature:	18.0000 deg C	
Measured Shock Mach Number:	1.1829	Theoretical: 1.2975
Shock speed:	427.5627 m/sec	
Flow velocity behind shock:	96.1777 m/sec	
Adibatic wall temperature:	56.1688 deg C	
Reference temperature:	55.3119 deg C	
Recovery Factor:	0.8821	
Dynamic viscosity:	0.1981E-04	
Specific heat:	0.1008E+04	
Thermal conductivity:	0.2818E-01	
Air density:	1.5238	
Prandtl Number:	0.7087E+00	

Results based on Theoretical Heat Flux and Measured Mach Number

Re	x (m)	St	Nu	h	q (kW/m^2)
0.420E+06	0.568E-01	0.247E-02	0.736E+03	0.365E+03	0.139E+02
0.452E+06	0.611E-01	0.244E-02	0.780E+03	0.360E+03	0.137E+02
0.487E+06	0.659E-01	0.240E-02	0.829E+03	0.354E+03	0.135E+02
0.526E+06	0.710E-01	0.236E-02	0.880E+03	0.349E+03	0.133E+02
0.602E+06	0.814E-01	0.230E-02	0.981E+03	0.340E+03	0.130E+02
0.675E+06	0.913E-01	0.225E-02	0.108E+04	0.332E+03	0.127E+02
0.957E+06	0.129E+00	0.210E-02	0.142E+04	0.310E+03	0.118E+02

Results based on Measured Heat Flux and Mach Number

x (m)	St	Nu	h	q (kW/m^2)	Qm/Qth
0.568E-01	0.499E-02	0.148E+04	0.737E+03	0.281E+02	0.202E+01
0.710E-01	0.407E-02	0.152E+04	0.601E+03	0.230E+02	0.172E+01
0.913E-01	0.400E-02	0.192E+04	0.591E+03	0.226E+02	0.178E+01
0.129E+00	0.436E-02	0.296E+04	0.645E+03	0.246E+02	0.208E+01

****
* r060 *
****

Driven Pressure:	28.9300 inches Hg	
Driver Pressure:	60.0000 inches Hg, gauge	
Pressure behind shock:	46.8849 inches Hg	
Driven Temperature:	18.0000 deg C	
Temperature behind shock:	62.1353 deg C	
Stagnation Temperature:	69.5763 deg C	
Driver Temperature:	18.0000 deg C	
Measured Shock Mach Number:	1.2377	Theoretical: 1.2691
Shock speed:	454.2223 m/sec	
Flow velocity behind shock:	122.4789 m/sec	
Adibatic wall temperature:	68.6965 deg C	
Reference temperature:	67.2998 deg C	
Recovery Factor:	0.8818	
Dynamic viscosity:	0.2035E-04	
Specific heat:	0.1008E+04	
Thermal conductivity:	0.2903E-01	
Air density:	1.6254	
Prandtl Number:	0.7068E+00	

Results based on Theoretical Heat Flux and Measured Mach Number

Re	x (m)	St	Nu	h	q (kW/m^2)
0.555E+06	0.568E-01	0.234E-02	0.918E+03	0.470E+03	0.238E+02
0.598E+06	0.611E-01	0.231E-02	0.974E+03	0.463E+03	0.235E+02
0.644E+06	0.659E-01	0.227E-02	0.103E+04	0.456E+03	0.231E+02
0.695E+06	0.710E-01	0.224E-02	0.110E+04	0.449E+03	0.228E+02
0.796E+06	0.814E-01	0.218E-02	0.122E+04	0.437E+03	0.222E+02
0.893E+06	0.913E-01	0.213E-02	0.134E+04	0.427E+03	0.217E+02
0.127E+07	0.129E+00	0.198E-02	0.178E+04	0.398E+03	0.202E+02

Results based on Measured Heat Flux and Mach Number

x (m)	St	Nu	h	q (kW/m^2)	Qm/Qth
0.568E-01	0.351E-02	0.138E+04	0.704E+03	0.357E+02	0.150E+01
0.710E-01	0.293E-02	0.144E+04	0.587E+03	0.298E+02	0.131E+01
0.913E-01	0.322E-02	0.203E+04	0.645E+03	0.327E+02	0.151E+01
0.129E+00	0.303E-02	0.271E+04	0.607E+03	0.308E+02	0.152E+01

****
* r061 *
****

Driven Pressure:	28.9300	inches Hg	
Driver Pressure:	90.0000	inches Hg, gauge	
Pressure behind shock:	50.1861	inches Hg	
Driven Temperature:	18.0000	deg C	
Temperature behind shock:	69.2529	deg C	
Stagnation Temperature:	79.0558	deg C	
Driver Temperature:	18.0000	deg C	
Measured Shock Mach Number:	1.2766	Theoretical:	1.3477
Shock speed:	473.4467	m/sec	
Flow velocity behind shock:	140.5797	m/sec	
Adibatic wall temperature:	77.8943	deg C	
Reference temperature:	76.0564	deg C	
Recovery Factor:	0.8815		
Dynamic viscosity:	0.2074E-04		
Specific heat:	0.1008E+04		
Thermal conductivity:	0.2964E-01		
Air density:	1.6962		
Prandtl Number:	0.7055E+00		

Results based on Theoretical Heat Flux and Measured Mach Number

Re	x (m)	St	Nu	h	q (kW/m^2)
0.652E+06	0.568E-01	0.227E-02	0.104E+04	0.545E+03	0.326E+02
0.703E+06	0.611E-01	0.223E-02	0.111E+04	0.537E+03	0.322E+02
0.757E+06	0.659E-01	0.220E-02	0.118E+04	0.529E+03	0.317E+02
0.817E+06	0.710E-01	0.217E-02	0.125E+04	0.521E+03	0.312E+02
0.935E+06	0.814E-01	0.211E-02	0.139E+04	0.507E+03	0.304E+02
0.105E+07	0.913E-01	0.206E-02	0.153E+04	0.496E+03	0.297E+02
0.149E+07	0.129E+00	0.192E-02	0.202E+04	0.462E+03	0.277E+02

Results based on Measured Heat Flux and Mach Number

x (m)	St	Nu	h	q (kW/m^2)	Qm/Qth
0.568E-01	0.419E-02	0.193E+04	0.101E+04	0.603E+02	0.185E+01
0.710E-01	0.321E-02	0.185E+04	0.773E+03	0.463E+02	0.148E+01
0.913E-01	0.361E-02	0.267E+04	0.868E+03	0.520E+02	0.175E+01
0.129E+00	0.318E-02	0.333E+04	0.764E+03	0.457E+02	0.165E+01

****
* r063 *
****

Driven Pressure:	28.9300 inches Hg	
Driver Pressure:	70.0000 inches Hg, gauge	
Pressure behind shock:	43.7712 inches Hg	
Driven Temperature:	18.0000 deg C	
Temperature behind shock:	55.2247 deg C	
Stagnation Temperature:	60.6344 deg C	
Driver Temperature:	18.0000 deg C	
Measured Shock Mach Number:	1.1999	Theoretical: 1.2975
Shock speed:	435.7699 m/sec	
Flow velocity behind shock:	104.4319 m/sec	
Adibatic wall temperature:	59.9961 deg C	
Reference temperature:	58.9796 deg C	
Recovery Factor:	0.8820	
Dynamic viscosity:	0.1998E-04	
Specific heat:	0.1008E+04	
Thermal conductivity:	0.2844E-01	
Air density:	1.5555	
Prandtl Number:	0.7081E+00	

Results based on Theoretical Heat Flux and Measured Mach Number

Re	x (m)	St	Nu	h	q (kW/m^2)
0.461E+06	0.568E-01	0.243E-02	0.793E+03	0.397E+03	0.167E+02
0.497E+06	0.611E-01	0.239E-02	0.841E+03	0.392E+03	0.164E+02
0.536E+06	0.659E-01	0.236E-02	0.893E+03	0.386E+03	0.162E+02
0.578E+06	0.710E-01	0.232E-02	0.949E+03	0.380E+03	0.160E+02
0.662E+06	0.814E-01	0.226E-02	0.106E+04	0.370E+03	0.155E+02
0.742E+06	0.913E-01	0.221E-02	0.116E+04	0.361E+03	0.152E+02
0.105E+07	0.129E+00	0.206E-02	0.153E+04	0.337E+03	0.142E+02

Results based on Measured Heat Flux and Mach Number

x (m)	St	Nu	h	q (kW/m^2)	Qm/Qth
0.568E-01	0.452E-02	0.148E+04	0.739E+03	0.310E+02	0.186E+01
0.710E-01	0.372E-02	0.152E+04	0.608E+03	0.255E+02	0.160E+01
0.913E-01	0.394E-02	0.207E+04	0.646E+03	0.271E+02	0.179E+01
0.129E+00	0.380E-02	0.283E+04	0.622E+03	0.261E+02	0.185E+01

****
* r064 *
****

Driven Pressure:	28.9300	inches Hg	
Driver Pressure:	60.0000	inches Hg, gauge	
Pressure behind shock:	46.7927	inches Hg	
Driven Temperature:	18.0000	deg C	
Temperature behind shock:	61.9335	deg C	
Stagnation Temperature:	69.3114	deg C	
Driver Temperature:	18.0000	deg C	
Measured Shock Mach Number:	1.2366	Theoretical:	1.2691
Shock speed:	453.6804	m/sec	
Flow velocity behind shock:	121.9586	m/sec	
Adibatic wall temperature:	68.4391	deg C	
Reference temperature:	67.0543	deg C	
Recovery Factor:	0.8818		
Dynamic viscosity:	0.2034E-04		
Specific heat:	0.1008E+04		
Thermal conductivity:	0.2901E-01		
Air density:	1.6234		
Prandtl Number:	0.7068E+00		

Results based on Theoretical Heat Flux and Measured Mach Number

Re	x (m)	St	Nu	h	q (kW/m^2)
0.552E+06	0.568E-01	0.234E-02	0.915E+03	0.468E+03	0.236E+02
0.595E+06	0.611E-01	0.231E-02	0.971E+03	0.461E+03	0.232E+02
0.641E+06	0.659E-01	0.227E-02	0.103E+04	0.454E+03	0.229E+02
0.691E+06	0.710E-01	0.224E-02	0.109E+04	0.447E+03	0.225E+02
0.792E+06	0.814E-01	0.218E-02	0.122E+04	0.435E+03	0.219E+02
0.838E+06	0.913E-01	0.213E-02	0.134E+04	0.425E+03	0.214E+02
0.126E+07	0.129E+00	0.199E-02	0.177E+04	0.396E+03	0.200E+02

Results based on Measured Heat Flux and Mach Number

x (m)	St	Nu	h	q (kW/m^2)	Qm/Qth
0.568E-01	0.379E-02	0.148E+04	0.756E+03	0.381E+02	0.162E+01
0.710E-01	0.320E-02	0.156E+04	0.638E+03	0.322E+02	0.143E+01
0.913E-01	0.352E-02	0.221E+04	0.702E+03	0.354E+02	0.165E+01
0.129E+00	0.302E-02	0.268E+04	0.602E+03	0.304E+02	0.152E+01

****
* r080 *
****

Driven Pressure:	29.2800 inches Hg	
Driver Pressure:	100.0000 inches Hg, gauge	
Pressure behind shock:	54.6034 inches Hg	
Driven Temperature:	21.0000 deg C	
Temperature behind shock:	80.7623 deg C	
Stagnation Temperature:	93.6060 deg C	
Driver Temperature:	21.0000 deg C	
Measured Shock Mach Number:	1.3196	Theoretical: 1.3675
Shock speed:	497.5398 m/sec	
Flow velocity behind shock:	160.9128 m/sec	
Adibatic wall temperature:	92.0710 deg C	
Reference temperature:	89.6752 deg C	
Recovery Factor:	0.8814	
Dynamic viscosity:	0.2134E-04	
Specific heat:	0.1009E+04	
Thermal conductivity:	0.3057E-01	
Air density:	1.7762	
Prandtl Number:	0.7044E+00	

Results based on Theoretical Heat Flux and Measured Mach Number

Re	x (m)	St	Nu	h	q (kW/m^2)
0.760E+06	0.568E-01	0.220E-02	0.118E+04	0.635E+03	0.451E+02
0.819E+06	0.611E-01	0.217E-02	0.125E+04	0.625E+03	0.444E+02
0.882E+06	0.659E-01	0.214E-02	0.133E+04	0.616E+03	0.438E+02
0.951E+06	0.710E-01	0.210E-02	0.141E+04	0.607E+03	0.431E+02
0.109E+07	0.814E-01	0.205E-02	0.157E+04	0.591E+03	0.420E+02
0.122E+07	0.913E-01	0.200E-02	0.172E+04	0.577E+03	0.410E+02
0.173E+07	0.129E+00	0.187E-02	0.228E+04	0.538E+03	0.383E+02

Results based on Measured Heat Flux and Mach Number

x (m)	St	Nu	h	q (kW/m^2)	Qm/Qth
0.568E-01	0.372E-02	0.199E+04	0.107E+04	0.762E+02	0.169E+01
0.710E-01	0.278E-02	0.186E+04	0.801E+03	0.570E+02	0.132E+01
0.913E-01	0.310E-02	0.267E+04	0.895E+03	0.636E+02	0.155E+01
0.129E+00	0.257E-02	0.314E+04	0.741E+03	0.527E+02	0.138E+01

****
* r102 *
****

Driven Pressure:	29.1900 inches Hg	
Driver Pressure:	70.0000 inches Hg, gauge	
Pressure behind shock:	48.8772 inches Hg	
Driven Temperature:	20.0000 deg C	
Temperature behind shock:	67.8431 deg C	
Stagnation Temperature:	76.4323 deg C	
Driver Temperature:	20.0000 deg C	
Measured Shock Mach Number:	1.2562	Theoretical: 1.2958
Shock speed:	464.9193 m/sec	
Flow velocity behind shock:	131.5895 m/sec	
Adibatic wall temperature:	75.4144 deg C	
Reference temperature:	73.8041 deg C	
Recovery Factor:	0.8815	
Dynamic viscosity:	0.2064E-04	
Specific heat:	0.1008E+04	
Thermal conductivity:	0.2948E-01	
Air density:	1.6627	
Prandtl Number:	0.7058E+00	

Results based on Theoretical Heat Flux and Measured Mach Number

Re	x (m)	St	Nu	h	q (kW/m^2)
0.602E+06	0.568E-01	0.230E-02	0.978E+03	0.508E+03	0.282E+02
0.648E+06	0.611E-01	0.227E-02	0.104E+04	0.501E+03	0.277E+02
0.698E+06	0.659E-01	0.224E-02	0.110E+04	0.493E+03	0.273E+02
0.753E+06	0.710E-01	0.220E-02	0.117E+04	0.486E+03	0.269E+02
0.862E+06	0.814E-01	0.214E-02	0.131E+04	0.473E+03	0.262E+02
0.967E+06	0.913E-01	0.210E-02	0.143E+04	0.462E+03	0.256E+02
0.137E+07	0.129E+00	0.195E-02	0.189E+04	0.431E+03	0.239E+02

Results based on Measured Heat Flux and Mach Number

x (m)	St	Nu	h	q (kW/m^2)	Qm/Qth
0.568E-01	0.415E-02	0.176E+04	0.915E+03	0.507E+02	0.180E+01
0.913E-01	0.346E-02	0.236E+04	0.762E+03	0.422E+02	0.165E+01
0.129E+00	0.289E-02	0.280E+04	0.637E+03	0.353E+02	0.148E+01

****
* r103 *
****

Driven Pressure:	29.1900 inches Hg	
Driver Pressure:	80.0000 inches Hg, gauge	
Pressure behind shock:	50.5983 inches Hg	
Driven Temperature:	20.0000 deg C	
Temperature behind shock:	71.5226 deg C	
Stagnation Temperature:	81.3640 deg C	
Driver Temperature:	20.0000 deg C	
Measured Shock Mach Number:	1.2762	Theoretical: 1.3218
Shock speed:	474.8475 m/sec	
Flow velocity behind shock:	140.8556 m/sec	
Adibatic wall temperature:	80.1965 deg C	
Reference temperature:	78.3525 deg C	
Recovery Factor:	0.8814	
Dynamic viscosity:	0.2084E-04	
Specific heat:	0.1008E+04	
Thermal conductivity:	0.2979E-01	
Air density:	1.6990	
Prandtl Number:	0.7052E+00	

Results based on Theoretical Heat Flux and Measured Mach Number

Re	x (m)	St	Nu	h	q (kW/m^2)
0.652E+06	0.568E-01	0.227E-02	0.104E+04	0.547E+03	0.329E+02
0.702E+06	0.611E-01	0.224E-02	0.111E+04	0.539E+03	0.325E+02
0.756E+06	0.659E-01	0.220E-02	0.117E+04	0.531E+03	0.320E+02
0.816E+06	0.710E-01	0.217E-02	0.125E+04	0.523E+03	0.315E+02
0.934E+06	0.814E-01	0.211E-02	0.139E+04	0.509E+03	0.307E+02
0.105E+07	0.913E-01	0.206E-02	0.152E+04	0.498E+03	0.300E+02
0.149E+07	0.129E+00	0.192E-02	0.202E+04	0.464E+03	0.279E+02

Results based on Measured Heat Flux and Mach Number

x (m)	St	Nu	h	q (kW/m^2)	Qm/Qth
0.568E-01	0.387E-02	0.178E+04	0.933E+03	0.562E+02	0.170E+01
0.710E-01	0.291E-02	0.168E+04	0.703E+03	0.423E+02	0.134E+01
0.913E-01	0.314E-02	0.232E+04	0.758E+03	0.456E+02	0.152E+01
0.129E+00	0.273E-02	0.286E+04	0.658E+03	0.396E+02	0.142E+01

****
* r104 *
****

Driven Pressure:	29.1900	inches Hg	
Driver Pressure:	115.0000	inches Hg, gauge	
Pressure behind shock:	56.7254	inches Hg	
Driven Temperature:	20.0000	deg C	
Temperature behind shock:	84.2586	deg C	
Stagnation Temperature:	98.9052	deg C	
Driver Temperature:	20.0000	deg C	
Measured Shock Mach Number:	1.3448	Theoretical:	1.3990
Shock speed:	509.5541	m/sec	
Flow velocity behind shock:	171.9212	m/sec	
Adibatic wall temperature:	97.1583	deg C	
Reference temperature:	94.4235	deg C	
Recovery Factor:	0.8816		
Dynamic viscosity:	0.2155E-04		
Specific heat:	0.1010E+04		
Thermal conductivity:	0.3089E-01		
Air density:	1.8214		
Prandtl Number:	0.7045E+00		

Results based on Theoretical Heat Flux and Measured Mach Number

Re	x (m)	St	Nu	h	q (kW/m^2)
0.825E+06	0.568E-01	0.216E-02	0.126E+04	0.685E+03	0.528E+02
0.888E+06	0.611E-01	0.213E-02	0.133E+04	0.675E+03	0.521E+02
0.957E+06	0.659E-01	0.210E-02	0.142E+04	0.665E+03	0.513E+02
0.103E+07	0.710E-01	0.207E-02	0.151E+04	0.655E+03	0.505E+02
0.118E+07	0.814E-01	0.201E-02	0.168E+04	0.637E+03	0.492E+02
0.133E+07	0.913E-01	0.197E-02	0.184E+04	0.623E+03	0.480E+02
0.188E+07	0.129E+00	0.184E-02	0.243E+04	0.581E+03	0.448E+02

Results based on Measured Heat Flux and Mach Number

x (m)	St	Nu	h	q (kW/m^2)	Qm/Qth
0.568E-01	0.375E-02	0.218E+04	0.119E+04	0.916E+02	0.173E+01
0.710E-01	0.298E-02	0.217E+04	0.943E+03	0.728E+02	0.144E+01
0.913E-01	0.341E-02	0.319E+04	0.108E+04	0.833E+02	0.173E+01
0.129E+00	0.276E-02	0.365E+04	0.872E+03	0.673E+02	0.150E+01

****
* r105 *
****

Driven Pressure:	29.1900	inches Hg
Driver Pressure:	120.0000	inches Hg, gauge
Pressure behind shock:	56.3514	inches Hg
Driven Temperature:	20.0000	deg C
Temperature behind shock:	83.4955	deg C
Stagnation Temperature:	97.8483	deg C
Driver Temperature:	20.0000	deg C
Measured Shock Mach Number:	1.3407	Theoretical: 1.4087
Shock speed:	507.4619	m/sec
Flow velocity behind shock:	170.1035	m/sec
Adibatic wall temperature:	96.1322	deg C
Reference temperature:	93.4555	deg C
Recovery Factor:	0.8813	
Dynamic viscosity:	0.2151E-04	
Specific heat:	0.1009E+04	
Thermal conductivity:	0.3082E-01	
Air density:	1.8142	
Prandtl Number:	0.7040E+00	

Results based on Theoretical Heat Flux and Measured Mach Number

Re	x (m)	St	Nu	h	q (kW/m^2)
0.814E+06	0.568E-01	0.217E-02	0.124E+04	0.676E+03	0.515E+02
0.877E+06	0.611E-01	0.214E-02	0.132E+04	0.666E+03	0.507E+02
0.945E+06	0.659E-01	0.211E-02	0.140E+04	0.656E+03	0.500E+02
0.102E+07	0.710E-01	0.208E-02	0.149E+04	0.646E+03	0.492E+02
0.117E+07	0.814E-01	0.202E-02	0.166E+04	0.629E+03	0.479E+02
0.131E+07	0.913E-01	0.197E-02	0.182E+04	0.615E+03	0.468E+02
0.186E+07	0.129E+00	0.184E-02	0.241E+04	0.573E+03	0.436E+02

Results based on Measured Heat Flux and Mach Number

x (m)	St	Nu	h	q (kW/m^2)	Qm/Qth
0.568E-01	0.378E-02	0.217E+04	0.118E+04	0.896E+02	0.174E+01
0.710E-01	0.298E-02	0.214E+04	0.926E+03	0.705E+02	0.143E+01
0.913E-01	0.345E-02	0.318E+04	0.107E+04	0.817E+02	0.175E+01
0.129E+00	0.265E-02	0.347E+04	0.826E+03	0.629E+02	0.144E+01

VITA

Captain Richard K. Rockwell

and attended the Ohio State University, from which he received the degree of Bachelor of Science in Aeronautical and Astronautical Engineering in June 1985. He received his commission in June 1985, after having completed the Reserve Officer Training Corp program at Ohio State University. From October 1985 to May 1988 he was assigned to the 31st Test and Evaluation Squadron, Edwards AFB, California, as an Operational Test and Evaluation Systems Analyst for the B-52 CSRL, B-1B and B-2 test programs. He entered the Master of Science in Aeronautical and Astronautical Engineering program at the Air Force Institute of Technology in June 1988.

SECURITY CLASSIFICATION OF THIS PAGE

REPORT DOCUMENTATION PAGE

Form Approved
OMB No. 0704-0188

1a. REPORT SECURITY CLASSIFICATION UNCLASSIFIED	1b. RESTRICTIVE MARKINGS
2a. SECURITY CLASSIFICATION AUTHORITY	3. DISTRIBUTION/AVAILABILITY OF REPORT Approved for public release; distribution unlimited
2b. DECLASSIFICATION/DOWNGRADING SCHEDULE	
4. PERFORMING ORGANIZATION REPORT NUMBER(S) AFIT/GAE/ENY/89D-31	5. MONITORING ORGANIZATION REPORT NUMBER(S)
6a. NAME OF PERFORMING ORGANIZATION School of Engineering 6b. OFFICE SYMBOL (If applicable) AFIT/EN	7a. NAME OF MONITORING ORGANIZATION
6c. ADDRESS (City, State, and ZIP Code) Air Force Institute of Technology Wright-Patterson AFB, Ohio 45433	7b. ADDRESS (City, State, and ZIP Code)
8a. NAME OF FUNDING/SPONSORING ORGANIZATION 8b. OFFICE SYMBOL (If applicable)	9. PROCUREMENT INSTRUMENT IDENTIFICATION NUMBER
8c. ADDRESS (City, State, and ZIP Code)	10. SOURCE OF FUNDING NUMBERS PROGRAM ELEMENT NO. / PROJECT NO. / TASK NO. / WORK UNIT ACCESSION NO.

11. TITLE (Include Security Classification)
TRANSIENT HEAT TRANSFER MEASUREMENTS ON A FLAT PLATE IN TURBULENT FLOW USING AN ELECTRICAL ANALOG

12. PERSONAL AUTHOR(S)
Richard K. Rockwell, B.S., Capt, USAF

13a. TYPE OF REPORT	13b. TIME COVERED	14. DATE OF REPORT (Year, Month, Day)	15. PAGE COUNT
M.S. Thesis	FROM _____ TO _____	1989 December	155

16. SUPPLEMENTARY NOTATION

17. COSATI CODES			18. SUBJECT TERMS (Continue on reverse if necessary and identify by block number)
FIELD	GROUP	SUB-GROUP	Heat Transfer, Turbulence, Shock Tube, Electrical Analog, Flat Plate, Transient
21	05		
20	13		

19. ABSTRACT (Continue on reverse if necessary and identify by block number)

Thesis Advisor: Lt Col Paul I. King

20. DISTRIBUTION/AVAILABILITY OF ABSTRACT	21. ABSTRACT SECURITY CLASSIFICATION
☒ UNCLASSIFIED/UNLIMITED ☐ SAME AS RPT. ☐ DTIC USERS	UNCLASSIFIED

22a. NAME OF RESPONSIBLE INDIVIDUAL	22b. TELEPHONE (Include Area Code)	22c. OFFICE SYMBOL
Lt Col Paul I. King	(513) 255-2362	AFIT/ENY

DD Form 1473, JUN 86 *Previous editions are obsolete.* SECURITY CLASSIFICATION OF THIS PAGE

ABSTRACT

In this study an electrical analog, for heat flux measurement from surface mounted thin film temperature gauges, was built and tested. Typically, the determination of heat transfer from thin film gauges requires the numerical evaluation of an integral. The electrical analog enables the heat transfer to be recorded directly without incorporating numerical error.

Once built and tested, the analog is used to measure transient flat plate heat flux with free-stream turbulence. The time varying flow is produced using a low pressure shock tube, with free stream turbulence generated by flow injectiBon upstream of the flat plate. The "steady flow" portion of the test data is compared to the theoretical flat plate solution for constant free stream and constant plate temperatures.

A constant temperature hot-wire technique is used to determine free stream turbulence. The hot-wire procedure requires performing several experiments with the same flow conditions, but different hot-wire operating temperatures. A quadratic least squares curve fit is performed using the data from the hot-wire experiments to determine the turbulence level.